Publications of the Internal Combustion Engine Laboratory
Helsinki University of Technology
Teknillisen korkeakoulun polttomoottorilaboratorion julkaisuja
Espoo 2003 77

DIESEL FUEL INJECTION SYSTEM SIMULATION

Jukka Kiijärvi

Dissertation for the degree of Doctor of Technology to be presented with due permission for public examination and debate in Auditorium Kolab-118 at Helsinki University of Technology (Espoo, Finland) on the 28th of August, 2003, at 12 o'clock noon.

Helsinki University of Technology
Department of Mechanical Enginering
Internal Combustion Engine Laboratory

Teknillinen korkeakoulu
Konetekniikan osasto
Polttomoottorilaboratorio

Distribution:
Helsinki University of Technology
Internal Combustion Engine Laboratory
P. O. Box 4300
FIN-02015 HUT
Tel. +358-9-451 3460
Fax. +358-9-451 3454
E-mail: Seija.Erander-Luukkanen@hut.fi

ISBN 951-22-6657-1
ISSN 1459-5931

Otamedia Oy
Espoo 2003

Kiijärvi, J., Diesel Fuel Injection System Simulation. Espoo 2003, Publications of the Internal Combustion Engine Laboratory, Helsinki University of Technology, No. 77, 126 pp. ISBN 951-22-6657-1, ISSN 1459-5931.

Keywords: diesel engine, diesel fuel injection system, simulation

Abstract

The injection process of a medium-speed diesel engine was studied in detail, using a computer program developed for this purpose. In the program, the injection pump was replaced with the measured pressure at the junction between the pump and high-pressure pipe. The results were calculated with a full and approximately a half load. The calculated and measured results corresponded moderately well with each other. In the calculation, special interest was paid to the flow of the injection valve holes. Most of the fuel was injected into the cylinder from the cavitating flow of these holes. During the after-injection, no cavitation occurred in the holes. Models of different hydraulic systems can be built from the components of the program.

Preface

This research work was carried out in the Internal Combustion Engine Laboratory of Helsinki University of Technology. A new computer code was written for this work using the computers of CSC, the Finnish IT Center for Science.

During the work, the Internal Combustion Engine Laboratory had three professors: Proffessor Emeritus Jorma Pitkänen, Proffessor Matti Kleimola and, currently Proffessor Martti Larmi. I thank each one of them for their help and support during the work.

At the beginning of this study, I received valuable help and advice from Professor Emeritus Ilmari Kurki-Suonio. In addition, Dr.Raimo Turunen always helped me when needed. Dr. Seppo Niemi read through the manuscript and provided good comments. Mr. Ossi Kankkunen helped me with the English. Mrs. Kirsti Mäkinen translated the text. The translation was edited by Mrs. Ruth Vilmi. I am deeply indebted to these people for their help.

I received financial support from the Henry Ford Foundation, the Foundation of Technology in Finland, the Jenny and Antti Wihuri Foundation and the Research Foundation of Helsinki University of Technology. Without the support of these foundations, this work had been impossible to realize.

I wrote most of the computer code in a project that formed part of the Energy Technology Research Program Mobile. The Technology Development Centre (TEKES) admministered this research program. The manuscript was mainly written with the financial support of the Power Engineering Graduate School (PEGS). In both the Mobile project and PEGS, I was able to work full-timely on this study.

Veikkola, August 2003

Jukka Kiijärvi

Contents

Symbols

A	point of the characteristic grid, area
A_g	geometric cross-section area
A_s	smallest flow cross-section area
a	half-width of the range
a_{c0}, a_{c1}, a_{c2}	polynome coefficients of the speed of the pressure pulse in diesel oil
$a_{\rho 0}, a_{\rho 1}, a_{\rho 2}$	polynome coefficients of diesel oil density
$a_0 \dots a_n$	coefficients of the polynome
a_{00}	measured constant term of the straight line for fictive flow coefficient of laminar flow
a_-	lower bound of the range
a_+	upper bound of the range
B	point of the characteristic grid
C	point of the characteristic grid
c	speed of pressure pulse
d	diameter
F_0	spring initial force
f	Darcy-Weisbach friction factor, damping coefficient
g	acceleration due to gravity
i	pipe node
K	bulk modulus of elasticity
k	spring rate
l	length
M	molar mass
m	mass
n	number
n_{in}	number of volumetric flows entering the container
n_m	number of moving parts
n_{out}	number of volumetric flows discharging from the container
n_v	number of controlling pressures
P	point of the characteristic grid
p	pressure, exponent
p_n	pressure at point n
p_v	vapor pressure
p_0	initial pressure
q_m	mass flow rate
q_v	volume flow rate

q_{vin}	volume flow rate into a node of the characteristic grid or into container of unknown pressure
q_{vout}	volume flow rate out of a node of the characteristic grid or out of container of unknown pressure
R	point of the characteristic grid, molar gas constant
Re	Reynolds number
Re_{lt}	Reynolds number at which the flow turns from a laminar into a turbulent one
S	point of the characteristic grid
T	temperature
t	time
U	expanded uncertainty
u	standard uncertainty
u_c	combined standard uncertainty
V	volume
V_{cav}	cavitation volume
v	velocity
v_n	velocity at point n
x	lift, distance, input estimate
y	estimate of the measurand

α	angle
Δt	time step
Δx	length step
$\Delta\mu'/\mu'_0$	relative change of fictive flow coefficient
$\Delta\Pi$	dimensionless pressure drop, Equation 35
$\Delta\Pi_b$	critical dimensionless pressure drop
δ	clearance, thickness
δ/d	relative roughness
η	dynamic viscosity
θ	characteristics grid mesh ratio
μ	flow coefficient
μ'	fictive flow coefficient
μ'_t	fictive flow coefficient for turbulent flow
μ'_{t0}	measured fictive flow coefficient for turbulent flow
μ'_0	measured fictive flow coefficient
ξ	amount of interpolation
ρ	density
ρ_v	vapor density
ρ_0	initial density

ψ'	fictive contraction coefficient
ψ'_0	measured fictive contraction coefficient

1 Introduction

Combustion in the cylinder of a diesel engine has a critical effect on the efficiency of the engine and the contamination caused by the engine. In a diesel engine, combustion is controlled by means of fuel injection. Therefore, it is of great importance that the injection process of the fuel is controlled in a proper manner.

The formation and combustion of the jet is presently calculated using three-dimensional computational fluid dynamics programs. As one of the initial values, the programs need information about the flow in the holes of the injection valve as a function of time.

The injection process in a diesel engine can be studied experimentally or by means of a model. In an experimental method, test equipment has to be constructed. Making changes in the test equipment is cumbersome and time-consuming. There is no experimental method, through which all the valuable information concerning injection process can be achieved.

With the aid of a prefabricated model, the injection process can be examined more easily, more rapidly, more economically, and more precisely than experimentally. It is less cumbersome to study different injection systems using a model than with an experimental method. A model for an injection system is particularly useful when combined with a combustion model. However, modeling an injection system is difficult.

Conventionally, the injection system of a diesel engine comprises a pump, a high-pressure pipe, and an injection valve. Because the fuel is compressible, pressure waves are formed in the system. The flow at a given point of the injection system changes as a function of time. This kind of flow is referred to as time-dependent. When the flow is not dependent on time, the flow is referred to as steady.

In a simple injection system model, an assumption is made that the fuel is incompressible. In this case, no pressure waves occur in the system. At each point of the high-pressure pipe, an equal pressure is prevailing at any given moment in time. Such a model can be used for dimensioning the components of the injection system [30, p. 14].

Alliévi [1] may have been the first to derive a motion and continuity equation for one-dimensional time-dependent pipe flow. He assumed the flow to be frictionless. Some minor terms are lacking from Alliévi's partial differential equations.

The injection process has been calculated using various graphical methods [5] [26] [27]. In these methods, the speed of the pressure pulse in the fluid is assumed to be constant. Conventionally, a fluid is assumed to flow without any friction. Graphical methods are appropriate for the basic dimensioning

of the injection system. The calculation methods intended for the computer have replaced the use of graphical methods.

General wave equations have commonly been used for calculating the time-dependent flow in a high-pressure pipe, for instance [34], [29], [10], and [32]. When Alliévi's equations are solved, they result in general wave equations. The solutions to Alliévi's equations are found on pages 3–5 of the appendix in Köhler's dissertation [29]. According to the solution, the pressure in an arbitrary cross-section of the pipe comprises of constant pressure and two pressure waves traveling in different directions. After the solution to Alliévi's equations is derived, the speed of the pressure pulse in the liquid is assumed to be constant. In the general wave equations, the viscous friction can be taken into account by means of correction.

In the method of general wave equations, the time taken by the pressure wave to progress from one end of the pipe to the other end is used as the time step. The pipe can be divided into parts so that the boundary conditions between the parts are solved.

The general wave equations do not correspond most accurately to the actual time-dependent pipe flow. The reasons are the simplifications in deriving Alliévi's equations.

The method of characteristics is highly appropriate for calculating time-dependent, one-dimensional pipe flow with the computer. The characteristic equations are derived from the motion and continuity equation comprising all terms. According to Wylie and Streeter [46, p. 14], the method of characteristics includes for instance the following advantages:

1. stability criteria are firmly established;
2. boundary conditions are easily programmed;
3. minor terms may be retained if desired;
4. very complex systems may be handled;
5. it has the best accuracy of any of the finite difference methods;
6. programs are easy to debug because a steady state satisfies all conditions, and
7. it is a detailed method which allows complete tabular results to be printed out.

The method of characteristics has been criticized in the following points:

1. the method utilizes a great deal of computational capacity [28] [32];

2. the cavitation examination of the method is awkward [28].

The computational capacity of modern computers is adequate for the use of the method of characteristics.

According to Kumari's [28] group, the cavitation examination of the method of characteristics involves difficulties. Therefore, they made experiments with the modeling of time-dependent pipe flow using Lax-Wendroff's method and the Leap-Frog method. The use of the two methods has not, however, become more general in calculating the pipe flows of the injection system. According to Chaudry [4, p. 45], the method of characteristics has proved to be superior to other methods in solving time-dependent pipe flow in a number of ways.

In the method of characteristics, the starting point for cavitation can be calculated precisely. In addition, the method offers a reasonably good view of the susceptibility of the system to cavitation [33].

In this present research work, the time-dependent, one-dimensional pipe flow is modeled using the method of characteristics.

The boundary conditions of the end to the injection pump and the injection valve are solved both in the method of general wave equations and in the method of characteristics utilizing the same principles. The containers are assumed to be concentrated volumes. In such a volume the pressure is of equal magnitude everywhere in the entire container at any given moment. The movements of the valves are solved with motion equations. The equations related to concentrated volume and motion are ordinary differential equations. These equations are solved numerically. Since the events at the end to the injection pump and the injection valve are rapid, solving these ordinary differential equations has occasionally been difficult.

The target of the present study is to develop a computer program with which the flow in the high-pressure pipe and the injection valve can be studied. The program is based on the mathematical model of the injection system introduced in Reference [24].

The cavitation is taken into account in the high-pressure pipe, in the concentrated volume, and in the holes of the injection valve. Detailed information is output about the flow. As our intention is to achieve good program portability, the code is written in a standardized programming language. The program is built from the subroutines representing the components of the injection system. From these subroutines, models describing general hydraulic systems can be assembled.

Adding the model of the injection pump to the program takes a lot of time. Therefore, the injection pump is omitted from the program. The

injection pump is replaced by the pressure measured at the pump end of the high-pressure pipe.

Particular attention is paid to the flow in the holes of the injection valve. One aim of the study is to examine the mass flow rate and the velocity of the fuel in the holes of the injection valve as a function of time.

Very few findings have been published concerning the injection systems of medium-speed diesel engines. Therefore, the injection system of a medium-speed Wärtsilä 324 TS diesel engine was selected as the target application of the program. The calculated results are compared to the values measured from the injection system of the test engine.

2 Injection system models

This chapter deals with models of the injection system of a diesel engine, in which the time-dependent one-dimensional pipe flow is solved using the method of characteristics. The models are dealt with in chronological order, starting from the earliest and ending with the most recent. The models are named according to the author or authors. If the calculated and the measured injection process are compared in the references, an example is given.

The speed of the pressure pulse refers to the velocity at which the pressure wave propagates in a liquid. The loss at a compression point of the system is described by the use of a fictive flow coefficient. The compression point in the present study is referred to as the flow passage. The holes in the injection valve are one example of the flow passages of the injection system. The fictive flow coefficient is defined in Equation 34 (p. 46).

2.1 Fomin's model

Sitkei's work [37, p. 32] presents a picture of the characteristic grid of a high-pressure pipe from the year 1959 used by Fomin [15]. Fomin most probably calculated the injection process of a medium-speed diesel engine with the aid of the method of characteristics. Unfortunately, no other information concerning Fomin's work is available.

2.2 El-Erian's model

The dissertation of El-Erian [7] is probably the first study in which the injection system of the diesel engine was modeled with the aid of a computer and the method of characteristics. In addition to the dissertation, the findings achieved by El-Erian are presented in References [45], [8], [9], and [46, pp. 325–329].

El-Erian studied measures to reduce after-injection. Figure 1 presents the injection system used by El-Erian. A relief valve has been added in the feed chamber of the pump. The injection pump is controlled by the plunger. The side of the plunger is provided with a longitudinal groove and a helical guide groove. When the piston rises so high that the helical guide groove combines the high-pressure side and the suction side of the pump via the longitudinal groove, the injection ends. Since the guide groove is helical, the effective stroke can be regulated by rotating the piston. The pump and the injection valve are connected by a high-pressure pipe. The delivery valve is a constant-volume valve.

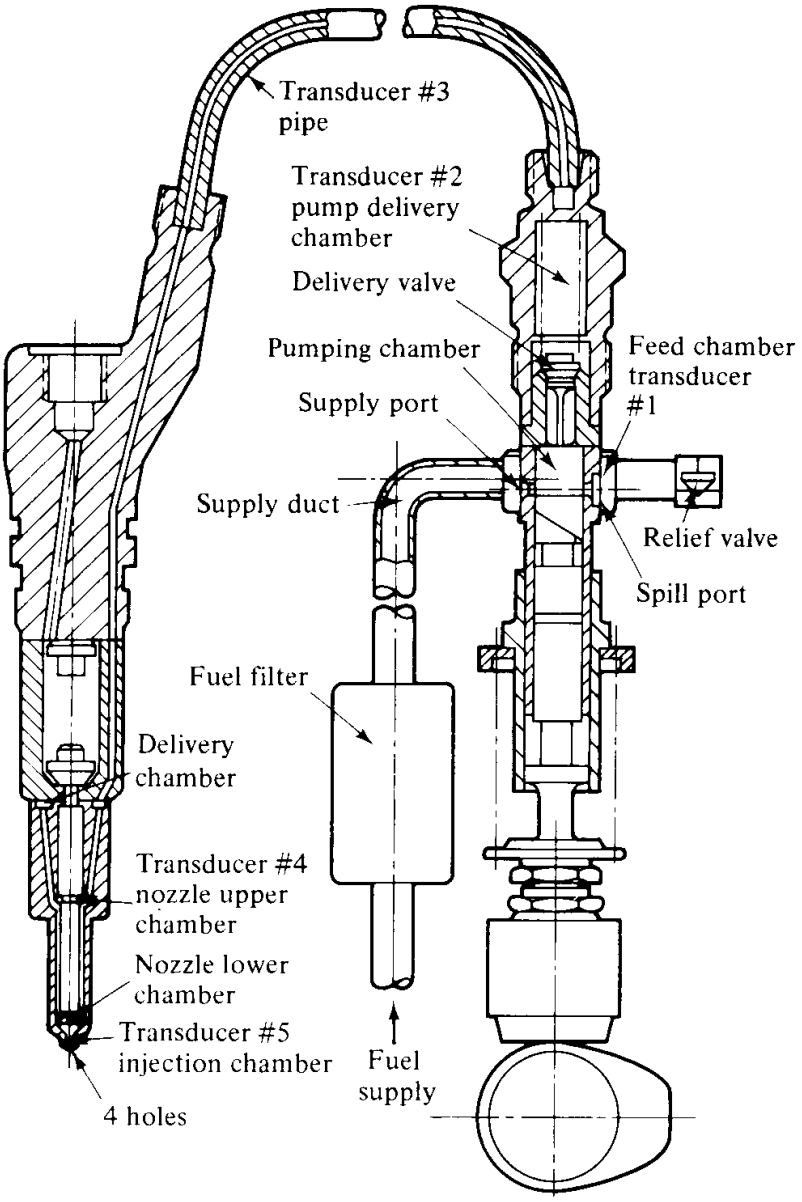

Figure 1. The injection system used by El-Erian and points of pressure measurement [46, p. 326].

In El-Erian's model, the properties of the fluid are dependent on the pressure. If at some point of the pipe section the pressure goes below the vapor pressure of the fluid, the vapor is assumed to be segregated from the fluid at that point. The pressure at this section is set to be of the magnitude of the vapor pressure of the fluid. The vapor cavitation is modeled with the aid of the equations describing the flow of the pipe and the continuity equation of the local mass. The description of the vapor cavitation in El-Erian's model is inadequate. When referring to the model, neither a local model continuity equation nor any other equations needed for calculating cavitation are given.

The ordinary differential equations of the end of the injection pump and the injection valve are solved using Hamming's predictor-corrector method [35]. First, El-Erian tried to solve the equations concerning the boundary conditions both with an iterative method and with Runge-Kutta's method. In both methods, a very short time-step had to be selected compared with the time-step required in the method of characteristics.

The supply port, the spill port, the gap between the delivery valve and the seat, the gap between the needle of the injection valve and the seat, and the holes in the injection valve form the flow passages in Figure 1. The assumption is made in the El-Erian model that the flow is not cavitating in the flow passage. According to Reference [45], the fictive flow coefficient may be dependent on the Reynolds number. However, in El-Erian's dissertation [7] this flow coefficient is constant.

When the base pressures of two injection processes, calculated in succession, are sufficiently close to one another, the calculation is ended.

In Figure 2, measured and calculated values are compared as a function of the cam angle of the injection pump. The positions of the transducers are shown in Figure 1. The lift of the delivery valve and of the needle and the pressure in the pumping chamber were not measured. The measured and calculated results are very similar. El-Erian's model is appropriate only for the injection system of the type studied.

2.3 Goyal's model

Goyal [18] created a universal model for the injection system. He modeled a variety of different injection systems.

In Goyal's model, the properties of a fluid are dependent on the pressure. The cavitation is modeled in a fashion similar to the El-Erian model (p. 17). In addition, the effect of vapor on the bulk modulus of elasticity and the density of the fluid are taken into account. When the entire element is filled with vapor, the pressure of the element may be lower than the vapor

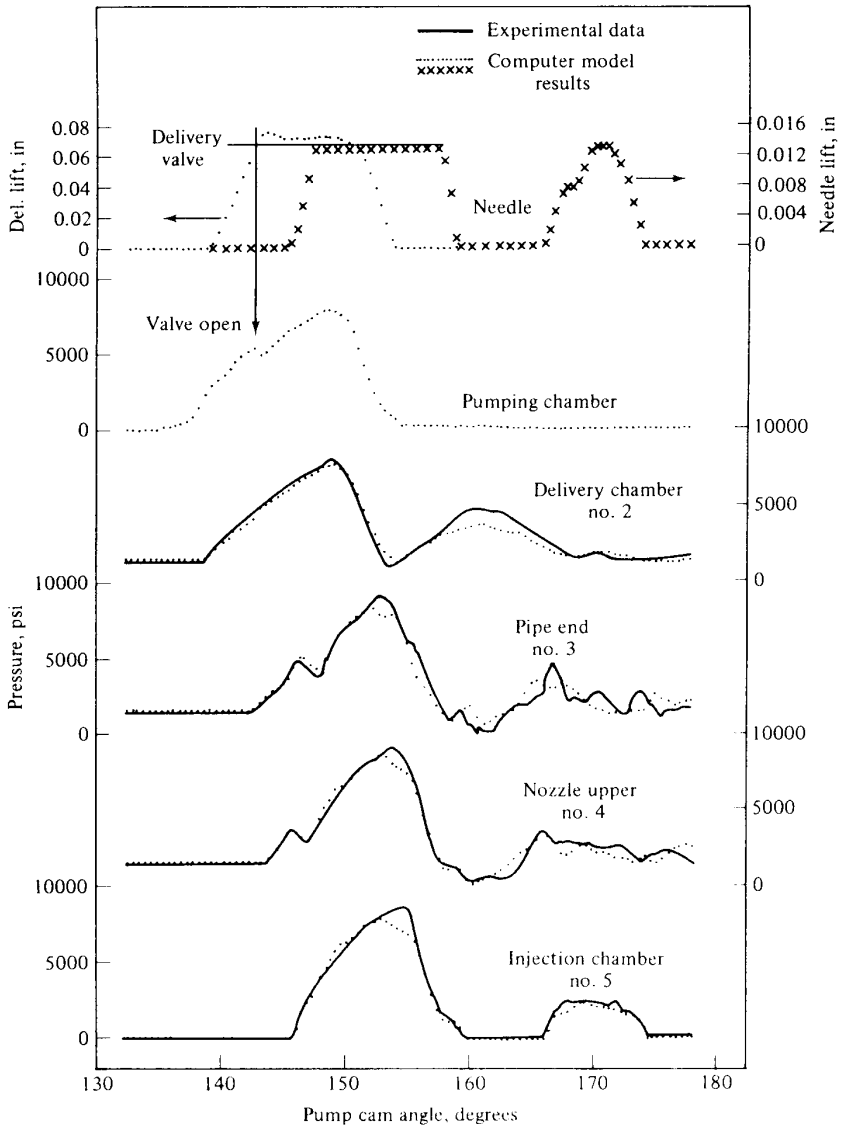

Figure 2. Comparison of the results calculated and measured using the El-Erian model as a function of cam angle [46, p. 328].

pressure of the liquid. Goyal does not introduce any equations for computing cavitation, and neither does he determine what is meant by an element.

In the model, the ordinary differential equations are solved with the Runge-Kutta method. The fictive flow coefficient of the flow passage is a function of the Reynolds number.

Goyal divided his model of the injection system into modules, in which the injection process is calculated in different parts of the system. When the injection system comprises of a plunger-regulated pump, a high-pressure pipe, and an injection valve, the program modules, the pump, the pipe and the injection valve illustrate the system. The modules, the pump, and the injection valve are divided further into lower-level modules.

According to Goyal, the results calculated with his model correspond well to the measured values. However, Goyal did not present any comparisons between the calculated and measured results.

The division of the Goyal model into modules is, in the programming sense, an acceptable solution. As these modules can be combined in a number of ways, a great number of different injection systems can be modeled.

2.4 The model of Kumar's group

A plunger-controlled pump, a high-pressure pipe and an injection valve form the model for the injection system of Kumar's group [28]. A constant-volume valve is used as the delivery valve.

In the model, the characteristics of the fuel are not constant. Kumar et al. do not, however, provide any explanation as to which factors the characteristics of the fuel are dependent on.

Kumar's group experimented with three different methods in order to solve the time-dependent pipe flow. In addition to the method of characteristics, the pipe flow is calculated with the Leap-Frog and the Lax-Wendroff method.

In the method of characteristics, the cavitation is modeled as concentrated vapor cavitation (Item 4.4.5, p. 43). When the pressure goes below the vapor pressure of the fluid at some point of the system, the cavitation starts. The pressure at a cavitating point is assumed to be of the magnitude of the vapor pressure of the fluid. The cavitation volume (Equation 29, p. 44) during a time-step is calculated at the point of cavitation. When the cavitation volume becomes zero, the cavitation ends.

Both in the Leap-Frog method and the Lax-Wendroff method the cavitation is assumed to be divided uniformly between the sections of the pipe.

Using the method of characteristics, the Leap-Frog method, and the Lax-Wendroff method, it is assumed that relatively good results must have been

obtained. No comparison of the results using the different methods with the measured values are given, however.

The boundary conditions are solved with the Runge-Kutta and the Newton-Raphson methods. The Newton-Raphson method is intended for solving non-linear equations. From the ordinary differential equations of the boundary conditions Kumar et al. formed equations of finite differences, and these were elaborated to become appropriate for the Newton-Raphson method. According to the authors, the Newton-Raphson method is more appropriate for solving the boundary conditions than the Runge-Kutta method. It is presumable that no variable time-step was included in the Runge-Kutta method which they applied.

It is not disclosed in the publication of Kumar's group how the fictive flow coefficients of the flow passages were defined.

2.5 Wannenwetsch and Egler's model

Wannenwetsch and Egler [43] created modeling programs of hydraulic transients, which are extremely easy to use. Bosch, a well-known manufacturer of injection systems, performs calculations concerning the injection process using Wannenwetsch and Egler's model.

The Wannenwetsch and Egler model divides the hydraulic system into twelve elements. In this model these elements are represented by figures which can be connected with each other at a computer terminal. By connecting these figures together at the computer terminal, it is possible to construct the correct hydraulic system with the Wannenwetsch and Egler model.

In the article by Wannenwetsch and Egler, it is not disclosed how the characteristics of the fuel and the cavitation are taken into account.

The ordinary differential equations of the boundary conditions are solved in two ways. In both methods, implicit equations of finite differences are formed from ordinary differential equations.

Wannenwetsch and Egler do not give any indication of the definition of the fictive flow coefficients of flow passages.

Wannenwetsch and Egler calculated the injection process for the injection system formed by a plunger-controlled pump, a high-pressure pipe, and an injection valve. For the delivery valve, a constant-volume valve was used. They compared the calculated and measured results. Figure 3 shows the measured and calculated pressures at both ends of the high-pressure pipe. The injector needle lift is also given. The calculated and measured values correspond well to each other.

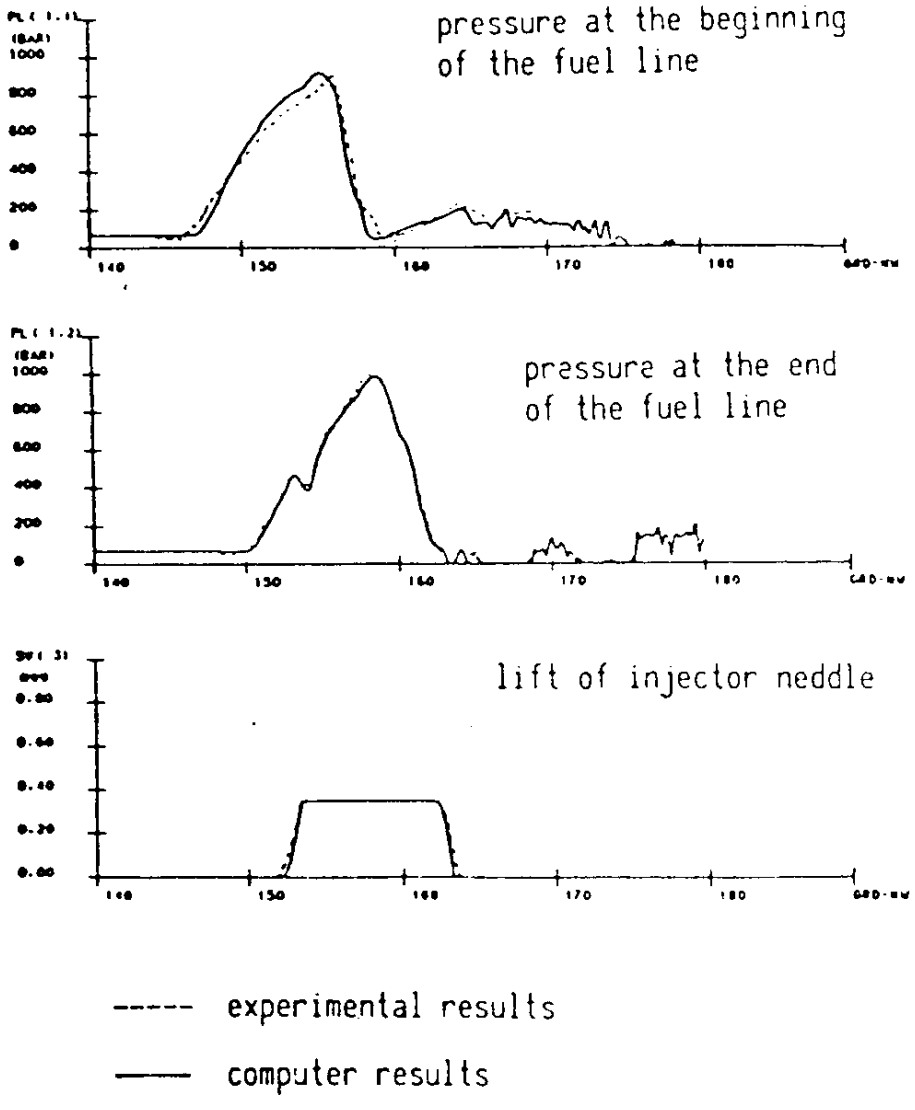

Figure 3. Measured and calculated pressures at both ends of the high-pressure pipe and injector needle lift as a function of cam angle. Calculations were based on the Wannenwetsch and Egler model. Plunger-controlled pump, constant-volume delivery valve, high-pressure pipe, and injection valve [43].

A novel element in the Wannenwetsch and Egler model is the program generator. It was most demanding to create it. No other models are known in which the boundary conditions have been solved using an implicit method. Since implicit methods are highly stable, ordinary differential equations are reliably solved with these methods.

2.6 Sobel and Lehrach's model

In modern injection systems, a very high injection pressure is used. Because the high pressure causes deformations in the high-pressure pipe and leakage in the injection valve, Sobel and Lehrach [38] wanted to find out the effect of the high pressure on the injection process. Their model was created as a universal model which is easy to use.

In the model of Sobel and Lehrach the properties of the fluid dependent on pressure. The cavitation is calculated according to the same principle as in the El-Erian model (p. 17). Sobel and Lehrach introduced an equation with which the volumetric portion of fluid and vapor can be calculated in a pipe segment during the cavitation. They derived this equation from the mass continuity equation. It is not disclosed in the article what a pipe segment means. The effect of the vapor portion on the properties of the fluid was also included.

In the model of Sobel and Lehrach, a change in the cross-section area of the pipe is calculated after each time step as a consequence of the effect of the local pressure. When a change in the cross-sectional area is known, a change in the volume of the element can be calculated. The pressure of the pipe is corrected on the basis of the volumetric change of the element.

The boundary conditions of the end to the injection pump and the injection valve are solved with the Runge-Kutta method.

The fictive flow coefficients of the flow passages are assumed to be constant in the Sobel and Lehrach model.

Sobel and Lehrach calculated the effects of distension with a simple model (Figure 4), where a volume is closed at one end by a piston. A tube wall outer-to-inner diameter ratio of 2 is usual in high-pressure pipes. In this case, when the difference is measured from the figure, at a pressure of 100 MPa the effect of deformation on the pressure is about 3 % and at a pressure of 50 MPa less than 1 %.

In Figure 5, the calculated injection pressures are compared with the measured ones. The injection system was composed of a plunger-controlled pump, a high-pressure pipe, and a delivery valve. For the delivery valve, a round snubber valve, provided with a little hole in the middle, was used. The

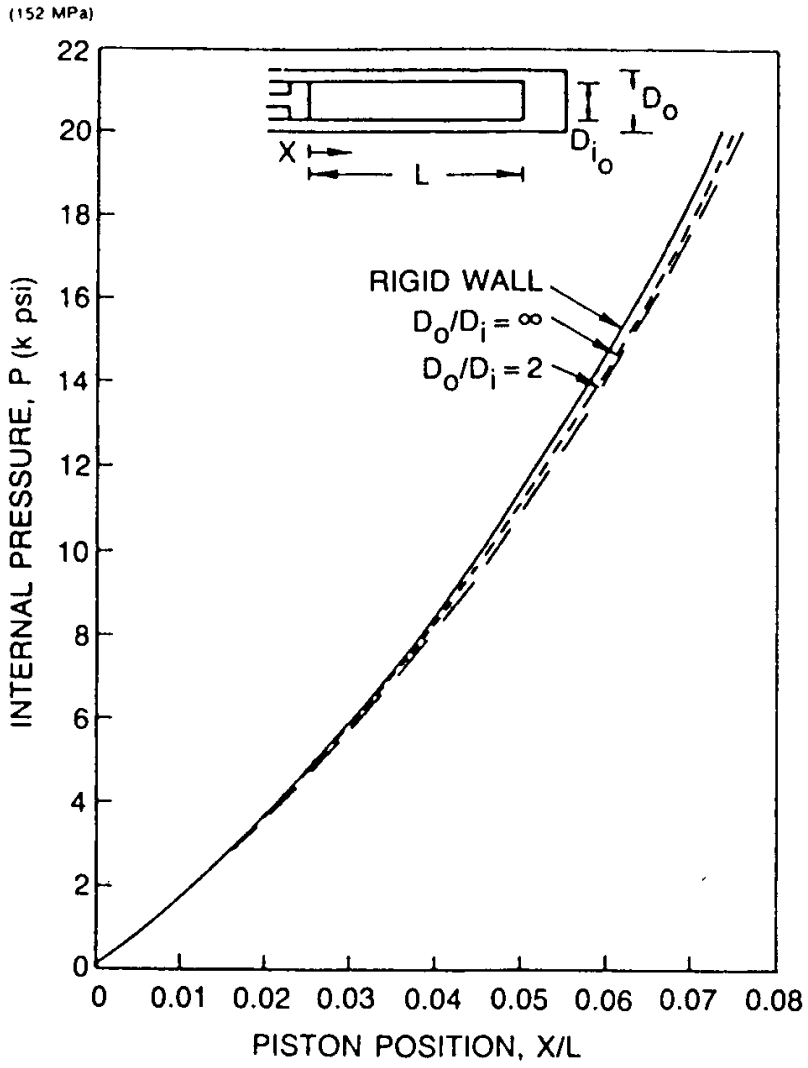

Figure 4. Distension effects [38].

valve choked the return flow from the high-pressure pipe. The measured and the calculated values correspond well to each other.

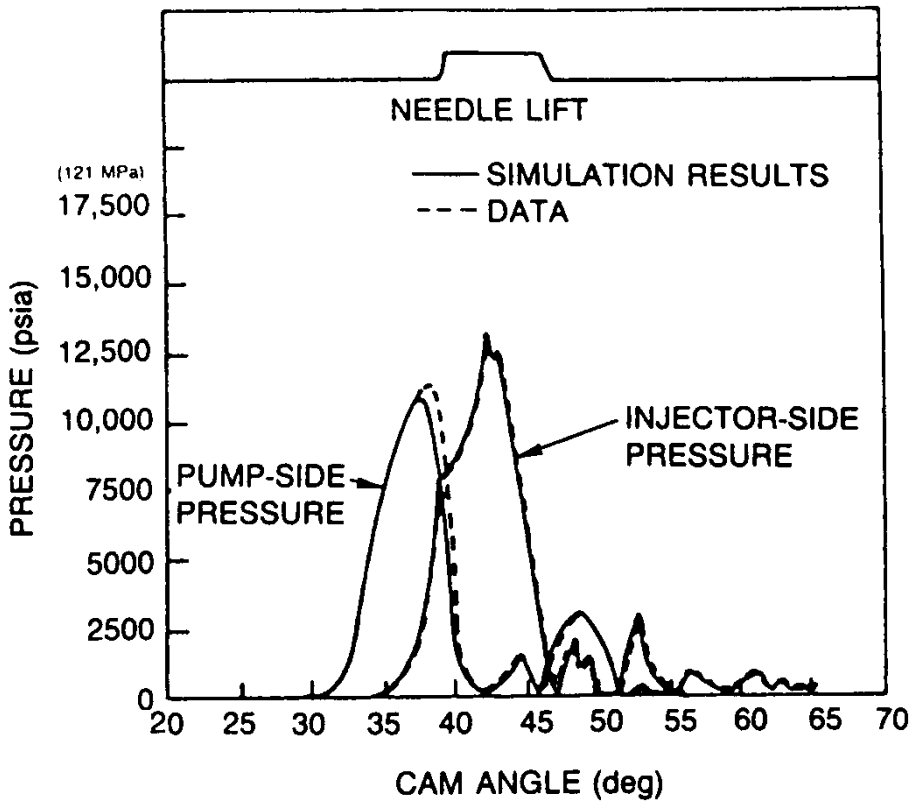

Figure 5. Comparison of the measured and calculated results as a function of cam angle; Sobel and Lehrach's model [38].

It is known that Sobel and Lehrach were the first to pay attention to the effect of the deformations of the high-pressure pipe on the injection process.

2.7 Ficarella and Laforgia's model

The objective of Ficarella and Laforgia [13] [14] was to ascertain what kind of effect the geometric and mechanical composition of the injection system exerts on the injection process.

In the model of Ficarella and Laforgia, the pump is plunger-controlled. The delivery valve can be a constant-volume, constant-pressure, or a choke valve. The pump and the injection valve are connected by a high-pressure pipe.

In Ficarella and Laforgia's model, the bulk modulus of elasticity and the density of the fluid depend on the pressure and the volume of air entrapped in the fluid. The air released from the fluid forms bubbles which dampen pressure waves. Thus, the released air exerts a powerful influence on the bulk modulus of elasticity and on the speed of the pressure pulse [46, pp. 9–10]. Obviously, Ficarella and Laforgia use the term air quantity to refer to the air released from the fluid.

Ficarella and Laforgia do not introduce an equation to illustrate the air released from the fluid. Therefore, it is possible to assume that in their model the fluid contains a constant proportion of released air.

Cavitation is modeled in two ways. In the first model, the pressure at the cavitating point is assumed to be of the magnitude of the vapor pressure of the fluid. Since the pressure wave cannot penetrate through the cavitating spot, the cavitating spot acts as a damper. For the cavitating spot a continuity equation is derived. An equation couple is formed from this equation and from the motion equation of the pipe flow, wherein the flow rate and the degree of evaporation are solved numerically.

In the other cavitation model, the pressure wave may propagate through a cavitating spot. The flow of two phases at a cavitating spot is modeled using a half-experimentally-derived equation for a one-phase flow.

When, in the Ficarella and Laforgia model, the fluid flows from the pipe into a container, no pressure losses take place. Instead, pressure loss arises when the fluid flows from the container into the pipe.

The ordinary differential equations of the boundary conditions are solved using Eulero's technique. It is assumed that this refers to one of Euler's methods.

The elasticity of the injection valve needle, the spring and the shim is modeled. Each of the parts is divided into elements which are connected by a spring and a dampening element. The equations of motion of the elements are solved using the predictor-corrector method.

As far as is known, Ficarella and Laforgia were the first to pay attention to cavitation in the flow passage in their model. In their view, the cavitation in the flow passage exerts an effect on the results.

Ficarella and Laforgia do not give any results, in which the effect of air is shown.

In Figure 6, the measured results are compared with the values calculated with Laforgia and Ficarella's model. The fluid was injected into the air pressure. The authors do not indicate in what injection system the results were obtained. The calculated and measured results correspond well to each other.

In Figure 7, the relative volumetric portion of the vapor in the pipe, cal-

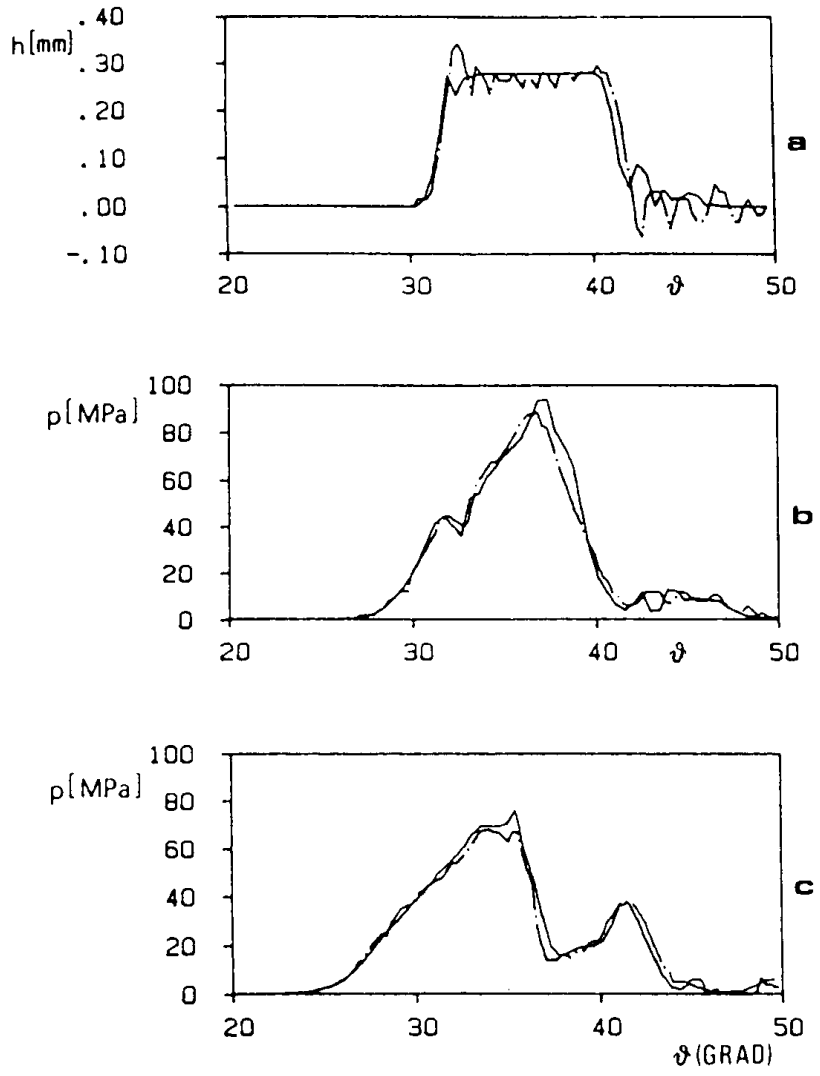

Figure 6. Comparison of the injection process, calculated with Ficarella and Laforgia's model, with the measured values as a function of cam angle. a) needle lift, b) pressure at the end to the injection valve, c) pressure at the end of the injection pump. Dashed line experimental, continuous line numerical [14].

culated using both cavitation models, is presented as a function of cam angle and the distance. The results calculated with the cavitation models differ significantly from each other. The portion of the vapor and the cavitation time were not measured.

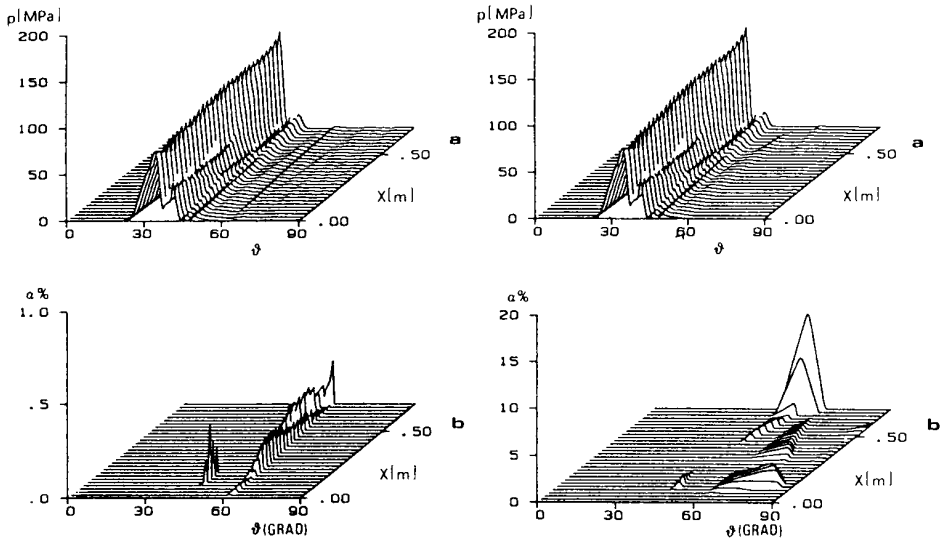

Figure 7. Pressure and the relative volumetric proportion of the vapor in the pipe as a function of cam angle and distance. In the figure on the left, the pressure wave is able to travel through the cavitating point, in the figure on the right: the speed of the pressure pulse in the cavitation point is zero [14].

2.8 Fairbrother's model

Fairbrother [11] also aimed to model the injection system. The results calculated with the model are compared with the values measured in the test bench.

The injection system modeled by Fairbrother comprises of a Bosch VE distributor pump, a high-pressure pipe, and a Stanadyne injection valve. A constant-volume delivery valve is used in the pump. The nozzle of the injection valve is provided with a number of holes.

In the first model, Fairbrother merely calculated the flow in the injection valve. The pressure measured at the high-pressure pipe of the injection

valve end is given as the initial value in this model. The other model was constructed from a pump, a high-pressure pipe, and an injection valve. In the latter model, the pressure measured in the upper chamber of the injection pump piston is used as the initial value.

Calibration fluid at over 40 °C was used in the tests. The bulk modulus of elasticity of the fluid as a function of pressure is calculated with an equation by Dow and Fink [6]. The density of the fluid is dependent on the pressure according to the quadratic polynomial. The effect of the separated vapor on the bulk modulus of elasticity of the fluid and on the density is calculated. The vapor pressure of the fluid is low, and due to this the pressure is assumed to be zero.

The flow of the pipe is solved with the method of characteristics. Fairbrother derived the characteristic equations from a simplified equation of motion and continuity. The pipe is divided into portions of equal length. As every portion is assumed to be a concentrated volume, the pressure in one part of the pipe is the same. The pressure of a subsequent point in time at the junction spots of the parts is solved using the method of characteristics. The pressure of the opposite ends of one part calculated in this manner is not necessarily equal in magnitude. Nothing was mentioned in the study as to how the pressure of the opposite ends of the part is distributed relative to the pressure of the entire part. When a part of the pipe is assumed to be a concentrated volume, according to Fairbrother, no significant error is caused in the calculated results.

The Darcy-Weisbach friction factor of the pipe flow is calculated with three equations. The first equation is used for the laminar flow and the second for a Reynolds number up to 4000. At Reynolds numbers higher than that, the friction factor is calculated with Blasius' equation. In all equations, the friction factor is merely a function of the Reynolds number.

If the pressure in a part of the pipe is below the vapor pressure of the fluid, the flow starts to cavitate. Therefore, the pressure is set at the magnitude of the vapor pressure of the fluid, and the volume of the separated vapor is calculated. Once the volume of the vapor of the cavitating part is zero, the cavitation ends. The way of calculating the cavitation occasionally resulted in incorrect high-frequency pressure oscillations in the system.

In the other cavitation model, the pressure in the cavitating pipe part is of the order of the vapor pressure of the fluid. No fluid flows through this part as in the first cavitation model. In the results calculated with the latter method, no incorrect pressure oscillations occurred, but the accuracy of the method was not specified.

Fairbrother assumes the containers to be concentrated volumes. No cavitation is allowed to occur in the containers.

The collision of the injection valve needle with the upper limiter and the seat is modeled. The collision is illustrated by a differential equation for which a solution has been sought. The elasticity of both the needle and the base is accounted for in the differential equation. The solution includes one coefficient only, the value of which has to be determined experimentally.

The fictive flow coefficient of the gap between the needle and the seat of the injection valve, and of the holes of the injection valve is dependent merely on the needle lift.

The ordinary differential equations at the end to the injection pump and the injection valve are solved using the Runge-Kutta method.

Fairbrother created his program in the Windows environment. The program is composed of modules describing the parts of the injection system. The program was compiled with Microsoft QuickC compiler, with which, according to Fairbrother, a good user interface can be obtained.

The calculated and the measured results are compared at three different rotational frequencies of the injection pump. At the lowest rotational frequency, the fuel rack is resting at the lower limiter, and, on the highest rotational frequency, at the upper limiter. At the middle rotational frequency, the rack is located halfway between the lower and the upper limiters. Below, the results obtained with the model comprising a pump, a high-pressure pipe and an injection valve are examined.

Compared with the measured injection quantity, the quantity per shot is 34 % less at the lowest rack setting, 20 % less at the middle setting, and 17 % less at the extreme setting.

In Figure 8, the calculated and the measured results are compared when the rack is at the upper setting and the rotational frequency of the pump is 2000 r/min.

The calculated and the measured pressure valve lifts and the pressure in the high-pressure pipe at the injection pump end differ from each other to a relatively high degree. The pressure calculated at the end of the injection valve is slightly lower during the injection than the measured pressure.

The calculated and the measured needle lifts correspond to each other relatively well. When the needle collides with the seat, the needle and the base give up about 0.06 mm, as shown in the figure. This is approximately 20 % of the greatest needle lift. The needle and the lift limiter give up very little when the needle collides with its upper limiter.

The transient volume flow rate of the fluid through the nozzle holes was measured with a Bosch pipe. According to Fairbrother, the volume flow rate measured with the Bosch pipe was not completely reliable.

Fairbrother's model has been tested thoroughly with one injection system. As far as is currently known, Fairbrother was the first to use the motion of

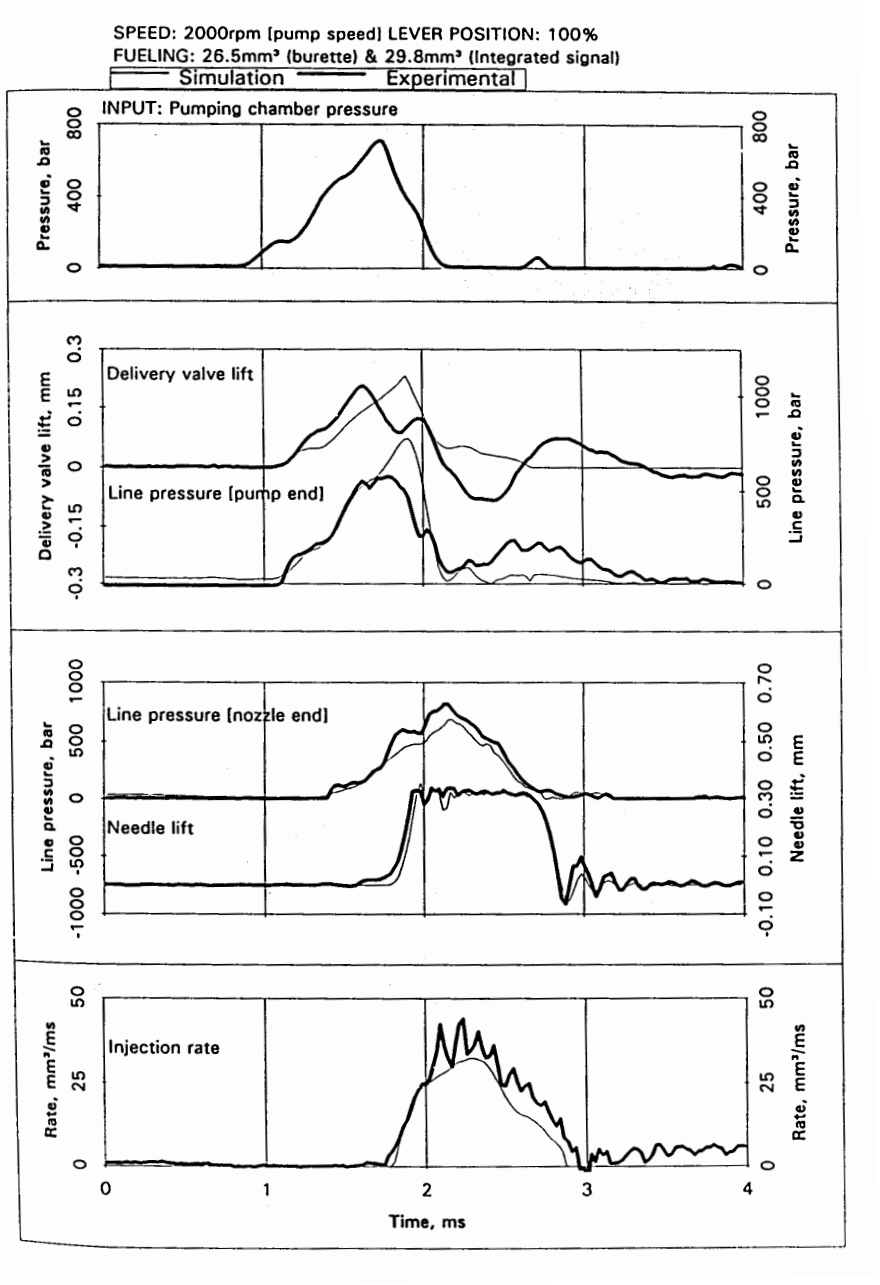

Figure 8. Comparison of the measured and calculated results; calculations made with Fairbrother's model, rack setting 100 %, pump speed 2000 r/min [11, p. 145].

the delivery valve for the assessment of the quality of the calculated results. Fairbrother's model is not, however, accurate in all respects. Particularly, the difference between the measured and calculated fuel injection quantity per shot is great.

The speed of the pressure pulse is not constant. Therefore, the points of the characteristic grid of a preceding point of time have to be interpolated (p. 40). When the pressure is assumed to be the same in one part of the pipe, the interpolation becomes easier. On the other hand, Fairbrother did not deal with interpolation at all. In addition, Fairborther's assumption of the pressure being equal in a pipe part aids the understanding the effect of vapor on the properties of the fluid.

Fairbrother did not separate the actual program and the user interface. Therefore, it is obviously difficult to transfer the program to any environment other than Windows.

3 Model is4 for the injection system

The injection pump of the test engine is plunger-controlled. For the delivery valve of the pump, a constant-volume valve is used. A high-pressure pipe connects the pump and the injection valve.

Figure 9 presents the injection valve of the test engine. After the junction of the high-pressure pipe and the injection valve, the fluid is directed into two bores which are continued to the junction of the body and the tip of the injection valve. At that point, four bores lead to the pressure container. These four bores lie symmetrically, if viewed from above. When the needle opens, the fluid flows via a gap between the needle and the seat to the sac container. From the sac container the fluid is injected through eight holes into the cylinder. Some of the fluid flows from the pressure container via the gap between the needle and the control into a leakage container.

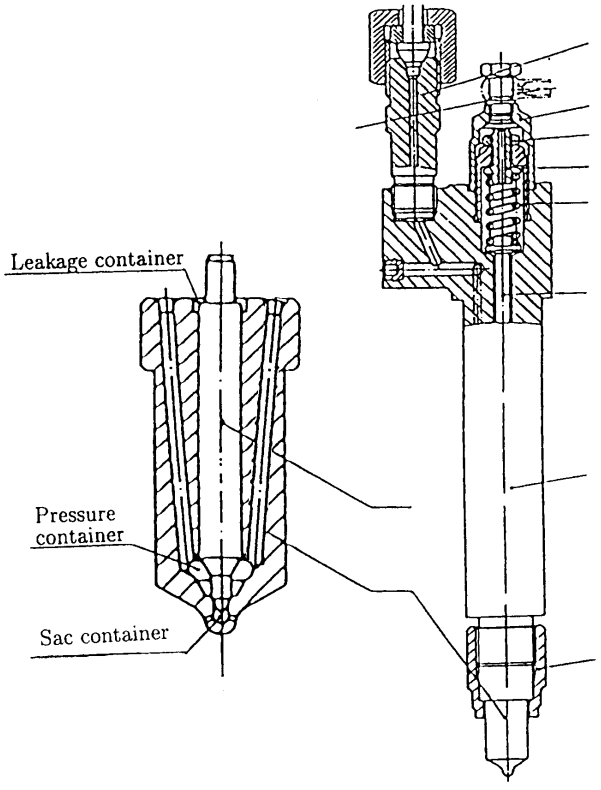

Figure 9. Injection valve of Wärtsilä 324 TS engine.

The model is composed of elementary units, the figure markings and

symbols of which are depicted in Figure 10. In addition, the fluid is one of the elementary units of the model, although it does not have a figure sign of its own. The symbol for fluid is *dl*.

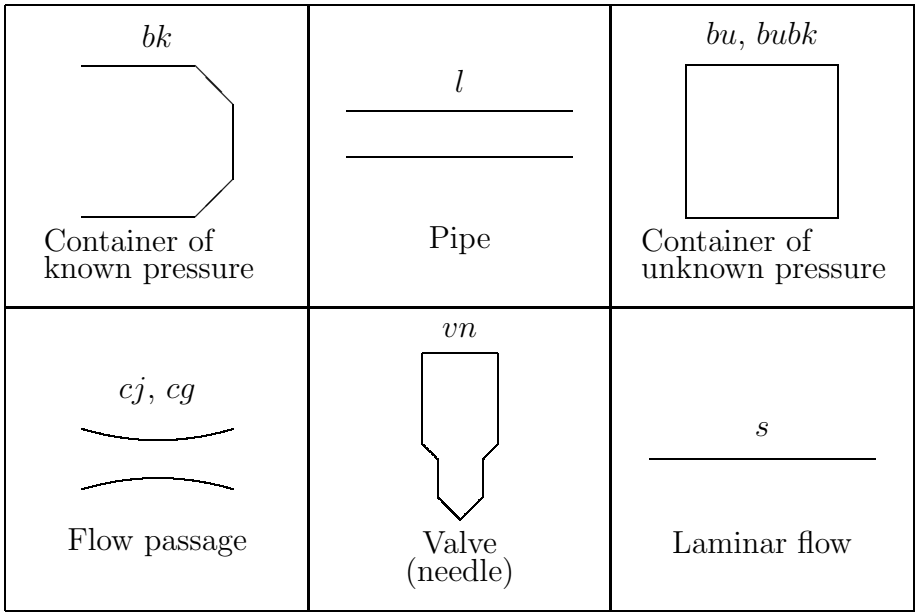

Figure 10. Elementary units of the mathematical model.

The pressure in the containers *bu* and *bubk* of unknown pressures is solved using the same equations. The flow passage *cj* is determined as valve-controlled and the passage *cg* as a constant-aperture passage. The needle is classified as a valve.

Figure 11 presents a model for an injection system composed of elementary units. The model is dimensioned according to the injection system of the test engine.

The injection pump has been replaced by Container bk_1 of known pressure. The pressure measured at the pump end of the high-pressure pipe as a function of time is fed from this container to the system. Pipe l_1 describes the high-pressure pipe.

The bores of the frame and the tip of the injection valve, the junctions of the ports, and the pressure container are modeled with Container bu_1 of unknown pressure. The volume of the container is the sum of the bores, the junctions, and the volume of the pressure container.

Flow passage cj_1 controlled by the valve illustrates the flow passage between the needle and the seat of the injection valve. A hypothesis that the

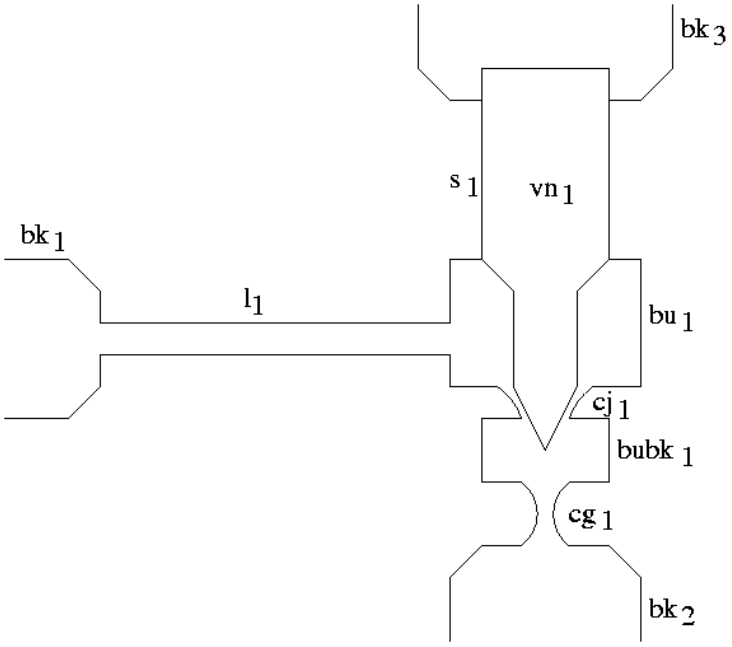

Figure 11. Model is4 for the injection system.

fluid can flow in the passage merely from Container bu_1 into Container $bubk_1$ is presented in the model. This hypothesis probably corresponds to the behavior of the actual flow.

The sac container is modeled using Container $bubk_1$ of unknown pressure. When the needle of the injection valve is closed, the pressure in Container $bubk_1$ is assumed to be equal to the pressure in Container bk_2.

Flow passage cg_1 with constant aperture illustrates the holes of the injection valve. During the injection, the pressure of Container $bubk_1$ is assumed to be higher than or equal to the pressure in Container bk_2. Therefore, a hypothesis presented in the model is that the fluid is able to flow in Passage cg_1 only from Container $bubk_1$ into Container bk_2.

The pressure in Container bk_2 of known pressure is the same as the pressure measured in the cylinder of the test engine as a function of time.

The needle of the injection valve is modeled by Needle vn_1. The leakage between the needle and the control is calculated as Laminar flow s_1. Container bk_3 of known pressure illustrates the leakage container.

4 Mathematical model

The mathematical model of the injection system is composed of elementary units. Since there are a variety of ways in which elementary units can be combined, models of various injection and hydraulic systems can be built. New elementary units may also be added to the model.

The mathematical model of the injection system is dealt with in detail in Reference [24, pp. 29–87].

4.1 Hypotheses

The following aspects are hypothesized in the model for an injection system:

1. the properties of the fluid are functions of pressure and temperature;
2. the temperature of the fluid is constant in one elementary unit. However, the temperature of the fluid need not be the same in different elementary units;
3. the properties of the fluid are not affected by the vapor and gas bubbles;
4. the cross-section of the pipe is circular;
5. the pipe is in a horizontal position;
6. the pipe is assumed to be rigid;
7. the pipe is straight;
8. the fluid flows one-dimensionally in the pipe.
9. in a time-dependent pipe flow, the fluid friction is equal to the steady flow;
10. the fluid flows from the container into the pipe and from the pipe into the container without losses;
11. the container is rigid;
12. in the time-dependent flow, the fictive flow coefficient of the flow passage is equal to the steady flow, and
13. the valve stem, the seat, and the upper limiter of the valve are stiff.

4.2 Fluid

The fluid is assumed to be homogeneous. The following properties of the fluid are necessary in the model as a function of pressure and temperature: speed of pressure pulse, density, bulk modulus of elasticity, cinematic viscosity, and vapor density. In addition, the vapor pressure of the fluid as a function of temperature must be known.

When the temperature of the fluid is constant, the speed of the pressure pulse in diesel oil is calculated in this study with Equation [10, p. 35] [41] [24, p. 32]

$$c = a_{c0} + a_{c1}p + a_{c2}p^2, \tag{1}$$

where

c	speed of pressure pulse in diesel oil
$a_{c0} \dots a_{c2}$	polynomial coefficients of the speed of pressure pulse
p	pressure.

At a constant temperature, the density of diesel oil as a function of pressure can be calculated by Equation [21]

$$\rho = \rho_0 + \int_{p_0}^{p} \frac{1}{c^2} dp, \tag{2}$$

where

ρ	density
ρ_0	density of diesel oil at initial pressure
p_0	initial pressure.

For diesel oil, quadratic polynomial [24, p. 34] is applicable for the solution points of Equation 2

$$\rho = a_{\rho 0} + a_{\rho 1}p + a_{\rho 2}p^2, \tag{3}$$

where the symbols $a_{\rho 0} \dots a_{\rho 2}$ refer to polynomial coefficients of diesel oil density. Since the calculation of the value of the polynomial is reliable and rapid, the density of diesel oil in this present research work is calculated using Polynomial 3.

The bulk modulus of elasticity K of the fluid is solved using the expression

$$K = \rho c^2. \tag{4}$$

If the vapor of the fluid is assumed to behave like an ideal gas, the following expression can be achieved for vapor density:

$$\rho_v = \frac{M}{RT}\, p, \tag{5}$$

where

ρ_v	density of fluid vapor
M	molar mass of vapor
R	molar gas constant
T	temperature.

4.3 Container of known pressure

In the container of known pressure, the pressure is known as a function of time.

4.4 Pipe

One-dimensional, time-dependent pipe flow is solved by means of the application of the method of characteristics. The application is determined as a method of specified time intervals.

In the method of specified time intervals, the pipe is divided into parts of equal length. The cross-sections of the pipe restricting these parts are called nodes. The nodes at each end of the pipe are called edges. The nodes which are not edges are called inner nodes.

4.4.1 Characteristic equations

Wylie and Streeter [46, pp. 17–19] have derived an equation of motion through examination of the forces affecting a fluid element. For the equation of motion, they wrote as follows:

$$\frac{1}{\rho}\frac{\partial p}{\partial x} + v\frac{\partial v}{\partial x} + \frac{\partial v}{\partial t} + g\sin\alpha + \frac{fv|v|}{2d} = 0, \tag{6}$$

where

ρ	fluid density
p	pressure
x	distance along pipe axis
v	fluid velocity
t	time
g	acceleration due to gravity
α	pipe angle to horizontal plane
f	Darcy-Weisbach friction factor (Item 4.4.3)
d	pipe inside diameter.

The force caused by the mass of the fluid element is considerably smaller than the other forces affecting the element. Therefore, it can be assumed that the pipe is horizontal (Section 4.1) and the angle $\alpha = 0$.

The continuity equation can be written as [46, p. 22]

$$\frac{\dot{p}}{\rho} + c^2 \frac{\partial v}{\partial x} = 0, \tag{7}$$

where c is the speed of pressure pulse in fluid. Marking $\dot{p}$ refers to the total derivative of pressure in relation to time.

When the method of characteristics [46, pp. 31–33] [24, pp. 40–43] is applied to Equations 6 and 7, four ordinary differential equations are developed from two partial differential equations

$$\frac{1}{c\rho}\frac{dp}{dt} + \frac{dv}{dt} + \frac{fv|v|}{2d} = 0, \tag{8}$$

if

$$\frac{dx}{dt} = v + c \tag{9}$$

and

$$-\frac{1}{c\rho}\frac{dp}{dt} + \frac{dv}{dt} + \frac{fv|v|}{2d} = 0, \tag{10}$$

if

$$\frac{dx}{dt} = v - c. \tag{11}$$

Equations 8 and 10 are called positive and negative compatibility equations. Equations 9 and 11 are characteristics. A compatibility equation is valid only along its characteristics.

4.4.2 Finite-difference equations

Figure 12 presents a characteristic grid. A pipe has been divided into parts of Δx length. On the vertical axis, the time-step is Δt. The characteristics are assumed to be straight lines in the plane formed by the x- and t-axes. The positive characteristic travels from point R to point P, and the negative characteristic from point S to point P. The pressure and the volume flow rate at points A, C and B of the characteristic grid are assumed to be known.

The following finite-difference equations are deduced from characteristic equations [46, pp. 33–35] [24, pp. 43–46]

$$A(p_P - p_R) + \rho_R c_R (q_{vP} - q_{vR}) + \frac{f_R \rho_R c_R}{2dA} q_{vR}|q_{vR}|\Delta t = 0, \tag{12}$$

if

$$x_P - x_R = (v_R + c_R)\Delta t \tag{13}$$

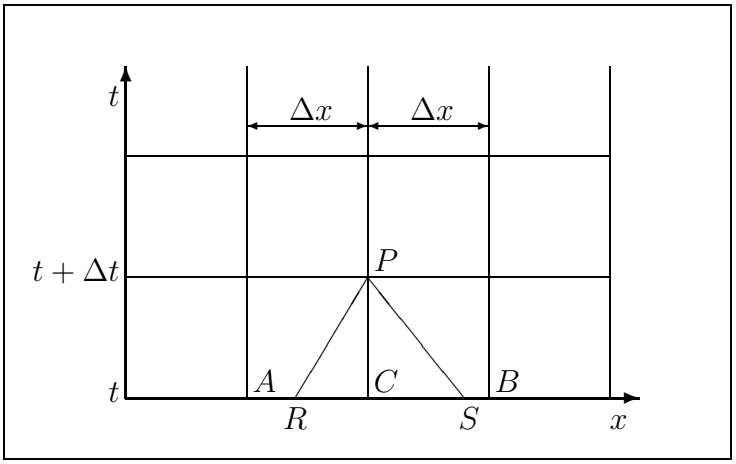

Figure 12. Characteristic grid.

and

$$A(p_P - p_S) - \rho_S c_S(q_{vP} - q_{vS}) - \frac{f_S \rho_S c_S}{2dA} q_{vS}|q_{vS}|\Delta t = 0, \tag{14}$$

if

$$x_P - x_S = (v_S - c_S)\Delta t, \tag{15}$$

where

A	pipe inside cross-section area
p	pressure
ρ	density
c	speed of pressure pulse
q_v	volume flow rate
f	Darcy-Weisbach friction factor.

The subscripts R, P, and S refer to the value of the quantity at the point of the characteristic grid indicated by the subscript.

The pressure and the volume flow rate are interpolated at points R and S of the characteristic grid. Interpolation is dealt with in Section 4.4.4.

The pressure and the volume flow rate at point P in the grid are solved through Equations 12 and 14. The values of pressure and volume flow rate in all the inner nodes of the pipe at the point of time $t + \Delta t$ are calculated in the manner described above. At the upstream end of the pipe, negative compatibility Equation 14 is solved at the same time as the equations of the boundary condition. At the downstream end, positive compatibility Equation 12 is solved simultaneously with the boundary condition.

4.4.3 Darcy-Weisbach friction factor

The Darcy-Weisbach friction factor f of laminar pipe flow is calculated using the well-known equation

$$f = \frac{64}{Re}, \tag{16}$$

where Re refers to the Reynolds number. The equation of laminar pipe flow is valid both for smooth and rough pipes.

When the Reynolds number exceeds a value of 2300, the flow in the pipe turns from a laminar into a turbulent one [16, p. 40]. In the known injection system models, the Darcy-Weisbach friction factor of turbulent pipe flow is usually either solved using Blasius' equation [16, p. 364], or nothing is mentioned regarding how the friction factor was determined. In Blasius' equation, the friction factor is merely a function of the Reynolds number. The equation is still valid when the Reynolds number is smaller than or equal to 10000 [16, p. 364].

In Colebrook's equation, the roughness of the inside surface of the pipe is taken into account. Therefore, the friction factor is mostly solved in the hydraulics using Colebrook's equation [16, p. 364]

$$\frac{1}{\sqrt{f}} = -2{,}0 \lg\left(\frac{\delta/d}{3{,}7} + \frac{2{,}51}{Re\sqrt{f}}\right), \tag{17}$$

where δ/d refers to the relative roughness of the inside surface of the pipe. Moody's drawing was made with the aid of Colebrook's equation [44, pp. 116–117]. On the basis of the drawing, the equation is valid at up to a Reynolds number of at least 10^8. In the model, the friction factor is iterated from Colebrook's equation. The first value of the iteration is estimated with Equation [16, p. 364] [39]

$$f = 0.25\left[\lg\left(\frac{\delta/d}{3.7} + \frac{5.74}{Re^{0.9}}\right)\right]^{-2}. \tag{18}$$

4.4.4 Interpolation

The markings of interpolation are shown in Figure 13. Since the pressure pulse speed is not constant, the values of pressure and volume flow rate have to be interpolated at points R and S of the characteristic grid. The values of the pressure and the volume flow rate are known at points A, C and B of the grid.

For the grid mesh ratio θ, the following is determined

$$\theta = \frac{\Delta t}{\Delta x}, \tag{19}$$

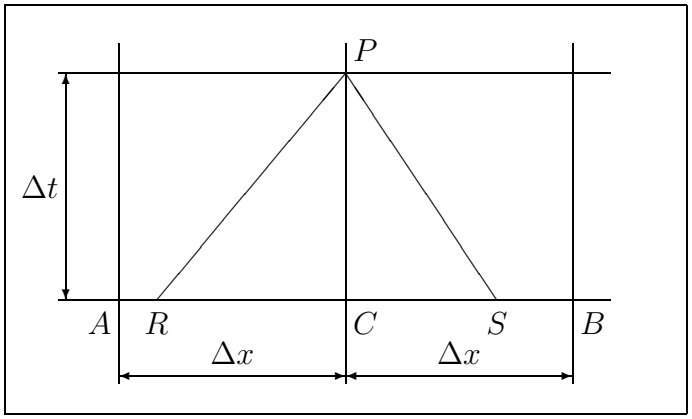

Figure 13. Markings of interpolation.

where Δt is a time step and Δx is a length step.

In linear interpolation [46, pp. 55–59] [24, pp. 48–51], we get the following equations

$$p_R = p_C - (\frac{q_{vR}\,\theta}{A} + \theta\, c_R)(p_C - p_A) \tag{20}$$

$$q_{vR} = \frac{q_{vCin} - \theta\, c_R(q_{vCin} - q_{vAout})}{1 + \frac{\theta}{A}(q_{vCin} - q_{vAout})} \tag{21}$$

$$p_S = p_C + (\frac{q_{vS}\,\theta}{A} - \theta\, c_R)(p_C - p_B) \tag{22}$$

$$q_{vS} = \frac{q_{vCout} - \theta\, c_S(q_{vCout} - q_{vBin})}{1 - \frac{\theta}{A}(q_{vCout} - q_{vBin})}, \tag{23}$$

where

p	pressure
q_v	volume flow rate
c	speed of pressure pulse
q_{vin}	volume flow rate into grid node
q_{vout}	volume flow rate out of grid node.

Subscripts A, R, C, S, and B refer to the value of a quantity at the corresponding point of the grid. Because of the cavity examination (4.4.5), the volume flow rates into a pipe node and out of a pipe node are separated.

In the model it is assumed that the temperature in an elementary unit is identical. Hence, the pressure pulse speed c is a function of pressure p. When Expression 1 of pressure wave speed is embedded in the interpolation equations 20–23, the computational precision of the computer is not sufficient

to reliably solve the interpolation points. In order to solve this problem, the hypothesis is made in this study that the speed of the pressure wave between two nodes is a linear function of the pressure.

In the method, the actual speed of a pressure pulse is first calculated in two consecutive nodes. Since the speed of the pressure wave is assumed to be a linear function of the pressure between two consecutive nodes, the coefficients a_0 and a_1 of equation

$$c = a_0 + a_1 p \tag{24}$$

can be solved. Finally, the pressure and the volume flow rate are calculated at the point of interpolation.

The calculation of the pressure and the volume flow rate is examined at point R of the grid. Equation 21 for volume flow rate and Expression 24 for pressure pulse speed are embedded in Equation 20. When the equation thus obtained is solved in relation to the pressure at point R, the following is received [25, p. 15]:

$$p_R = \frac{p_C A + p_C \theta \left(q_{vCin} - q_{vAout}\right) - q_{vCin} \theta \left(p_C - p_A\right) - a_0 A \, \theta \left(p_C - p_A\right)}{a_1 A \, \theta \left(p_C - p_A\right) + A + \theta \left(q_{vCin} - q_{vAout}\right)}. \tag{25}$$

Then, the speed of the pressure wave at point R is calculated using expression 24. Finally, the volume flow rate at point R is solved using Equation 21.

In Equations 22, 23 and 24, the pressure is solved at point S of the grid, resulting in [25, p. 15]:

$$p_S = \frac{p_C A - p_C \theta \left(q_{vCout} - q_{vBin}\right) + q_{vCout} \theta \left(p_C - p_B\right) - a_0 A \, \theta \left(p_C - p_B\right)}{a_1 A \, \theta \left(p_C - p_B\right) + A - \theta (q_{vCout} - q_{vBin})}. \tag{26}$$

In Equation 24, the speed of the pressure pulse at point S is calculated, and in Equation 23, the volume flow rate at point S.

The ratio of the distance between the interpolated point and point C to the length step is called the amount of interpolation. As according to Equation 13, $x_P - x_R = (q_{vR}/A + c_R)\Delta t$, and on the other hand $x_C = x_P$, the amount ξ of interpolation at point R will be

$$\xi_R = \frac{x_C - x_R}{\Delta x} = \frac{x_P - x_R}{\Delta x} = \frac{(q_{vR}/A + c_R)\Delta t}{\Delta x}. \tag{27}$$

With the aid of Equation 15, the amount of interpolation at point S will be

$$\xi_S = \frac{x_S - x_C}{\Delta x} = \frac{x_S - x_P}{\Delta x} = \frac{(c_S - q_{vS}/A)\Delta t}{\Delta x}. \tag{28}$$

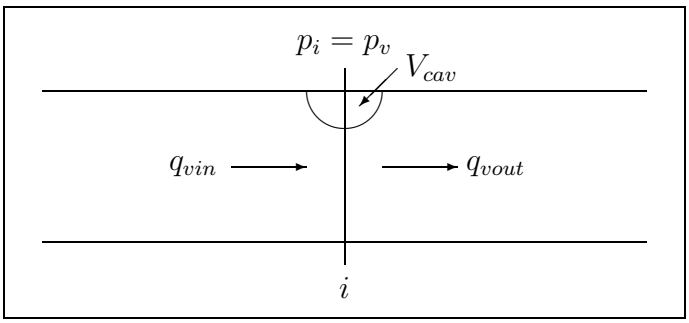

Figure 14. Concentrated vapor cavitation in a pipe node i.

The interpolation is required to meet Courant's condition [46, p. 58]: the distance of points R and S from point C must be less than or equal to the longitudinal step. Otherwise, the method of specified time intervals would be unstable.

Interpolation may result in an artificial numerical attenuation in the system [46, p. 58]. To keep this attenuation small, the amount of interpolation is required to be as small as possible, i.e., as close to one as possible. Using an appropriate time step, the maximum amount of interpolation is one in one or more nodes, and below one in the rest of the nodes.

4.4.5 Concentrated vapor cavitation

Cavitation refers to bubble formation and the action of bubbles in a fluid [47, p. 4]. The bubbles may contain vapor, gas or both gas and vapor. The vapor has been separated from the fluid. When a fluid contains gas, bubbles may be formed from the gas. Cavitation is a highly complex phenomenon, and no universal model has been successfully created for it. Cavitation is dealt with in this study at a macroscopic level, that is, no individual bubbles are examined.

In the present model, concentrated vapor cavitation (Figure 14) can be formed merely in an inner node of a pipe [46, pp. 137–139]. If the pressure in a node is below the vapor pressure of the fluid, concentrated vapor cavitation starts. The pressure in a node is set to be of the magnitude of the vapor pressure of the fluid and the cavitation volume is calculated. Concentrated vapor cavitation forms an internal boundary condition in the pipe. When the cavitation volume in the node becomes zero, the vapor cavitation ends.

The cavitation volume is calculated as a mean cavitation volume during

a time step, that is,

$$V_{cav}(t+\Delta t) = V_{cav}(t) + \frac{1}{2}\Delta t\{[q_{vout}(t+\Delta t) - q_{vin}(t+\Delta t)] + [q_{vout}(t) - q_{vin}(t)]\}, \quad (29)$$

where

V_{cav}	cavitation volume
t	time
Δt	time step
q_{vin}	volume flow rate into a node
q_{vout}	volume flow rate out of a node

Concentrated vapor cavitation is appropriate when the flow cavitates merely in part of the system. With the beginning of the first cavitation, the model is moderately valid. Since the effect of vapor on the speed of the pressure pulse is not considered, false pressure peaks may occur in the results calculated with the model. For the same reason, artificially abrupt pressure waves may be formed in the model.

4.5 Container of unknown pressure

The container of unknown pressure is short and its cross-sectional area is great compared with the dimensions of the pipes of the system. The container of unknown pressure is assumed to be a concentrated volume. No inertia resides in the concentrated volume, but merely elasticity [2]. This results in an equal pressure prevailing in different parts of the concentrated volume at any given moment. The pressure of the container of unknown pressure and the cavitation volume have to be solved.

When the flow is not cavitating in the container of unknown pressure, the pressure is solved by means of Equation [24, p. 68] derived from the definition of bulk modulus of elasticity

$$\frac{dp}{dt} = -\frac{K}{V}\frac{dV}{dt}, \quad (30)$$

where

p	pressure
t	time
K	bulk modulus of elasticity of fluid
V	volume.

The above equation yields

$$\frac{dp}{dt} = -\frac{K}{V - \sum_{i=1}^{n_m} A_i x_i}(-\sum_{i=1}^{n_{in}} q_{vini} + \sum_{i=1}^{n_{out}} q_{vout} - \sum_{i=1}^{n_m} A_i v_i) \tag{31}$$

where

n_m	number of moving parts
A	cross-section area of a moving part
x	lift of a moving part
n_{in}	number of volumetric flows entering the container
q_{vin}	volumetric flow entering the container
n_{out}	number of volumetric flow exiting the container
q_{vout}	volumetric flow exiting the container
v	velocity of the moving part.

The velocity of the moving part is positive when the motion of the part results in decreased container volume.

If the flow cavitates in the container of unknown pressure, the pressure prevailing in the container is of the magnitude of the vapor pressure of the fluid. Ficarella and Laforgia [14] deduced from the continuity equation for cavitation volume the following equation:

$$\frac{\rho - \rho_v}{\rho} \frac{dV_{cav}}{dt} = -\sum_{i=1}^{n_{in}} q_{vini} + \sum_{i=1}^{n_{out}} q_{vouti} - \sum_{i=1}^{n_m} A_i v_i, \tag{32}$$

where

ρ	density of homogeneous fluid
ρ_v	vapor density
V_{cav}	cavitation volume.

4.6 Flow passage

A short discontinuity point throttling the flow is called a flow passage. Pressure loss is created in a flow passage. The fluid is assumed to be incompressible in the flow passage. In the model for an injection system, the volume flow rate of a fluid flowing through a flow passage is needed. This is calculated with Equation [36, p. 5]

$$q_v = \mu A_g \sqrt{\frac{2}{\rho}(p_1 - p_2) + v_1^2}, \tag{33}$$

where

q_v	volume flow rate
μ	flow coefficient
A_g	geometric cross-section area of a flow passage
ρ	fluid density
p_1	pressure before the flow passage
p_2	pressure after the flow passage
v_1	velocity at the inlet point of the flow passage.

The geometric cross-section area of the flow passage refers to the smallest cross-section area of the passage.

In Equation 33 the velocity v_1 must be known, because of which the use of this equation is difficult. Therefore, the expression [36, p. 6] has been deduced from Equation 33

$$q_v = \mu' A_g \sqrt{\frac{2}{\rho}(p_1 - p_2)}, \tag{34}$$

where μ' denotes the fictive flow coefficient.

The flow passage is illustrated with two elementary units, in which the fictive flow coefficient is calculated in different ways.

4.6.1 Flow passage controlled by valve

The geometric cross-section area of the flow passage controlled by a valve is changed with the aid of a valve. The fictive flow coefficient of such a flow passage is assumed to be exclusively a function of valve lift (cf. Section 7, p. 69).

4.6.2 Constant-aperture flow passage

The geometric cross-section area of a constant-aperture flow passage is constant. The fictive flow coefficient of the constant-aperture flow passage is illustrated with the combined Giffen-Muraszew and Schmitt model [17, p. 69] [36]. In Figure 15, the fictive flow coefficient of the constant-aperture flow passage is presented as a function of the square root of the Reynolds number and the dimensionless pressure drop. The dimensionless pressure drop is determined using the equation

$$\Delta\Pi = \frac{p_1 - p_2}{p_2}, \tag{35}$$

where

$\Delta\Pi$	dimensionless pressure drop
p_1	pressure before flow passage
p_2	pressure after flow passage.

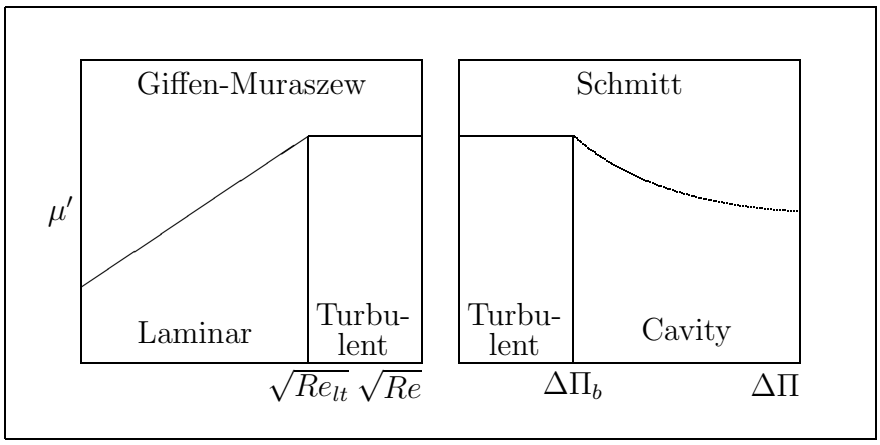

Figure 15. Fictive flow coefficient μ' of a constant-aperture flow passage as a function of the square root of the Reynolds number Re and the dimensionless pressure drop $\Delta\Pi$ in the combined Giffen-Muraszew and Schmitt model. Re_{lt} refers to the Reynolds number at which the flow turns into a turbulent from laminar one, $\Delta\Pi_b$ to the critical dimensionless pressure drop.

According to Giffen and Muraszew, the fictive flow coefficient in a laminar flow is linearly proportional to the square root of the Reynolds number, i.e.

$$\mu' = a_0 + a_1\sqrt{Re}, \tag{36}$$

where

μ'	fictive flow coefficient
a_0, a_1	straight line coefficients.

The flow turns from a laminar into a turbulent one at the Reynolds number Re_{lt}. In Giffen-Muraszew's model, the fictive flow coefficient of a turbulent non-cavitating flow is constant.

Schmitt models the fictive flow coefficient of the turbulent non-cavitating flow in a manner similar to Giffen and Muraszew. When the dimensionless pressure drop exceeds the critical dimensionless pressure drop $\Delta\Pi_b$, the flow starts to cavitate. According to Schmitt, the fictive flow coefficient in the cavitating turbulent flow is calculated with the equation

$$\mu' = \psi'\sqrt{1 + 1/\Delta\Pi}, \tag{37}$$

where ψ' is the fictive contraction coefficient. This value is constant.

In Reference [24, pp. 97–100] it is shown that the Giffen-Muraszew model and the Schmitt model can be combined at least when determining the fictive

flow coefficient for the injector tip holes of the test engine. The fictive flow coefficient of the non-cavitating turbulent flow constitutes a compatibility condition between the fictive flow coefficients of these two models.

4.7 Valve

In this model, the part where the motion depends on the hydraulic pressure is called a valve. When the force caused by the hydraulic pressure is able to move the valve, this pressure is said to control the area. The area which the controlling pressure influences is defined as the controlling area. The injection valve needle is included in valves. The needle contains three controlling areas.

The motion of the valve is calculated from the motion equations

$$\frac{dv}{dt} = \frac{1}{m}(\sum_{i=1}^{n_v} p_i A_i - F_0 - kx - fv) \tag{38}$$

and

$$\frac{dx}{dt} = v, \tag{39}$$

in which

v	valve velocity
t	time
m	moving mass of valve
n_v	number of controlling pressures
p	pressure
A	controlling area
F_0	spring initial force
k	spring rate
x	valve lift
f	viscous damping coefficient.

The moving mass of the valve includes the mass of the valve stem and one third of the mass of the valve spring.

Viscous damping is caused by the dry friction, the spring and the ambient fluid [33]. For the coefficient of viscous damping, Vogel [42] introduced the equation

$$f = 0.2\sqrt{km}. \tag{40}$$

Vogel does not mention how the equation was obtained.

After the valve collides with the upper limiter, the valve is left open or it starts to close immediately. The valve is left open if the pressure force created by the controlling pressures is higher than the spring force affecting

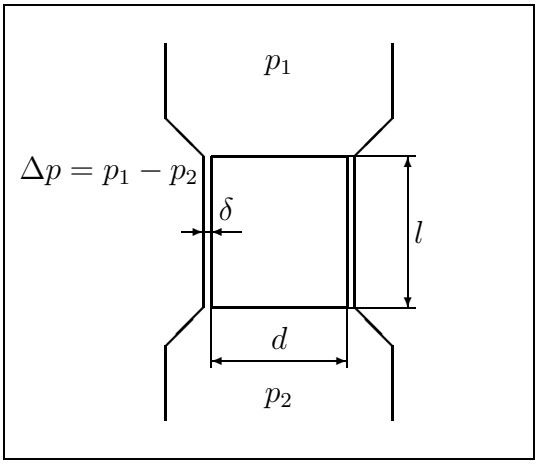

Figure 16. Laminar flow in the gap between the non-moving piston and the sleeve.

the valve. If the valve starts to close immediately, the velocity of the valve is assumed to be downwards 1/5 of the absolute value of the collision rate.

The collision of the valve with the seat is modeled according to the same principles as the collision of the valve with the upper limiter. The valve remains closed after the collision if the spring force affecting the valve is higher than the pressure force created by the controlling pressures. The valve starts to open immediately after the collision if the pressure force created by the controlling pressures is higher than the spring force. In this case, the valve speed upwards is assumed to be 1/5 of the absolute value of the collision rate.

4.8 Laminar flow

Figure 16 shows a sleeve which connects two containers. A non-moving piston is contained in the sleeve. When the clearance between the sleeve and the piston is small, the flow in the gap between the bushing and the piston can be assumed to be laminar. The volume flow rate in the gap is calculated with Equation [16, p. 338]

$$q_v = \frac{\delta^3 \Delta p \pi d}{12 \eta l}, \tag{41}$$

where

q_v	volume flow rate
δ	clearance between piston and sleeve
Δp	pressure difference between the sleeve ends
d	piston diameter
η	dynamic viscosity of the fluid
l	gap length.

5 Program is4

Program is4 was developed with IBM SP2 9076/24 and Digital Alpha-Server 8400 computers. The operating system in both computers is Unix, made by the computer manufacturer. For the programming environment, Emacs was used. The ultimate results were calculated with a Digital computer. The present program version is 0.622.

The writing of Program is4 was started in the Fortran 77 language. When a Fortran 90 compiler was acquired, the Fortran 90 language was adopted for programming. Since Fortran 77 is a subset of Fortran 90, there was no need to change the code written in Fortran 77. The program was successfully compiled both by the IBM xlf90 and Digital DEC Fortran compilers.

The mathematical NAG subroutine library includes appropriate routines for solving ordinary differential equations. Therefore, Version 17 of the library was selected for the sole subroutine library of Program is4.

The programming of the calculation code took approximately 6000 working hours. The time used for creating the pre- and post-processing software of the program was not counted.

5.1 Program diagram

The entity consisting of an elementary unit or units of a mathematical model is described by a subroutine which, in this study, is called an object. For instance, Pipe l_1 is represented by Object l1. Object is4 represents the entire Injection system is_4. The object is encapsulated as completely as possible. An encapsulated subroutine exerts minimal interaction with the environment.

Figure 17 shows the program diagram of Program is4. With Object is4, the progress of the program and the interaction of objects are controlled. The Subroutine isi reads the inputs of Object is4 from the file. Objects bk1, l1, iva1, bk2, and bk3 are initialized using Subroutine is4i. Subroutine is4c controls the calculation and printout.

Since objects of the end of the injection valve are interdependent, they have been gathered as part of Object iva1. The injection valve is illustrated by Object iva1, which consists of Objects bu1, cj1, bubk1, cg1, vn1, and s1.

The ordinary differential equations of the end of the injection valve are solved in Object iva1 using Subroutine D02QGF of the NAG library. The subroutine solves the ordinary differential equations by means of Adams'

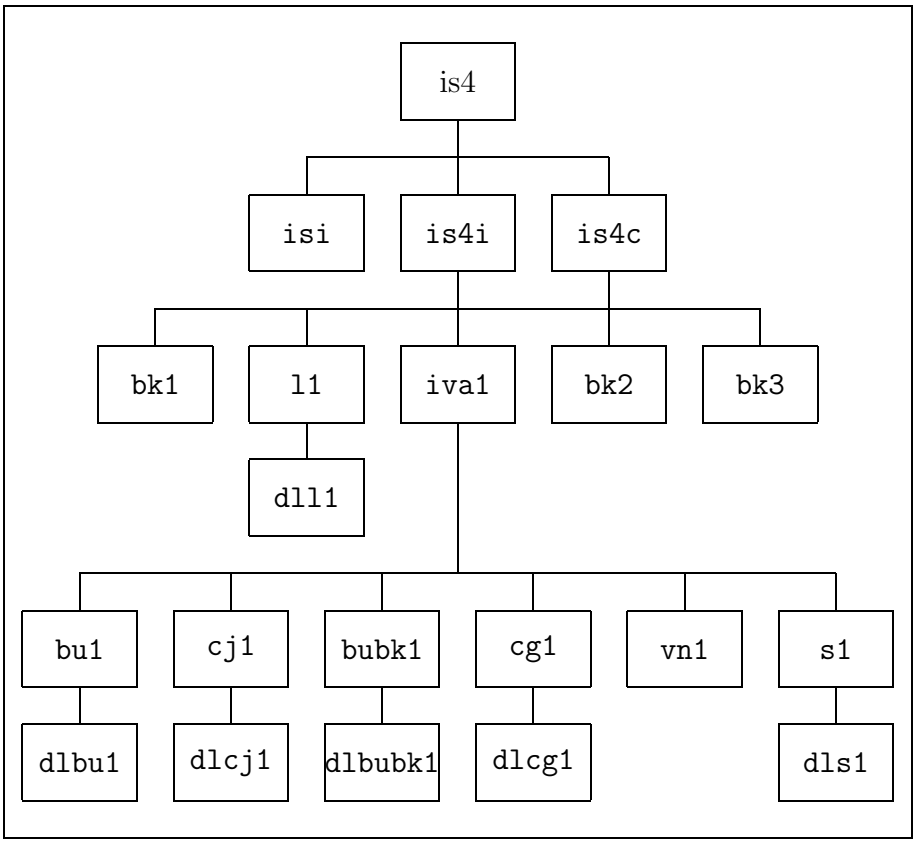

Figure 17. `is4` Version 0.622 program diagram.

predictor-corrector method. A variable order and time step are used for the solution.

A specific fluid object is associated with Objects `l1`, `bu1`, `cj1`, `bubk1`, `cg1`, and `s1`. Therefore, the characteristics of the fluid need not be the same in different objects. The name of a liquid object starts with the letters `dl`. The other letters indicate the object the fluid is associated with.

5.2 Subroutine `is4c`

Figure 18 shows the iterative structure of the calculation and output of Subroutine `is4c`. The calculation and the output have been combined in one subroutine. Thanks to this, the values of the variables in a potential error situation can be stated, and it is also easier to see how the error situation was reached. In the more recent versions of the program it is, however, worthwhile to consider transferring the output into the new Subroutine `is4w`. In this case, Subroutine `is4c` would have one task only.

At the beginning of the iterative structure, a request for an appropriate `time_step` is made from Pipe `l1`. For the present, Variable `itime` contains the number of the preceding time step. Object `l1` is written in Fortran 77. In Fortran 77 objects, alternative input locations are used, with the aid of which an object written in Fortran 77 can be encapsulated [31, pp. 376–379].

Next, the point of Time `time` and the number of Time step `itime` are specified with a new time step.

In Subroutine `is_4_end_1` it is tested whether the iteration should be ended. The iteration is ended if the tables are full. With Variable `time_dim_1`, the maximum number of potential time steps is determined. Another reason for terminating the calculation could be that the desired calculation time has been reached. Variable `t_end` of the Data type `is_input_data` includes the last calculation point of the time desired. If the iteration is ended, Variable `give_up` will be given the value `.true.`.

If iteration is continued, the flow in the inner nodes of Pipe `l1` is first calculated. Thereafter, Pressure `p_bk1` in Container `bk1` of known pressure is requested.

Object `iva1` describing the injection valve is written in Fortran 90. Therefore, the measure to be carried out can be sent as a message to the object. When Message `message` is given the value `calc_message`, the flow is solved in the Injection valve `iva1`. Object `l1` needs Pressure `p_bu1` in Container `bu1` of unknown pressure. After calculating the flow in Object `iva1`, the calculated results of the injection valve are immediately stored in the files without a separate message from Subroutine `is4c`.

```
DO
   !  Time step
   CALL l1dt (itime, &
      time_step)
   !  Time
   time = time + time_step
   !  Number of time step
   itime = itime + 1
   !  Exit the loop?
   CALL is_4_end_1 (itime, time_dim_1, time,
      is_input_data % t_end,&
      give_up)
   IF (give_up) EXIT
   !  Pipe inner nodes
   CALL l1innr (time_step, itime)
   !  Pressure at the pump
   CALL bk1c (time, p_bk1)
   !  Injection valve
   CALL iva1 (message = calc_message, &
      itime = itime, time = time, delta_t = time_step,&
      p_bu1 = p_bu1)
   !  Put the values at upstream boundary of the pipe
   CALL l1upp (time_step, itime, p_bk1)
   !  Put the values at downstream boundary of the pipe
   CALL l1dpp (time_step, itime, p_bu1)
   !  Write the pressure in the container bk1 into a file
   CALL bk1w (itime, time)
   !  Write the results of the pipe into a file
   CALL l1w (itime)
   !  Write the pressure in the container bk2 into a file
   CALL bk2w (itime, time)
   !  Write the pressure in the container bk3 into a file
   CALL bk3w (itime, time)
END DO
```

Figure 18. The iterative structure of the calculation and output of Subroutine is4c.

Pressure p_bk1 is given for Pipe l1 at the upstream and Pressure p_bu1 at the downstream end. Now, Object l1 calculates the flow at each end of the pipe.

Finally, the calculated results of Container of known pressure bk1, of Pipe l1, and of Container bk2 and bk3 of known pressure are stored in the output files of the objects.

5.3 Subroutine iva_calc_3

Figure 19 shows a simplified iteration structure of the calculation. By means of the subroutine, the flow in Injection valve iva1 at a given point in time is calculated.

The method for solving the ordinary differential equations at the end to the injection valve requires continuity of the derivatives. The derivatives show, however, a point of discontinuity, when the needle of the injection valve starts to lift, collides with the upper limiter, goes downwards from the upper limiter, or collides with the seat. In addition, the moments at which cavitation starts and ends in Container bu_1 of unknown pressure are defined as the points of discontinuity of the derivatives.

It is assumed that at the beginning of an iteration the equations of the derivatives of the previous moment are valid. The selection is made on the basis of Variable previous_alternative. The value of this variable indicates the location of Needle vn1 and the cavitation situation in Container bu1 of unknown pressure.

In the first alternative, the needle of the injection valve is closed and the flow is not cavitating in Container bu1. The input for Subroutine iva_calc_close_1 will be the desired moment of termination t_2 of the calculation and Pressure p_bu1_f in Container bu1 at the moment of starting the calculation. For the output, the subroutine yields Current alternative current_alternative and Pressure p_bu1 in Container bu1 at the moment of ending the calculation. For the input, Variable t_1 means the starting moment of the calculation, and for the output, the actual moment of terminating the calculation.

Other potential options are as follows:

- needle vn1 is closed and the flow is cavitating in container bu1;
- needle vn1 is located between the seat and the upper limiter;
- needle vn1 is completely open.

```
DO
   SELECT CASE (previous_alternative)
   CASE ("close")
      !  Needle vn1 closed, no cavity in bu1
      CALL iva_calc_close_1 (..., t_2, p_bu1_f, ..., &
         current_alternative, p_bu1, ..., t_1)
   CASE ("close_and_cavity")
      !  Needle vn1 closed, cavity in bu1
      CALL iva_calc_close_c_1 (..., t_2, p_bu1_f, ..., &
         current_alternative, p_bu1, ..., t_1)
   CASE ("opens_closes")
      !  Needle vn1 between seat and upper limiter
      CALL iva_calc_o_c_2 (..., t_2, p_bu1_f, ..., &
         current_alternative, p_bu1, ..., t_1)
   CASE ("open")
      !  Needle vn1 fully open
      CALL iva_calc_open_1 (..., t_2, p_bu1_f, ..., &
         current_alternative, p_bu1, ..., t_1)
   END SELECT
   IF (current_alternative == previous_alternative) THEN
      EXIT
   ELSE
      p_bu1_f = p_bu1
      ...
   END IF
END DO
```

Figure 19. Simplified iteration structure of the calculation of Subroutine `iva_calc_3`.

The flow might be cavitating in Container `bu1` only when Needle `vn1` is closed. As regards the other options, the pressure of Container `bu1` is assumed to be higher than the vapor pressure of the liquid.

If the current and the previous alternatives are identical, the iterative structure is abandoned. In this case, the value of variable `t_1` is equal to the moment `t_2` of terminating the calculation.

If the current and the previous alternatives deviate from each other, Pressure `p_bu1` at Moment `t_1` is set as the Pressure `p_bu1_f` of the moment of starting the calculation. In such a case, Variable `t_1` includes the end moment of the previous alternative, this being smaller than the desired End moment `t_2` of calculation.

Using the iterative structure, the point in time can be calculated accurately when the discontinuity point of the derivative is reached. In theory, all conceivable discontinuity points may occur once or several times during one time step. With the iterative structure, the points of time at each point of discontinuity can be calculated. Consequently, the ordinary differential equations of the end of the injection valve are solved throughout the calculation from the proper derivatives. The points of time at the points of discontinuity are stored in a file.

The ordinary differential equations of various alternatives of Subroutine `iva_calc_3` are solved using Adams' predictor-corrector method. With this method, a solution is not always reached. In the method, a time-step is required which must not be too short or too long. If a time-step is not of the proper length, the number of nodes of the pipe has to be changed.

6 Measurements

The measurements of the fictive flow coefficients of the present model are described in Reference [24, pp. 88–96]. The engine measurements related to the assessment of the quality of the model are described in Reference [27, pp. 36–42]. Only the main aspects of the measurements are dealt with below.

6.1 Fictive flow coefficient

6.1.1 Experimental setup

The fictive flow coefficient of the gap between the needle and the seat of the injection valve and of the holes was determined from the steady flow. The pressure and the temperature of the fluid were measured before the flow passage. The fluid was flowing from the passage into a container resting on a scale. When the time that had passed in the change of the fluid mass of the container was measured, the mass flow through the flow passage could be calculated.

The examined tip of the injection valve was of the type Bosch DL 150 T 1139. For the fluid, diesel oil of winter quality No. 1 was used. The fluid flowed from the flow passage under the fluid surface of the container. In this way, the formation of liquid fog could be prevented.

The pressure before the holes of the injection valve was measured with three manometers, their measuring ranges being 0–0.6 MPa, 0–4 MPa, and 0–10 MPa.

The needle lift was 4 mm, when the fictive flow coefficient of the injection valve holes was measured.

When the tip including the holes of the injection valve, was abraded away, the fictive flow coefficient between the needle and the seat could be measured. The fictive flow coefficient was measured on six needle lifts. The pressure prior to the gap between the needle and the seat was measured with two strain gauge transducers with measuring ranges of 0 to 2 MPa and 0 to 20 MPa.

The pressure after the flow passage could not be adjusted. It was assumed to be of the magnitude of the ambient pressure.

For financial reasons, defects in the measuring equipment could not be avoided. The pressure drop across the flow passage is dependent on the dimensionless pressure drop and the pressure after the passage according to the equation $\Delta p = \Delta\Pi p_2$. In the foregoing, Δp denotes pressure drop across the flow passage, $\Delta\Pi$, the dimensionless pressure drop, and p_2 the pressure after the passage. When the dimensionless pressure drop is kept constant and the

pressure after the flow passage increases, the pressure drop is increased across the flow passage. The Reynolds number is dependent on the pressure drop across the flow passage. If we wish to measure the turbulent non-cavitating flow, the pressure drop must be sufficient. Therefore, particularly at low dimensionless pressure drops, the pressure after the flow passage should be adjustable. This function would have necessitated a pressure chamber after the flow passage.

In the measurement system, the highest conceivable pressure before the flow passage was about 8 MPa. This pressure was far too low to explain the fictive flow coefficients of the flow passages of the injection valve.

The display range of the scale was 0–160 kg. For most measurements, this was too wide, but the scale could not be replaced during the measurements.

6.1.2 Measurement results

Figure 20 shows the fictive flow coefficient measured from the gap between the needle and the seat as a function of the square root of the Reynolds number. The parameter is the needle lift. For the measuring points of the fictive flow coefficient of one lift an exponential curve was fitted [24, p. 102]

$$\mu' = a_{e0} + a_{e1} e^{-a_{e2}\sqrt{Re}}, \tag{42}$$

where

μ'	fictive flow coefficient
$a_{e0} \dots a_{e2}$	coefficients of the function
Re	Reynolds number.

The coefficients of the exponential function 42 are presented in Table 1 as a function of needle lift.

Figure 21 shows the fictive flow coefficient of the injection valve holes fitted in the Giffen-Muraszew model. In laminar flow, the fictive flow coefficient conforms to the equation

$$\mu' = 0.422 + 4.652 \cdot 10^{-3}\sqrt{Re}. \tag{43}$$

When the Reynolds number reaches a value of 2230, the flow turns from a laminar into a turbulent one. The fictive flow coefficient of the turbulent cavitationless flow receives a value of 0.642.

When Schmitt's model (Figure 22) is fitted to the measured values of the fictive flow coefficient of the cavitating flow of the injection valve holes, the following is received

$$\mu' = 0.543\sqrt{1 + 1/\Delta\Pi}, \tag{44}$$

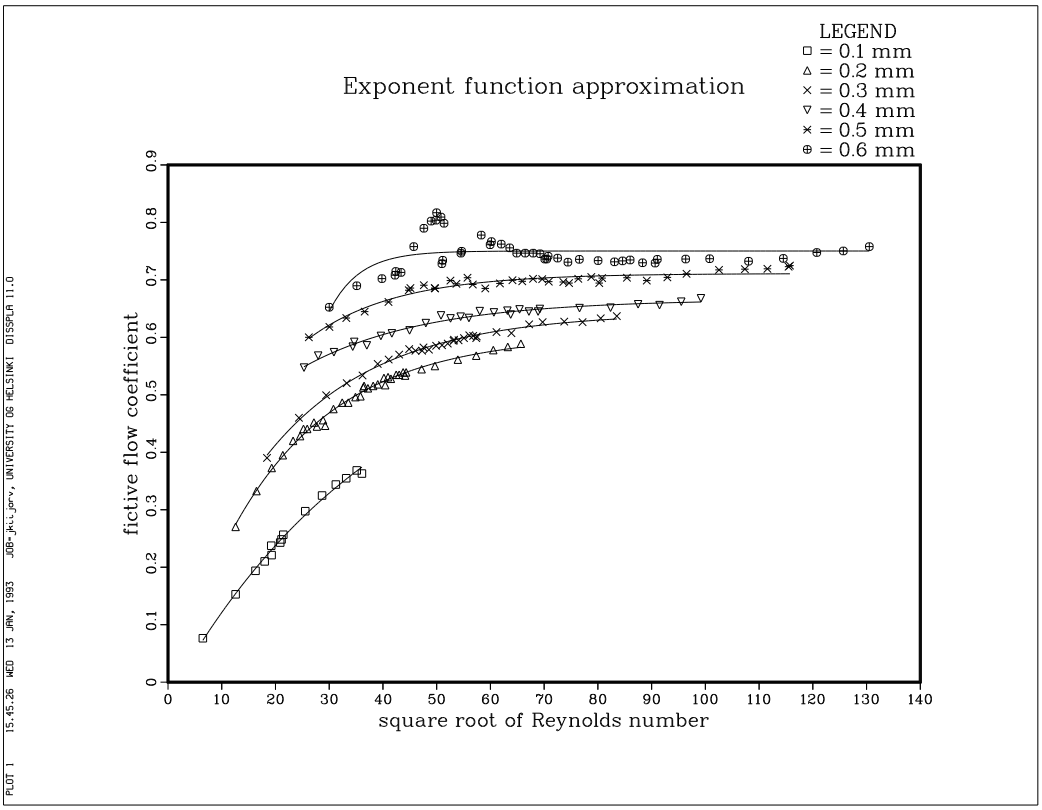

Figure 20. The fictive flow coefficient of the gap between the needle and the seat as a function of the square root of the Reynolds number, the needle lift as the parameter [24, p. 101]. The curves have been fitted with Function 42 to the measuring points corresponding to the needle lift.

Table 1. The coefficients of the exponential function 42 fitted to the measured fictive flow coefficients of the gap between the needle and the seat with different needle lifts x [24, p. 103].

x [mm]	a_{e0}	a_{e1}	a_{e2}
0.1	0.65373	−0.68189	$2.4715 \cdot 10^{-2}$
0.2	0.60504	−0.62608	$5.0782 \cdot 10^{-2}$
0.3	0.64339	−0.59441	$4.7347 \cdot 10^{-2}$
0.4	0.66604	−0.35835	$4.4144 \cdot 10^{-2}$
0.5	0.71104	−0.56574	$6.1408 \cdot 10^{-2}$
0.6	0.75024	−21.345	0.17712

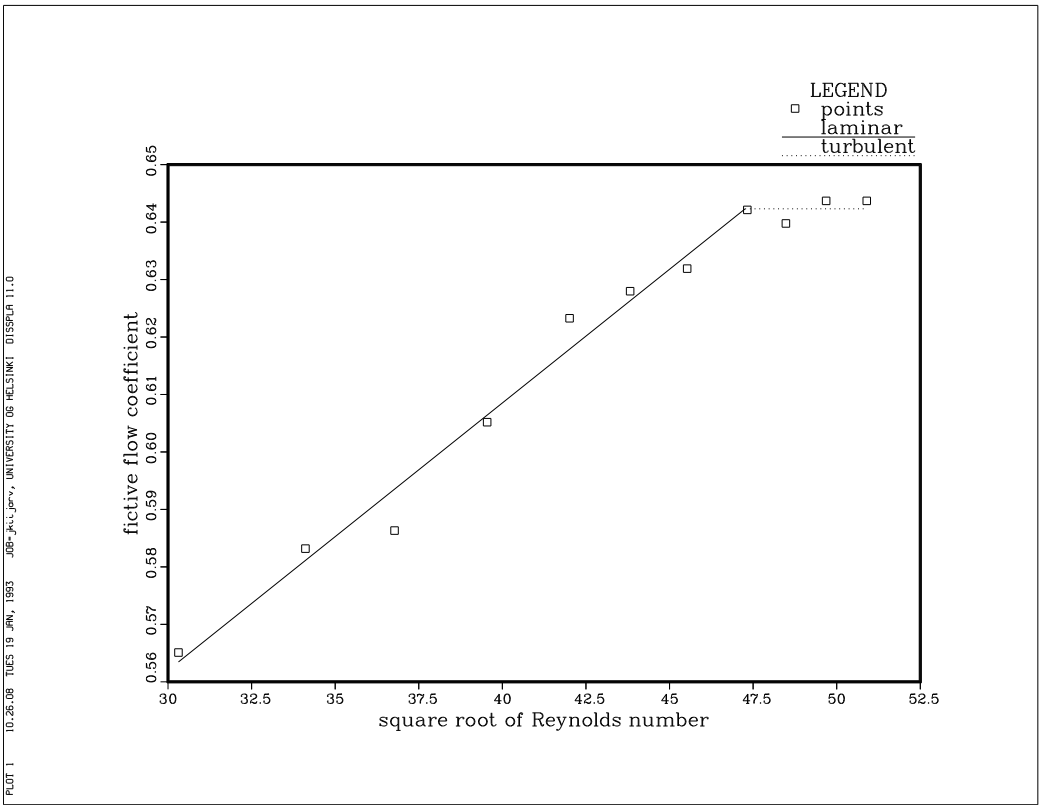

Figure 21. The fictive flow coefficient of the injection valve holes in laminar flow and in non-cavitating turbulent flow versus the square root of the Reynolds number [24, p. 98].

where $\Delta\Pi$ denotes dimensionless pressure drop. The fictive flow coefficient of the turbulent non-cavitating flow is almost equal to the value of the flow corresponding to the flow value in the Giffen-Muraszew model. When the dimensionless pressure drop exceeds a value of 2.50, the turbulent flow starts to cavitate.

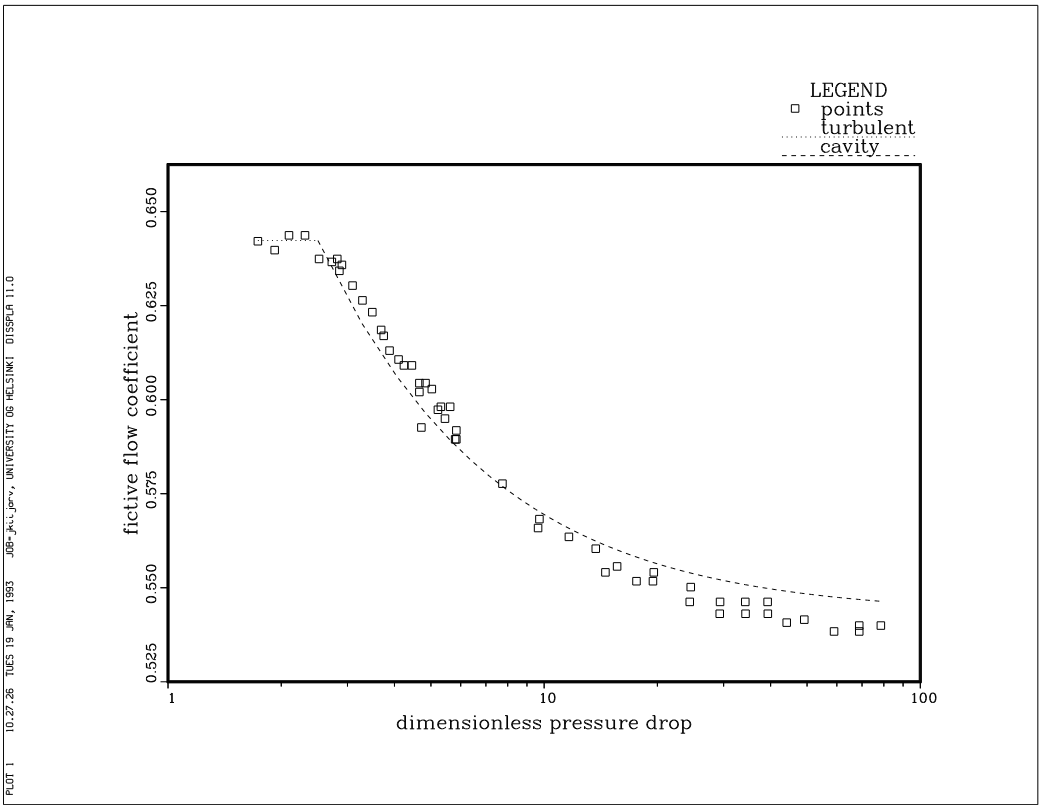

Figure 22. The fictive flow coefficient of the injection valve holes in the non-cavitating flow and in the cavitating turbulent flow as a function of dimensionless pressure drop [24, p. 99].

6.1.3 Uncertainty in measurement

The uncertainty in the measurement is estimated according to Reference [19]. Because no statistical analysis of a series of observations was made, type B evaluation of standard uncertainty is used.

It is assumed that

- the distribution is uniform.

- the input estimate x_i is the midpoint within the range from a_- to a_+. Thus we get $x_i = (a_- + a_+)/2$. The symbol a_- means the lower and a_+ the upper bound of the range.

- a is the half-width of the range and $a_+ - a_- = 2a$.

In this case the standard uncertainty $u(x_i)$ is

$$u(x_i) = \frac{a}{\sqrt{3}}. \tag{45}$$

The relative combined standard uncertainty $u_c(y)/y$ is calculated with Equation [19, p. 18]

$$\frac{u_c(y)}{y} = \sqrt{\sum_1^n \left[p_i \frac{u(x_i)}{x_i} \right]^2}, \tag{46}$$

in which y is the estimate of the measurand, p the exponent of the parameter in the original equation, and $u(x_i)/x_i$ the relative standard uncertainty of the input estimate.

At first the uncertainty in measurement is estimated in the flow passage between needle and seat. In this gap the fictive flow coefficient μ' is calculated from the measured data with Equation

$$\mu' = \frac{m}{A\, t\sqrt{2\rho\Delta p}}, \tag{47}$$

where

m	mass
A	geometric flow area of the flow passage
t	time
ρ	density of the liquid
Δp	pressure difference over the flow passage.

The geometric flow area A in the gap between needle and seat is

$$A = f(\alpha_1, \alpha_2, d_1, d_2), \tag{48}$$

in which (Figure 23)

α_1	the enlarged angle of the tip of the needle
α_2	the angle of the needle tip
d_1	diameter of the sac
d_2	diameter, where the angle of the needle tip changes.

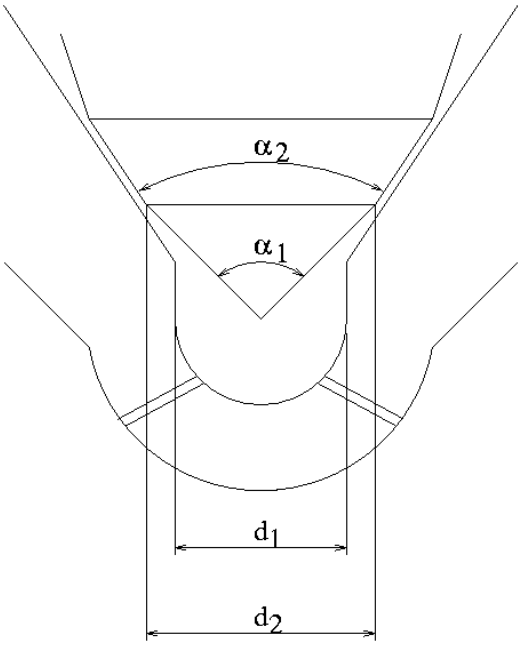

Figure 23. Tip of the injection valve.

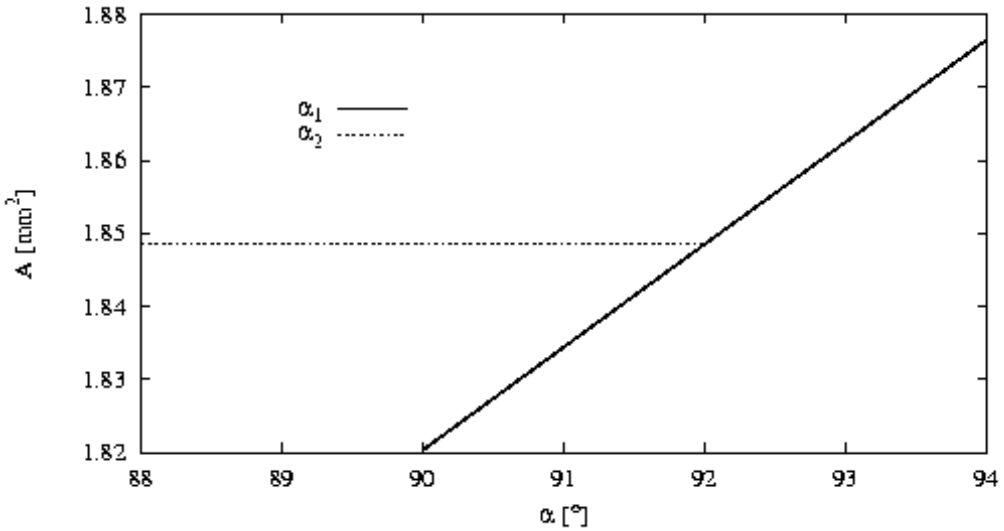

Figure 24. Geometric flow area A in the flow passage between needle and seat as a function of angle α. Needle lift 0.6 mm. The angles are shown in Figure 23.

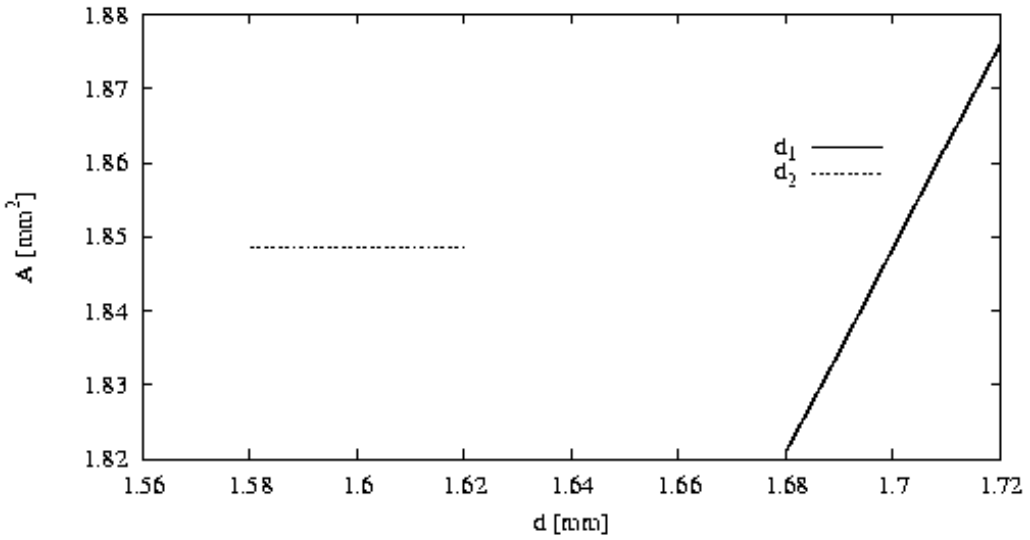

Figure 25. Geometric flow area A in the flow passage between needle and seat as a function of diameter d. Needle lift 0.6 mm. The diameters are shown in Figure 23.

The dependence of the geometric flow area of the four parameters is complicated. During injection the gap between needle and seat is fully open most of the time. Therefore the effect of these four parameters is calculated with the NeedleSeat -program [24, pp. 124–127] at the maximum lift of the needle. The results of the calculation are shown in Figures 24 and 25.

When the needle lift is at its maximum, the angle α_2 and the diameter d_2 have no effect on the geometric flow area. The effect of the angle α_1 and diameter d_1 can be approximated linear. Thus we get

$$\frac{u_c(\mu')}{\mu'} = \sqrt{\left[\frac{u(m)}{m}\right]^2 + \left[\frac{u(t)}{t}\right]^2 + \left[\frac{u(\alpha_1)}{\alpha_1}\right]^2 + \left[\frac{u(d_1)}{d_1}\right]^2 + \left[0.5\frac{u_(\rho)}{\rho}\right]^2 + \left[0.5\frac{u(\Delta p)}{\Delta p}\right]^2} \quad (49)$$

From Equation 49 and Table 2 we achieve a relative standard uncertainty value of 1.86 %. When this is multiplied by the coverage factor $k = 2$, then the expanded uncertainty $U = 3.72$ %. Only the greatest value of the fictive flow coefficient in each lift is used in the calculations (p. 69). The uncertainty

Table 2. Estimation of relative standard uncertainties in Equation 49.

	m	t	α_1	d_1	ρ	Δp
a	± 50 g	± 1 s	$\pm 2°$	± 0.01 mm	± 2.5 kg/m^3	
x_i	10 kg	70 s	92°	1.69 mm	865.5 kg/m^3	
$u(x_i)/x_i$	0.29 %	0.82 %	1.26 %	0.34 %	0.67 %	2.00 %

limits of the measured fictive flow coefficient in the gap between needle and seat are shown in Figure 30 (p. 79).

Next, the uncertainty of the measured fictive flow coefficient of the injection valve holes is studied. The fictive flow coefficient of the holes is calculated from the measured data with Equation

$$\mu' = \frac{m}{n(\pi/4)d^2 t\sqrt{2\rho\Delta p}}, \tag{50}$$

in which n means the number of the injection valve holes and d the diameter of the hole.

From Equations 46 and 50 we arrive at the relative combined standard uncertainty Equation

$$\frac{u_c(\mu')}{\mu'} = \sqrt{\left[\frac{u(m)}{m}\right]^2 + \left[\frac{u(t)}{t}\right]^2 + \left[2\,\frac{u(d)}{d}\right]^2 + \left[0.5\,\frac{u(\rho)}{\rho}\right]^2 + \left[0.5\,\frac{u(\Delta p)}{\Delta p}\right]^2} \tag{51}$$

The estimated relative standard uncertainties of the parameters in Equation 50 are given in Table 3. The estimated standard uncertainty in the injection valve hole diameter is the greatest. The injection valve used in the measurements was an old one. It was no longer suitable for renovatione. Therefore the half width of the range 0.02 mm of the injection valve hole diameter seems rather small.

Table 3. Estimation of relative standard uncertainties in Equation 50.

	m	t	d	ρ	Δp
a	± 50 g	± 1 s	± 0.02 mm	± 2.5 kg/m^3	
x_i	5000 g	90 s	0.45 mm	856.5 kg/m^3	
$u(x_i)/x_i$	0.58 %	0.64 %	2.57 %	0.16 %	2.00 %

Using the values from Table 3 we arrive at a value of 5.30 % for the

combined standard uncertainty. When this uncertainty is multiplied by the coverage factor $k = 2$, the expanded uncertainty $U = 10.6$ %.

In the laminar flow, the value of fictive flow coefficient must be between the lines

$$0.377+4.135\cdot10^{-3}\sqrt{Re} \leq \mu'(\sqrt{Re}) \leq 0.467+5.115\cdot10^{-3}\sqrt{Re} \ \ (k=2), \quad (52)$$

in which Re is the Reynolds number.

The fictive flow coefficient for turbulent flow is

$$\mu'_t = 0.642 \pm 0.068 \ (k = 2) \quad (53)$$

When cavitation occurs, the value of the fictive flow coefficient must be

$$0.485\sqrt{1+\frac{1}{\Delta\Pi}} \leq \mu'(\Delta\Pi) \leq 0.601\sqrt{1+\frac{1}{\Delta\Pi}} \ \ (k=2), \quad (54)$$

where $\Delta\Pi$ is the dimensionless pressure drop (Equation 35).

The expanded uncertainties of the fictive flow coefficients in injection valve holes are shown in Figures 31 (p. 79) and 32 (p. 80).

6.2 Engine measurements

6.2.1 Experimental setup

The tests were carried out with a medium-speed Wärtsilä 324 TS engine. The engine was old-fashioned but it was appropriate for testing the injection system model. Before the tests the engine had run for only 250 hours in laboratory conditions.

The pressures of the high-pressure side of the injection system were measured at three locations. The first pressure transducer was positioned at the junction of the injection pump and the high-pressure pipe, the second transducer halfway along high-pressure pipe, and the third transducer at the junction of the high-pressure pipe and the injection valve.

The pressure transducers were piezo-resistive. With the transducers, the absolute pressure was measured. The measuring range of the first and the third transducers was 0–200 MPa and the resolution 0.02 MPa. The second transducer measured pressure in a range of 0–100 MPa. The resolution of the transducer was 0.01 MPa. The measured pressures are averages of ten working cycles.

The movement of the injection valve needle was measured with a transducer operating according to the Hall principle.

The fuel injection mass per shot was defined with the aid of a scale, a rotation counter, and a clock. An assumption was made, concerning the injection mass calculated from the fuel mass flow rate, that the injected mass of each cylinder is equal in size. Since the engine speed was 750 r/min and the measuring period at least one minute, the injection mass is an average of at least 325 working cycles.

6.2.2 Measured results

In Chapter 7 (p. 69), examples of the results of the engine measurements are given.

6.2.3 Uncertainty in measurement

The combined standard uncertainty of the pressure transducers is 0.01. When the coverage factor $k = 2$, the expanded uncertainty is 0.02. The pressure did not vary much during the measurement.

There exist no data about the accuracy of the needle lift transducer. The output of the measuring chain is voltage, which is calibrated according to the maximum needle lift.

The injected mass per stroke was measured as a mean value between different cylinders and over many working cycles. In truck-type engines the injected mass between different cylinders is allowed to differ from the mean value by ±1 %

In the medium-speed test engine each cylinder has its own injection pump. The pumps are adjusted according to the maximum pressure in the cylinder. There had been problems in adjusting equal maximum pressure in different cylinders of the test engine. Obviously, the injected mass per stroke of the test engine must differ a lot more between cylinders than in a truck-type engine.

The uncertainty in measurement is approximated with the same method as in Section 6.1.3. The combined standard uncertainty is assumed to be equal to 0.03. Thus the expanded uncertainty

$$U = 0.06 \ (k = 2), \tag{55}$$

in which k is the coverage factor.

When the rack setting is 22 mm, the injected mass per stroke is

$$m = 1.044 \text{ g} \pm 0.063 \text{ g} \ (k = 2) \tag{56}$$

With the smaller rack setting of 15 mm the injected mass per stroke is

$$m = 0.569 \text{ g} \pm 0.034 \text{ g} \ (k = 2) \tag{57}$$

The uncertainty in measuring fuel mass and the revs is negligible compared to the uneven injected mass between cylinders.

7 Calculated and measured results

The calculated and measured results are compared at two rack settings, which are 22 mm and 15 mm. The higher rack setting corresponds to the full load, and the lower to the 53 % load.

The initial values of the calculation are given in Appendix A. In the initial calculation, 11 nodes proved to be a good number for the pipe nodes. The temperature of the fuel in the entire system was assumed to be 40 °C.

The fictive flow coefficient of the gap between the needle and the seat of the injection valve forms a surface as a function of the square root of the Reynolds number and the needle lift. For the calculation, the surface was formed with the aid of Exponent function 42 of different needle lifts. When the value of the fictive flow coefficient was interpolated from this surface, the calculation ended in an error. The error was caused by not enough fuel running through the needle and the seat.

When it was assumed in the calculation that the fictive flow coefficient of the flow passage cj_1 is dependent merely on the needle lift, no further problems arose. For the measured fictive flow coefficient of the lift, the constant term a_{e0} of Exponent function 42 was adopted. Since the fictive flow coefficient for a given lift is constant, the flow between the injection valve and the seat can be assumed to be turbulent and non-cavitating.

7.1 Rack setting of 22 mm

The calculated and measured lift of Needle vn_1, and the pressure at the downstream end of Pipe l_1 and in the midmost node of Pipe l_1 are presented in Figure 26 as a function of the crank angle.

When Needle vn_1 collides for the first time with its upper limiter and with its seat, peaks are observed in the measured needle lift curve. The peaks are assumed to be errors due to the measuring transducer. The needle lifts measured and calculated during the main injection correspond well to one another. According to both the calculated and the measured needle lift, an after-injection occurs. The after-injection of the calculated lift starts later than that of the measured lift. The calculated and the measured after-injections end at the same crank angle.

The calculated and measured pressures at the injection valve end of Pipe l_1 conform well to each other during the main injection. only the pressure calculated at crank angles -7 to -5 °and the pressure in the proximity of the top pressure are slightly lower than the measured pressure. The highest calculated pressure is 64.5 MPa and the highest measured 65.4 MPa. Thus, the highest calculated pressure is only 1.4 % lower than the maximum measured

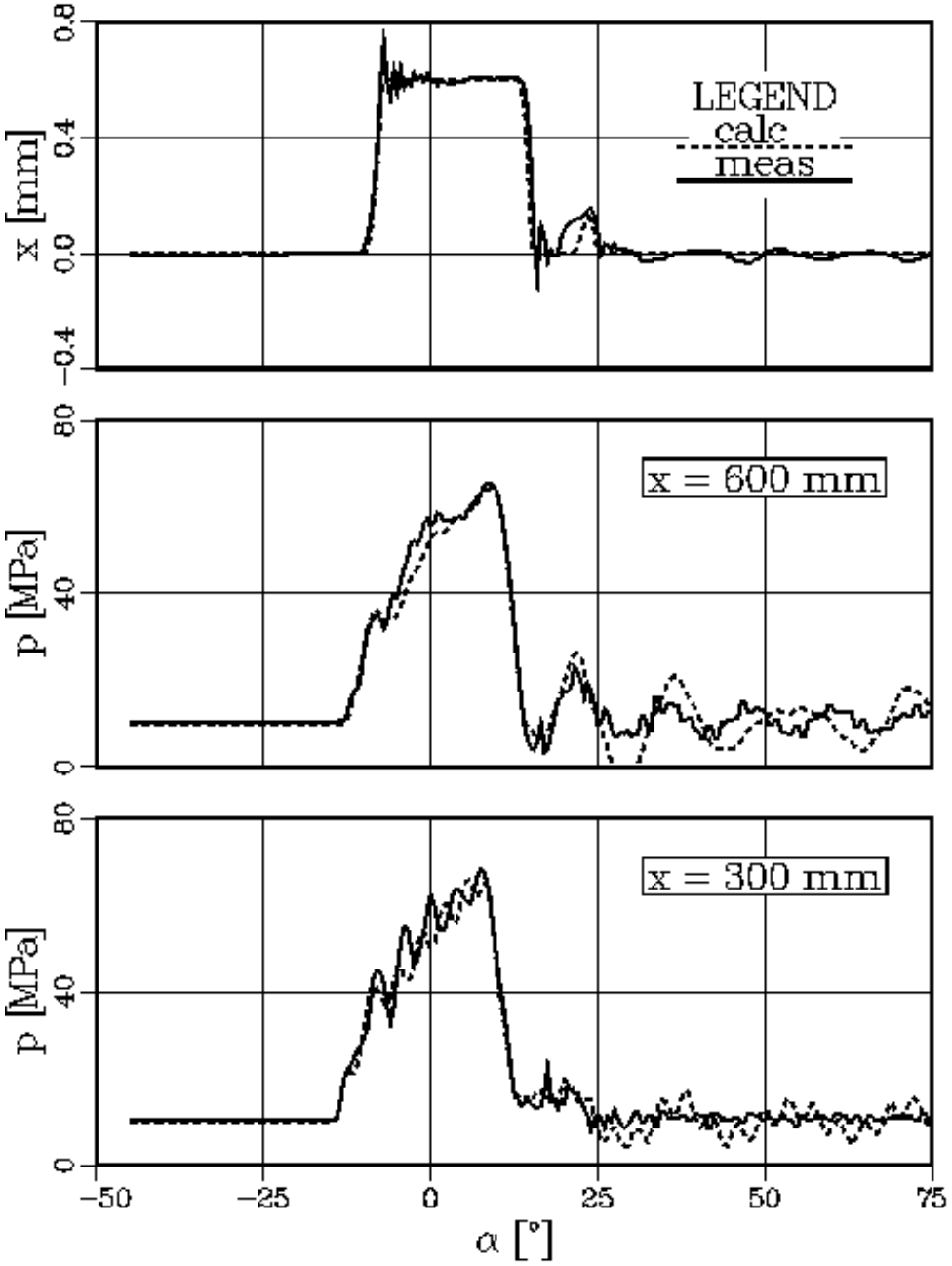

Figure 26. The calculated and measured lifts x of Needle vn_1, pressure p at the injection valve end of Pipe l_1 (x =600 mm) and in the middlemost node ($x = 300$ mm) as a function of the crank angle α. The rack setting was 22 mm.

pressure.

The calculated pressure in Pipe l_1 at the downstream end oscillates more strongly after the main injection than the measured pressure. The calculated pressure varies immediately after the main injection with the measured pressure at nearly the same frequency, but the pressure calculated and measured later oscillates at a different frequency.

When the crank angle is 27–31°, the calculated flow cavitates at the injection valve end of Pipe l_1. No cavitation is observed in the measured pressure in this range. The vapor pressure of the fuel is merely a fraction of the measurement range of the pressure transducers employed. Therefore, the pressure transducers are not appropriate for the reliable measuring of cavitation.

The calculated pressure and the measured pressure in the midmost node of Pipe l_1 resemble each other during the main injection. The highest calculated pressure is 65.8 MPa. For the highest pressure, 68.5 MPa was measured. Hence, the difference between the highest measured pressure and the highest calculated pressure is 3.9 %. The pressure calculated after the main injection oscillates more and after a crank angle of 25°, at different frequency than the measured pressure.

The injection mass per shot illustrates the success of the calculation during a longer period than the maximum pressure of the pipe node. For an injection mass, 0.883 g was calculated, and 1.044 g was measured. The calculated injection mass is 15.4 % lower than the measured mass. Because of the measurement arrangement of the injection mass, the size of the injection mass of the measured cylinder cannot be known precisely. Nevertheless, the difference between the measured and the calculated injection mass is large.

7.2 Rack setting of 15 mm

In Figure 27, the calculated and the measured lifts of Needle vn_1, the pressure at the injection valve end of Pipe l_1 and in the centremost node are compared. The curves are depicted as a function of the crank angle.

When Needle vn_1 collides with its limiter and its seat, the measured needle lift includes false peaks. In other respects, the calculated and measured needle lifts correspond excellently to each other.

The calculated and measured pressures in Pipe l_1 at the injection valve end have a small difference before starting the main injection. The pressure in the pipe is now assumed to be the same as the pressure measured at the injection pump end. This pressure is not entirely equal to the base pressure when measured at the injection valve end.

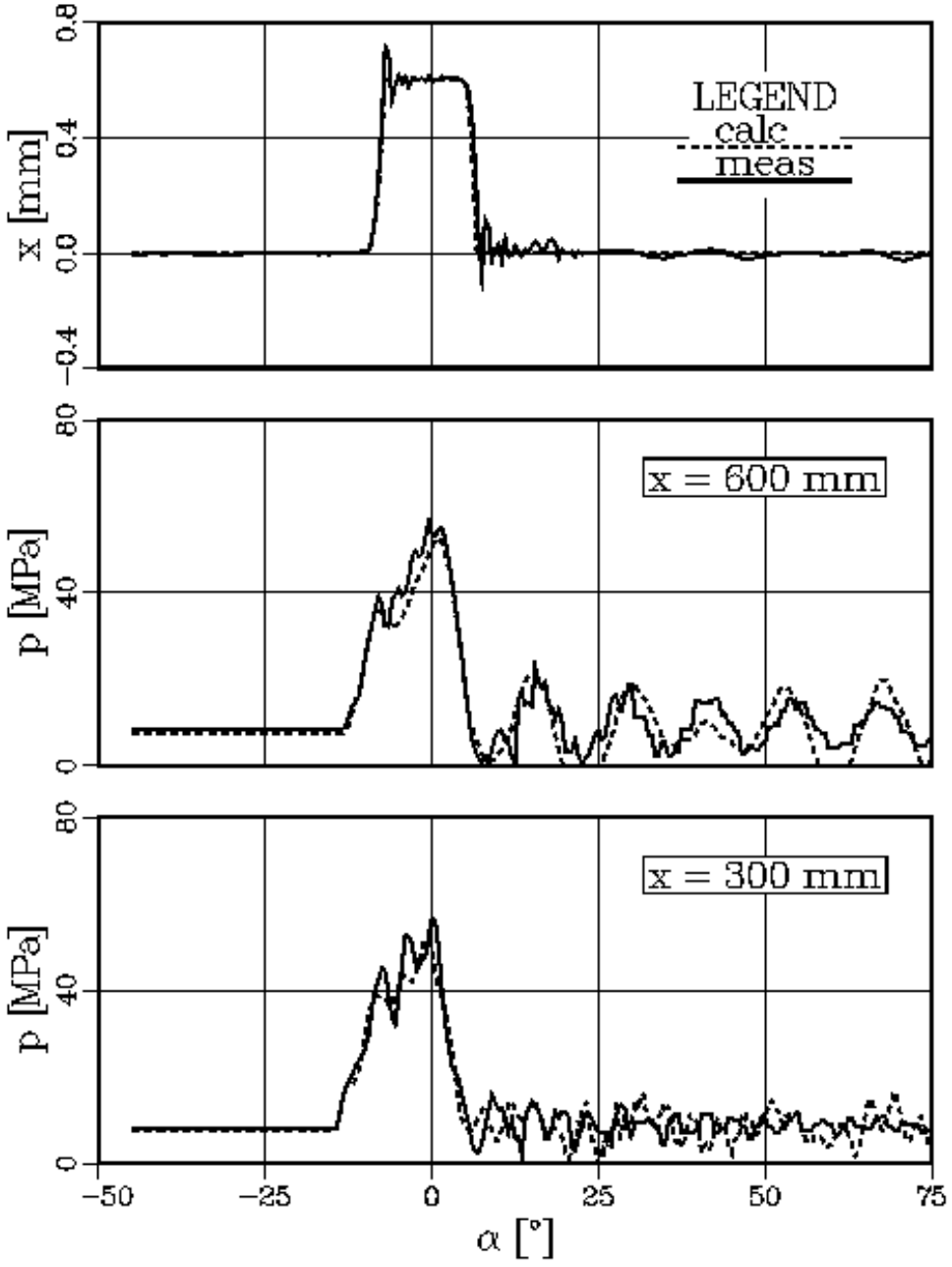

Figure 27. The calculated and the measured lift x of Needle vn_1 and pressure p at the downstream end of Pipe l_1 (x =600 mm) and in the midmost node (x =300 mm) as a function of the crank angle α. The rack setting was 15 mm.

During the main injection the curves for the calculated and the measured pressures in Pipe l_1 at the injection valve end are similar. The pressure curve calculated at a crank angle of a range from -9 to $-4°$ runs lower than the measured curve. The calculated maximum pressure is 52.7 MPa and the measured maximum pressure 56.8 MPa. Thus, the calculated maximum pressure is 7.2 % lower than the measured maximum pressure. The calculated and measured pressures after the main injection oscillate at nearly the same frequency. The amplitude of the after-oscillation is slightly different between the calculated and the measured pressure curves.

When the crank angle is 20–25° and 58–63°, the flow cavitates in Pipe l_1 at the injection valve end according to the curve. Again, no clear cavitation can be detected in the measured pressure curve.

The calculated and measured pressure in the midmost node of Pipe l_1 correspond well to each other in the course of the main injection. Both the calculated and the measured pressure oscillate after the main injection, though to some extent at different amplitudes and frequencies. For the maximum pressure, 51.9 MPa was calculated and 56.5 MPa was measured. The difference between the calculated and measured maximum pressures is 8.2 %.

The calculated injection mass per shot was 0.484 g and the measured mass, 0.569 g. The calculated injection mass is thus 14.9 % smaller than the measured mass. The calculated and measured injection masses differ considerably from each other, as is the case with the rack setting of 22 mm (p. 71).

8 Adaptation of fictive flow coefficients in the measured results

The expanded uncertainty of the measured injected mass per shot is 6 %. At both rack settings, 22 and 15 mm, the calculated injected mass is about 15 % smaller than the measured one. Thus, the calculated injected mass is too low compared to the measured mass.

At both rack settings the difference between the calculated and measured injected mass per shot is almost the same. This indicates that the reason for the too low calculated injected mass is systematic.

The fictive flow coefficients were measured from an old and used injection valve. The test engine had only been operated for a few hours.

There exist no reliable data of a value of the fictive flow coefficient in the flow passage between needle and seat. The shape of this gap is steady. Thus the value of the fictive flow coefficient in the passage can be expected to be higher than the measured maximum range from 0.61 to 0.75.

The fictive flow coefficient of the injection valve hole in non-cavitating turbulent flow varies normally from 0.7 to a little over 0.9. The value of 0.643 of measured fictive coefficient in this kind of flow is rather low. Obviously, the surface of the injection valve holes was no longer even.

There may have been deposits of soot on the surfaces of the measured injection valve holes. If the layer of deposit is uniform, then the relative change $\Delta A/A$ of the geometric flow area can be calculated with Equation

$$\frac{\Delta A}{A} = \left(1 - \frac{2\delta}{d}\right)^2 - 1, \tag{58}$$

where δ is the thickness of the deposit and d the diameter of the hole. The hole diameter of the injection valve is 0.45 mm. In Figure 28 the relative change of the geometric flow area is shown as a function of the thickness of the deposit. Obviously, the thickness of the deposit has a great influence on the geometric flow area.

The calculation may incorporate a systematic error, too. The program has been used to give boundary values to CFD-programs. The calculated and measured injected mass were almost the same in the study [23]. In this research the injection system of a medium-speed Wärtsilä 20 was modeled.

At first preliminary calculations were made. The fictive coefficients of the flow passages in the injection valve had the greatest effect on the injected mass per shot. So the main reason for the too low calculated injected mass seems to be the small values of these fictive flow coefficients. Therefore, new values for these fictive flow coefficients are sought in thus chapter by means

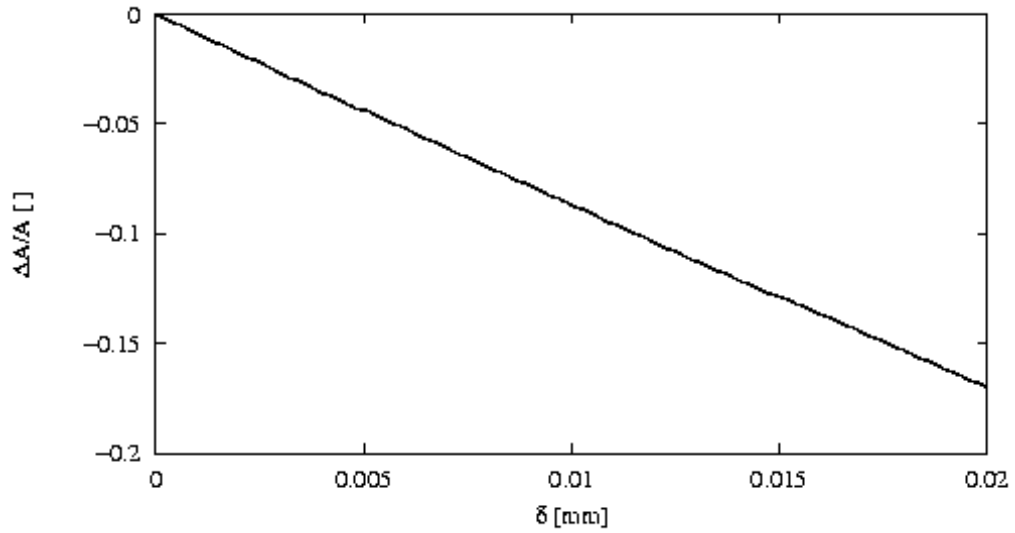

Figure 28. The relative change $\Delta A/A$ of the area of the hole of the injection valve as a function of the thickness δ of the soot deposit.

of calculation. The injection mass calculated using the new fictive flow coefficients is expected to correspond maximally to the measured injection mass. In addition, the pressure calculated with the new fictive flow coefficients is not allowed to differ to a great extent from the measured pressure.

The fictive flow coefficient of the gap between the needle and the seat and of the injection valve holes is not constant. For that reason, the relative change of each fictive flow coefficient is determined at the beginning of the chapter.

8.1 Relative change of the fictive flow coefficient of the gap between the needle and the seat of the injection valve

The fictive flow coefficient of the gap between the needle and the seat of the injection valve is assumed to be dependent only on needle lift. The fictive flow coefficient μ' changed at a given needle lift is calculated with the equation

$$\mu' = (1 + \frac{\Delta\mu'}{\mu'_0})\mu'_0, \tag{59}$$

where $\Delta\mu'/\mu'_0$ denotes a relative change in the fictive flow coefficient and μ'_0 denotes the measured fictive flow coefficient.

8.2 Relative change of the fictive flow coefficient of injection valve holes

When a relative change $\Delta\mu'/\mu'_0$ of the fictive flow coefficient of the injection valve holes is calculated, the following assumptions are made:

1. the Reynolds number Re_{lt}, by which the flow turns from a laminar to a turbulent one, remains the same as in the measured instance. The value of this Reynolds number is 2230;

2. the constant term of the straight line (Eq. 36) of the fictive flow coefficient for the laminar flow is calculated with the equation

$$a_0 = (1 + \frac{\Delta\mu'}{\mu'_0})a_{00}, \tag{60}$$

   where a_{00} is a measured constant term.

3. the fictive flow coefficient μ'_t for turbulent flow is solved using the equation

$$\mu'_t = (1 + \frac{\Delta\mu'}{\mu'_0})\mu'_{t0}, \tag{61}$$

   where μ'_t denotes the measured fictive flow coefficient for the turbulent flow;

4. the constant term a_0 for the straight line of the laminar flow of both the fictive flow coefficient and the fictive flow coefficient μ'_t for the turbulent flow are known. Moreover, when the Reynolds number Re_{lt} with which the flow turns from a laminar to a turbulent one, is konwn, the angular coefficient a_1 of the fictive flow coefficient for the laminar flow can be calculated by the equation

$$a_1 = \frac{\mu'_t - a_0}{\sqrt{Re_{lt}}}; \tag{62}$$

5. the fictive contraction ratio ψ' is solved by the clause

$$\psi' = (1 + \frac{\Delta\mu'}{\mu'_0})\psi'_0, \tag{63}$$

   where ψ'_0 denotes the measured fictive contraction ratio;

6. as the critical dimensionless pressure drop $\Delta\Pi_b$ is calculated by the equation

$$\Delta\Pi_b = \frac{1}{(\mu'_{t0}/\psi'_0)^2 - 1}\,, \tag{64}$$

the critical dimensionless pressure drop is constant in all cases. The value of the critical dimensionless pressure drop is 2.50.

8.3 Selection of values for fictive flow coefficients

Figure 29 presents the balance curves at rack settings of 22 and 15 mm, whereon no error occurred in the injection mass per shot. The curves are depicted as a function of the relative change of the fictive flow coefficient of the gap between the needle and the seat and of the injection valve holes.

It is assumed that in the gap between needle and seat there must occur a little loss. The maximum fictive flow coefficient was chosen with a value of 0.975. This corresponds to a value of 0.3 of the relative fictive flow coefficient at the maximum measured fictive flow coefficient.

The curve of the 15 mm rack setting runs slightly above the curve of the 22 mm setting. When the relative change of the fictive flow coefficient of the gap between the injection valve needle and the seat is 0.3, the zero curves are closest to each other. Hence, for the relative change of the fictive flow coefficient of the gap between the needle and the seat, the value 0.3 is selected. Appendix A.5 shows the original and the changed fictive flow coefficients of the gap between the needle and the seat as a function of needle lift.

For the relative change of the fictive flow coefficient of the injection valve holes, a value halfway between the zero curves is selected. At this point, the relative change in the fictive flow coefficient of the gap between the needle and the seat should be 0.3. Consequently, for the relative change of the fictive flow coefficient of the injection valve holes, a value of 0.168 is achieved. Appendix A.7 shows the original and the changed values for calculating the fictive flow coefficient of the injection valve holes.

In Figures 30, 31 and 32 both the optional and measured fictive flow coefficients with the expanded uncertainty limits are shown. The optional fictive flow coefficients are in every case greater than the upper limits of the expanded uncertainty. The reasons for this are explained at the beginning of the current chapter (p. 74).

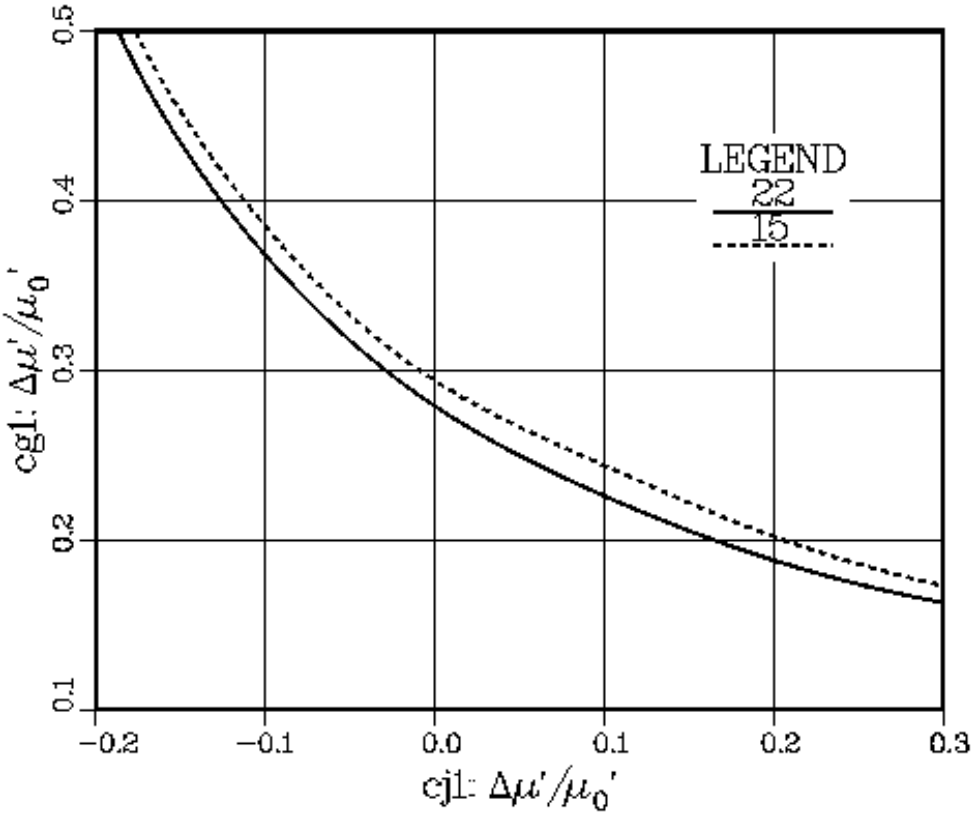

Figure 29. The balance curves, in which the error of the calculated injection mass per shot is zero, as a function of the relative change $\Delta\mu'/\mu_0'$ of the fictive flow coefficient of the gap cj_1 between the needle and the seat and the injection valve holes cg_1. The rack settings are 22 mm and 15 mm.

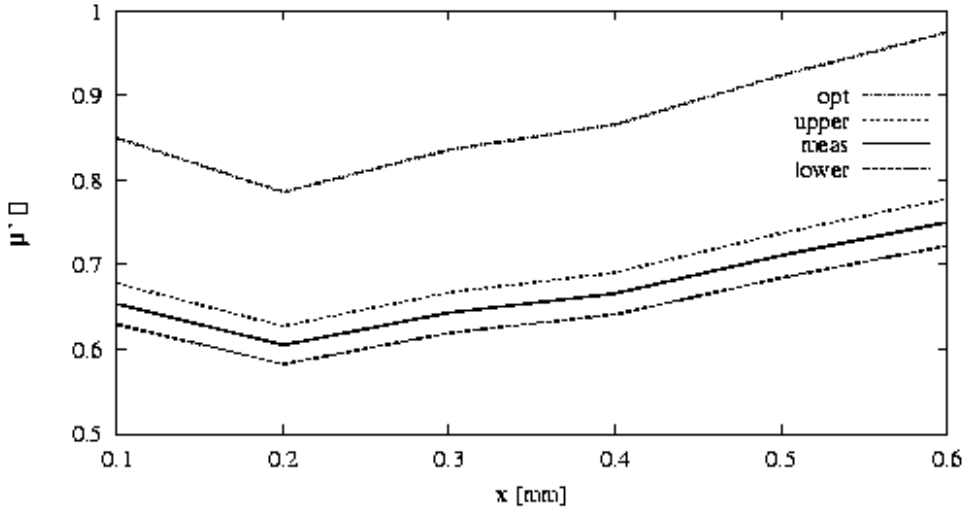

Figure 30. The fictive flow coefficient μ' in the flow passage between needle and seat as a function of the needle lift x. opt optional, upper expanded uncertainty , meas measured, lower expanded uncertainty.

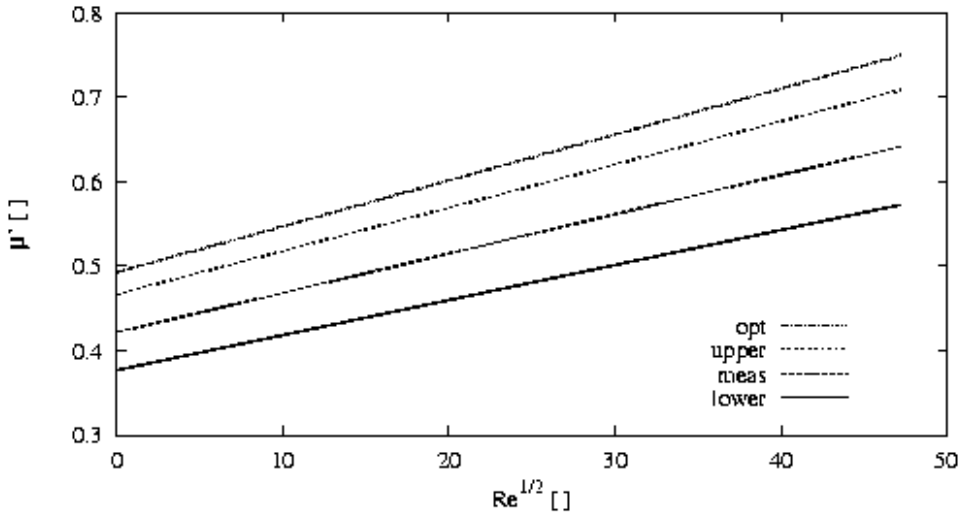

Figure 31. The fictive flow coefficient μ' in the injection valve hole as a function of the square root of the Reynolds number Re. Laminar flow. opt optional, upper expanded uncertainty, meas measured, lower expanded uncertainty.

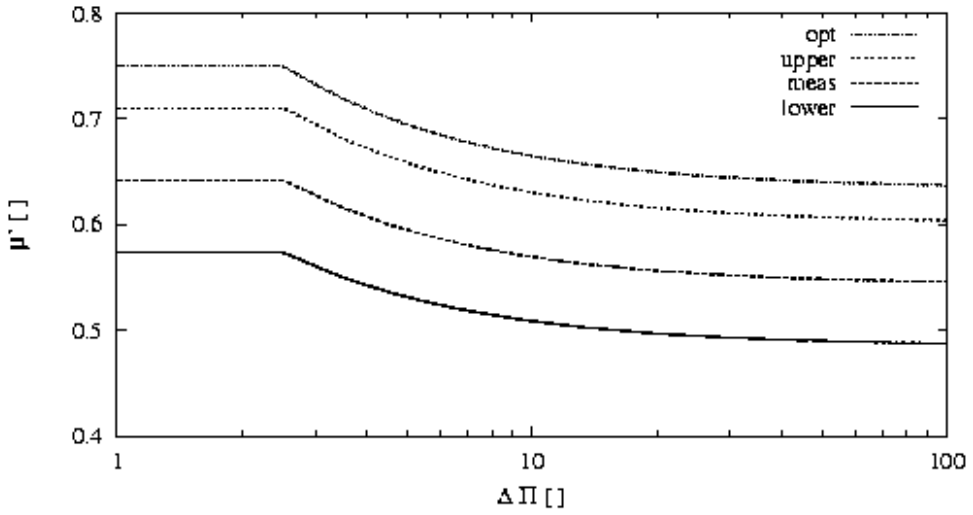

Figure 32. The fictive flow coefficient μ' in the injection valve hole as a function of dimensionless pressure drop $\Delta\Pi$. Turbulent flow without and with cavitation. opt optional, upper expanded uncertainty, meas measured, lower expanded uncertainty.

8.4 Quality of the results calculated using the optional fictive flow coefficients

8.4.1 Rack setting of 22 mm

Figure 33 presents a comparison of the curve of the lift of Needle vn_1 calculated by the measured and the optional fictive flow coefficients and the pressure curve of the last and centremost nodes of Pipe l_1 with the measured curves. The curves are depicted as a function of the crank angle.

The curves of the lift of Needle vn_1 calculated during the main injection correspond well to the measured needle lift. The curve of the needle lift calculated with the optional fictive flow coefficients illustrates the after-injection more accurately than the curve calculated with the original coefficients.

The pressure curves in Pipe l_1 at the injection valve end run nearly overlap at the beginning of the main injection. When the crank angle is 6°, the curve calculated by means of the optional fictive flow coefficients is lower than the curve calculated with the original coefficients. The curves calculated thereafter approach until they join at a crank angle of 2°. The curve calculated with coefficients selected after the main injection shifts the pressure oscillation so that it takes place slightly earlier compared with the curve

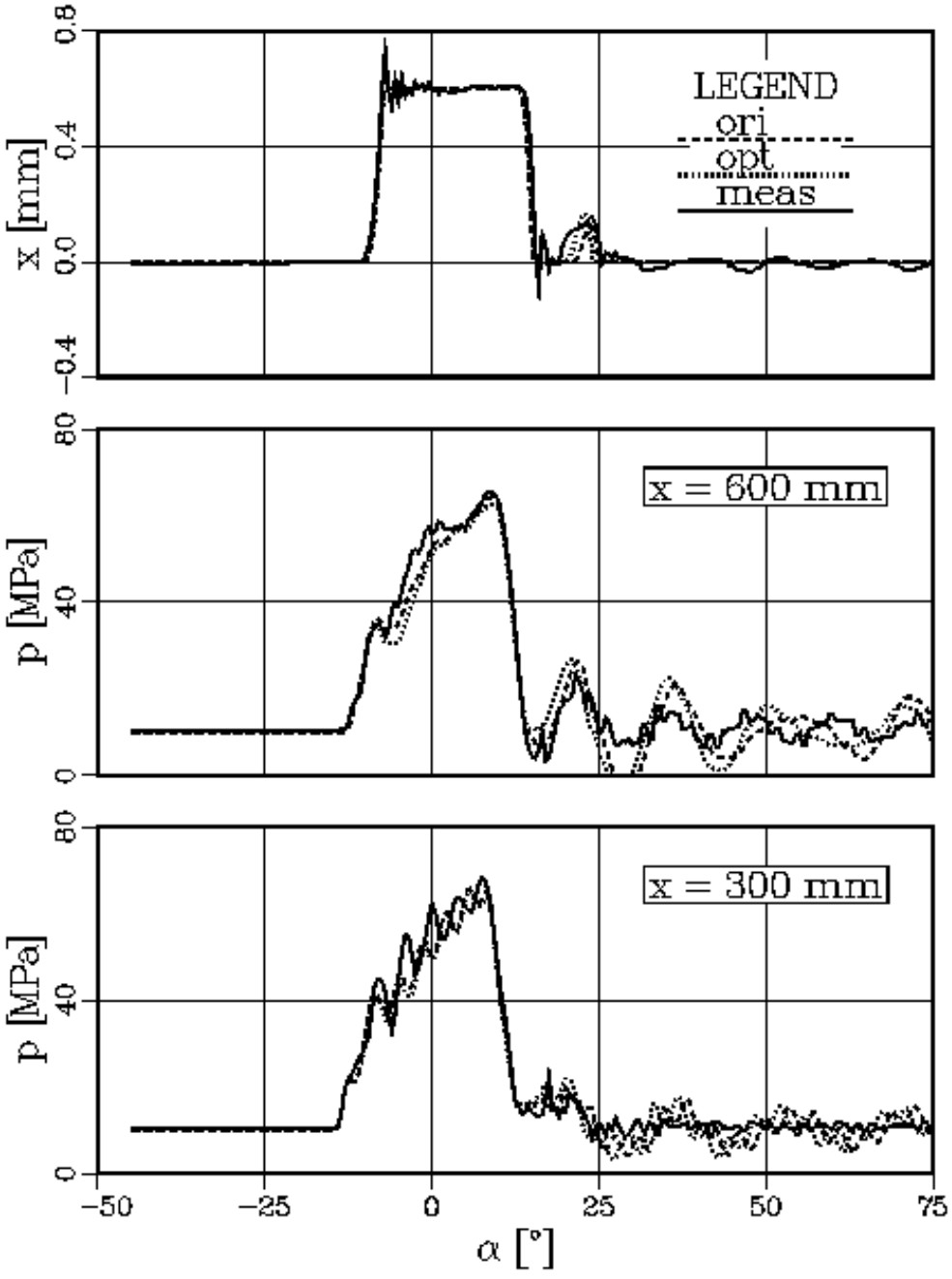

Figure 33. The calculated and the measured lift x of Needle vn_1, pressure p in the last ($x = 600$ mm) and the midmost ($x = 300$ mm) node of Pipe l_1 as a function of the crank angle α. The results are calculated with the original (ori) and the optional (opt) fictive flow coefficients. The rack setting was 22 mm.

calculated with the original coefficients. In addition, the frequency of the calculated oscillation changes slightly as a consequence of a change in the fictive flow coefficients.

The maximum pressure in Pipe l_1 at the injection valve end was 64.5 MPa with the original fictive flow coefficients and 62.5 MPa with the optional fictive flow coefficients. The maximum pressure calculated with the optional fictive flow coefficients is thus 4.4 % lower than the measured maximum pressure.

In the centremost node of Pipe l_1, a change in the fictive flow coefficient has no significant effect on the calculated pressure curve. The highest pressure calculated with the original fictive flow coefficients was 65.8 MPa and with the optional fictive flow coefficients 65.3 MPa. The maximum pressure of the midmost node calculated with the optional fictive flow coefficients is lower by 4.7 % than the measured maximum pressure.

When the injection mass per shot was calculated using the new fictive flow coefficients, the size of the mass was 1.048 g. This value is merely 0.4 % higher than the measured injection mass.

Enlarging the fictive flow coefficients at a rack setting of 22 mm changes significantly only the injection mass per shot. Consequently, the selection of new fictive flow coefficients at this rack setting is successful.

8.4.2 Rack setting of 15 mm

Figure 34 presents the needle lift and the pressure in Pipe l_1 at the end of the injection valve calculated with the original and the optional flow coefficients, and in the midmost node, as a function of the crank angle. In addition, the figure shows the measured curves of the same variables.

The lift curve of Needle vn_1 is not affected by a change in the fictive flow coefficient. The curves of needle lift calculated with the original and the optional fictive flow coefficients correspond well to the measured needle lift.

The pressure curves calculated in the last node of Pipe l_1 start to rise simultaneously. When the crank angle reaches a value of $-8°$, the calculated pressure curves start to deviate from each other. Now, the curve calculated with the optional fictive flow coefficients runs at its lowest. The calculated curves approach at a crank angle of $-6°$ and join at a crank angle of $2°$. The pressure calculated after the main injection oscillates in nearly the same fashion, in spite of the changes in the fictive flow coefficients.

With the original fictive flow coefficients, the highest pressure of the last node of Pipe l_1 was calculated to be 52.7 MPa. The maximum pressure of the same node calculated with the optional fictive flow coefficients was 51.4 MPa. The latter value is 9.5 % lower than the measured maximum pressure.

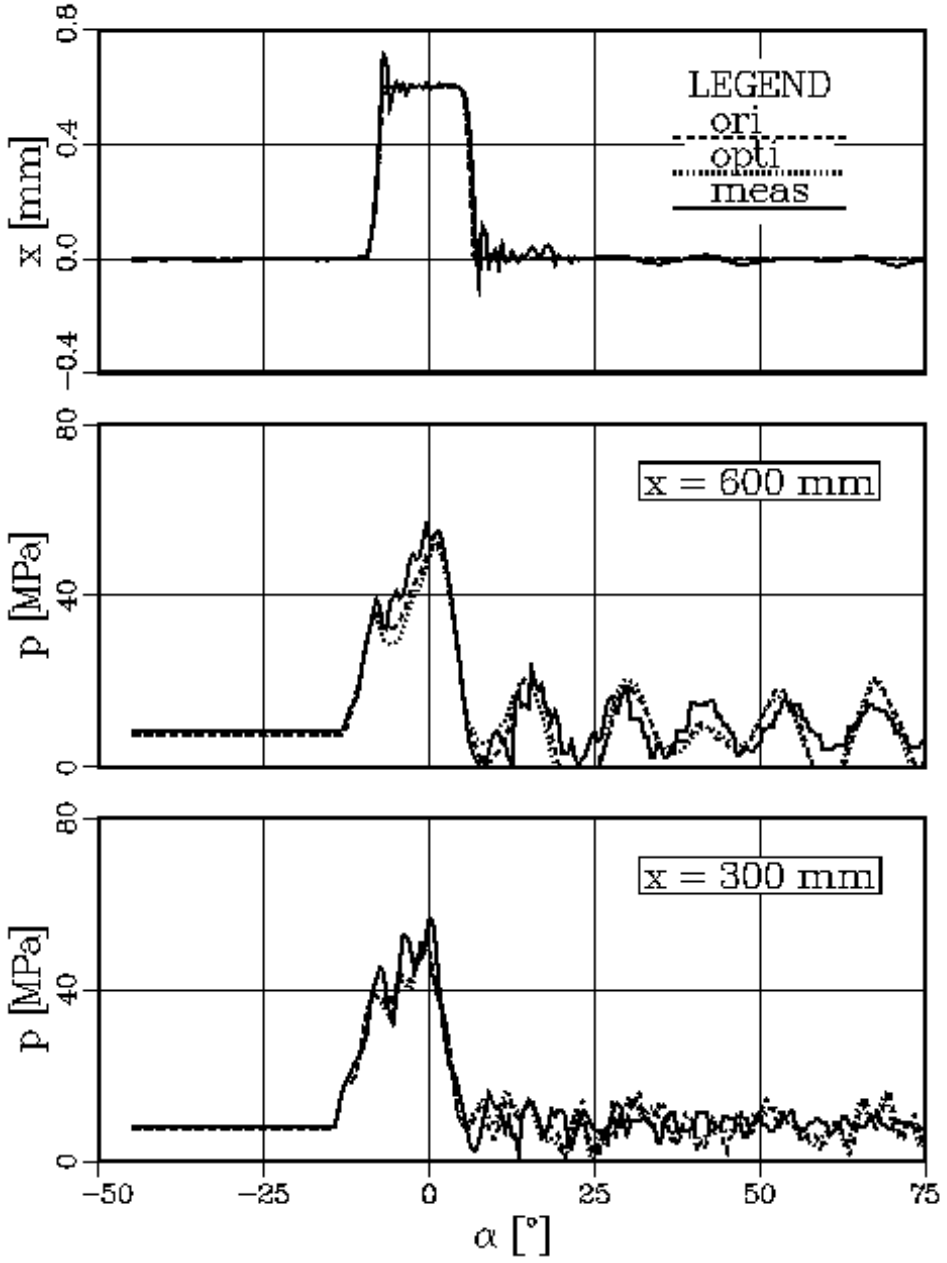

Figure 34. The calculated and the measured (meas) lift x of Needle vn_1 and pressure p in the last node (x = 600 mm) and the midmost node (x = 300 mm) of Pipe l_1 as a function of the crank angle α. The results were calculated using the measured (ori) and the optional (opt) fictive flow coefficients. The rack setting was 15 mm.

A change in the fictive flow coefficients at the centremost node of Pipe l_1 does not have any significant effect on the calculated pressure curve. For the highest pressure with the optional fictive flow coefficients, 51.1 MPa was calculated, and, with the original fictive flow coefficients, 51.9 MPa. The maximum pressure calculated with the optional fictive flow coefficients is 9.6 % lower than the measured maximum pressure.

The injection mass per shot with the optional fictive flow coefficients was calculated to be 0.567 g. This mass is only 0.4 % smaller than the measured mass.

At a rack setting of 15 mm, the option of new fictive flow coefficients can be considered as moderately successful. The injection mass calculated with the new fictive flow coefficients is approximately the same as the measured injection mass. On the other hand, the calculated pressures in Pipe l_1 do not correspond to the measured pressure very well for all parts.

9 Calculated results

The results have been calculated using the new fictive flow coefficients of the gap between the needle and the seat of the injection valve, as defined in Chapter 8, and of the injection valve holes. The initial values for the calculation are presented in Appendix A.

9.1 Pipe l_1

9.1.1 Amount of interpolation

When the rack setting was 22 mm, the smallest amount of interpolation at point R of the characteristic grid was 0.892. At a rack setting of 15 mm, the lowest amount of interpolation at point R of the grid was calculated to be 0.909. At the higher rack setting, the lowest amount of interpolation at point S of the characteristic grid was 0.899 and, at the lower setting, it was 0.895. The amount of interpolation never exceeded 1 at any point R or point S of the characteristic grid. Figure 35 shows an example of the amount of interpolation at points R and S of the characteristic grid as a function of the crank angle.

9.1.2 Pressure

In Figures 36 and 37, the pressure is presented as a function of the distance and crank angle in Pipe l_1 for rack settings of 22 mm and 15 mm. In the figures, the variation of pressure is distinctly discernible as a function of both place and time. At a rack setting of 22 mm, the high pressure range of the main injection extends significantly longer than at a setting of 15 mm.

When the rack setting was 22 mm, 67.6 MPa was calculated as the highest pressure of Pipe l_1. This pressure occurred at the first end of Pipe l_1 at a crank angle of 7°. With a 15 mm rack setting, the highest pressure was 52.4 MPa, occurring at a distance of 180 mm from the first end of Pipe l_1 at a crank angle of $-1°$.

Figure 38 shows the pressure in the eighth node of Pipe l_1 as a function of the crank angle at two rack settings. At both rack settings, the pressure starts to rise from the pressure at rest in a nearly similar fashion. At a rack setting of 15 mm, the pressure starts to go down, after the crank angle reaches the value of 0°. On the other hand, at a rack setting of 22 mm, the pressure continues to rise up to a crank angle of 9°. After the crank angle exceeds 25°, the pressure oscillates at both rack settings at approximately the same amplitude.

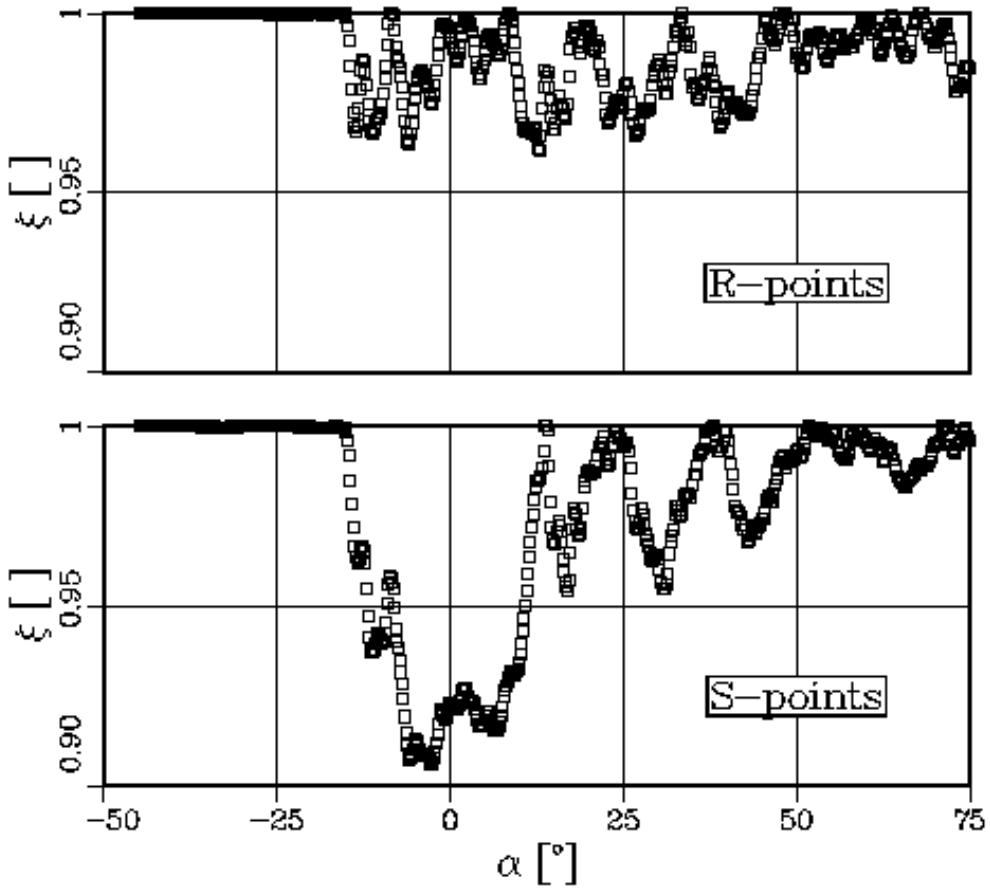

Figure 35. Amount ξ of interpolation at points R and S of the characteristic grid as a function of the crank angle α in the eighth node of Pipe l_1 ($x =$ 420 mm). The rack setting was 22 mm.

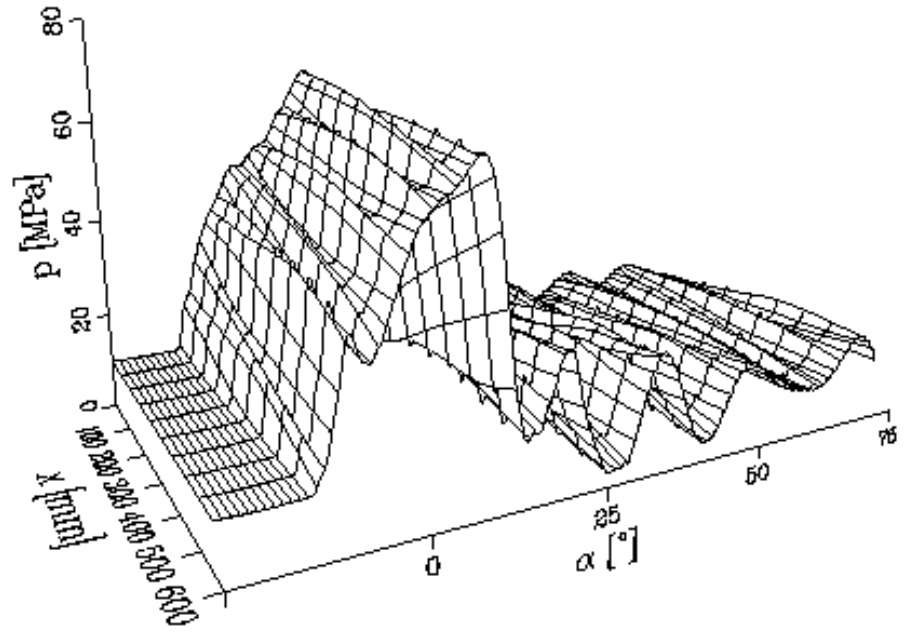

Figure 36. Pressure p in Pipe l_1 as a function of the distance x and the crank angle α. The rack setting was 22 mm.

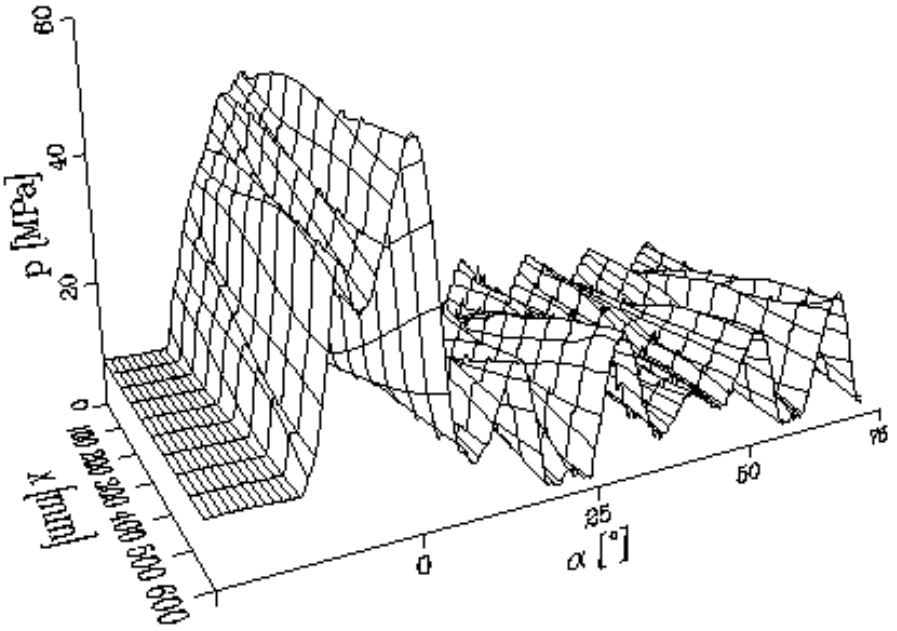

Figure 37. Pressure p in Pipe l_1 as a function of the distance x and the crank angle α. The rack setting was 15 mm.

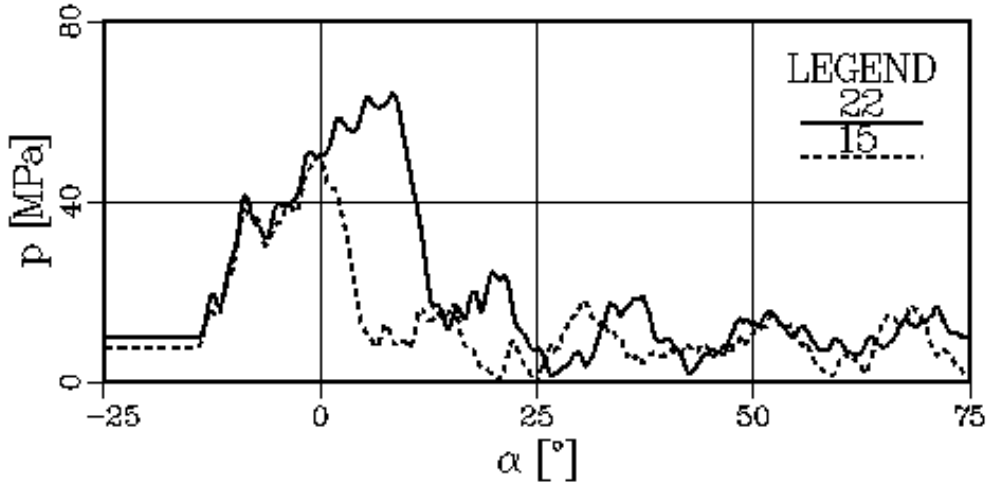

Figure 38. Pressure p in the eighth node of Pipe l_1 (x = 420 mm) as a function of the crank angle α. The rack settings were 22 and 15 mm.

9.1.3 Cavitation volume

When the rack setting was 22 mm, the flow did not cavitate in the inner nodes of Pipe l_1, while at a rack setting of 15 mm the flow cavitated only in the tenth, the ninth, and the eighth inner nodes (Figure 39). During the calculation period the average volume of cavitation in the tenth node was $3.79{\cdot}10^{-3}$, in the ninth node $5.44{\cdot}10^{-3}$, and in the eighth node $2.55{\cdot}10^{-3}$ mm^3.

In the tenth node of the pipe, the flow cavitated at three locations. The first two cavitations are clearly visible in the figure. The third cavitation starts just before the crank angle of 75 °. The cavitation does not end before the calculation is ended.

With a 21° crank angle, a very low cavitation peak can be detected. The maximum volume of the second cavitation is the highest of the calculated cavitations. A third cavitation is not detectable in the ninth node.

In the eighth node, the flow only cavitates at one location. The cavitation starts at the same time as the second cavitation of the ninth and the tenth node.

9.1.4 Flow velocity

The surface of the flow velocity is presented in Figure 40 as a function of the distance and the crank angle at a rack setting of 22 mm. The highest velocity is approximately 59 m/s. At a rack setting of 15 mm, the highest velocity is nearly the same as at the higher rack setting.

In Figure 41, the flow velocity is presented in the eighth node of Pipe l_1 as a function of the crank angle. In the course of the main injection, the average velocity of flow in the eighth node of the pipe is approximately 39 m/s at a rack setting of 22 mm, and 30 m/s at a rack setting of 15 mm.

9.1.5 Darcy-Weisbach friction factor

Figures 42 and 43 present the Darcy-Weisbach friction factor as a function of the crank angle in the eighth node of Pipe l_1. The friction factor has a very high value when the Reynolds number is small. Therefore, only a few curves of the friction factors are shown.

With a 22 mm rack setting, the injection starts at a crank angle of $-10°$ and ends at a crank angle of 15°. The friction factor is nearly constant, with the exception of the latter part of the injection.

With a 15 mm rack setting, the injection starts at a crank angle of $-10°$ and ends at a crank angle of 7°. At this rack setting, the friction factor is approaching constant only in the crank angle range -4–$+1$ °.

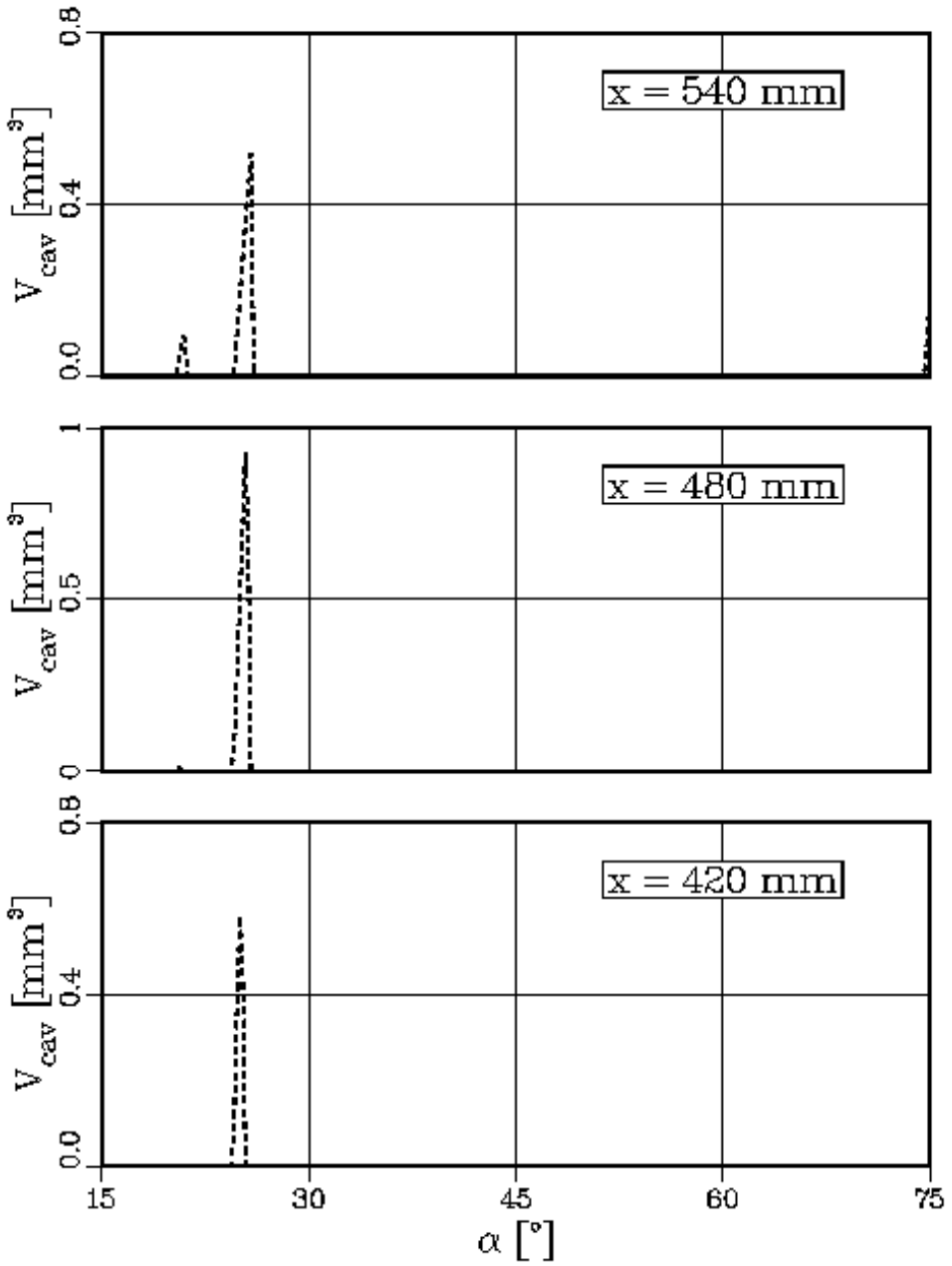

Figure 39. Cavitation volume V_{cav} in the tenth node (x = 540 mm), the ninth (x = 480 mm), and the eighth (x = 420 mm) nodes of Pipe l_1 as a function of the crank angle α. The rack setting was 15 mm.

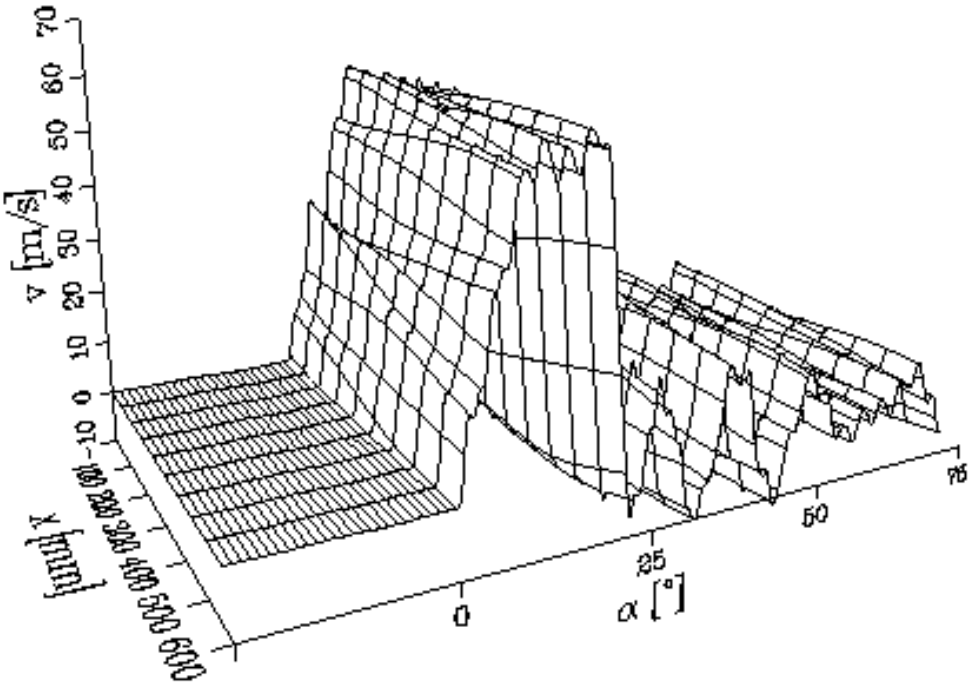

Figure 40. Flow velocity v in Pipe l_1 as a function of the distance x and the crank angle α. The rack setting was 22 mm.

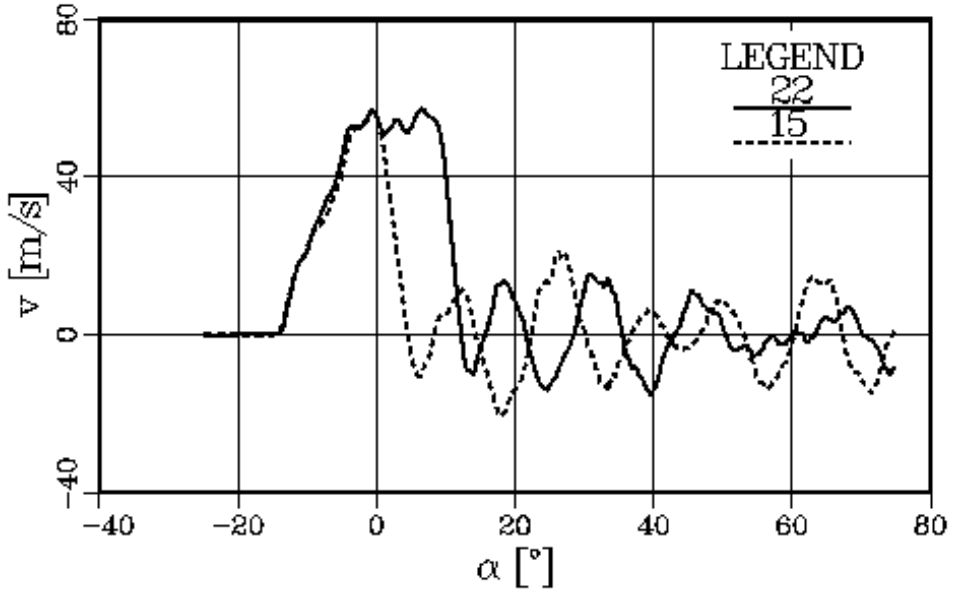

Figure 41. Flow velocity v in the eighth node of Pipe l_1 ($x = 420$ mm) as a function of the crank angle α. The rack settings were 22 mm and 15 mm.

9.1.6 Reynolds number

Figure 44 presents the Reynolds number in Pipe l_1 as a function of the distance and crank angle at a rack setting of 22 mm. The highest Reynolds number is approximately 75200 at the first end of Pipe l_1 at a crank angle of -2.0 °. At a rack setting of 15 mm, the Reynolds number is slightly higher than at a rack setting of 22 mm.

When the Reynolds number exceeds the value of 2300, the flow turns from a laminar into a turbulent one in Pipe l_1 . Consequently, the flow in Pipe l_1 is mostly turbulent after the beginning of the main injection. The Reynolds number is shown in Figure 45 in one pipe node as a function of the crank angle.

9.2 Container bu_1 of unknown pressure

Figure 46 shows the pressure in Container bu_1 of unknown pressure as a function of the crank angle at rack settings of 22 and 15 mm. At both settings, the pressure begins to rise at approximately the same time. The pressure curves are very close to each other up to a crank angle of 0°. Now, the pressure starts to drop at the smaller rack setting, whereas at the greater

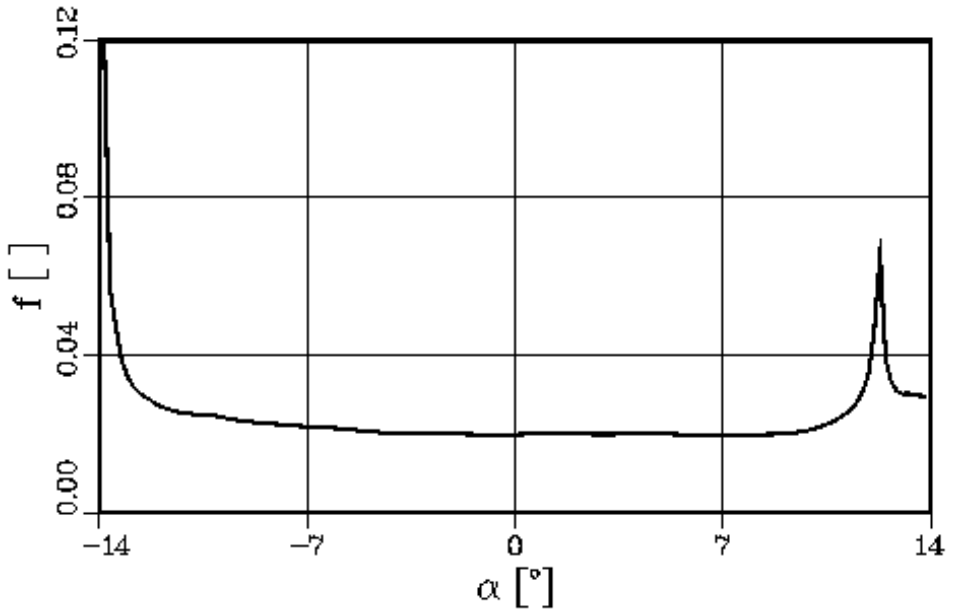

Figure 42. Darcy-Weisbach friction factor f in the eighth node of Pipe l_1 (x = 420 mm) as a function of the crank angle α. The rack setting was 22 mm.

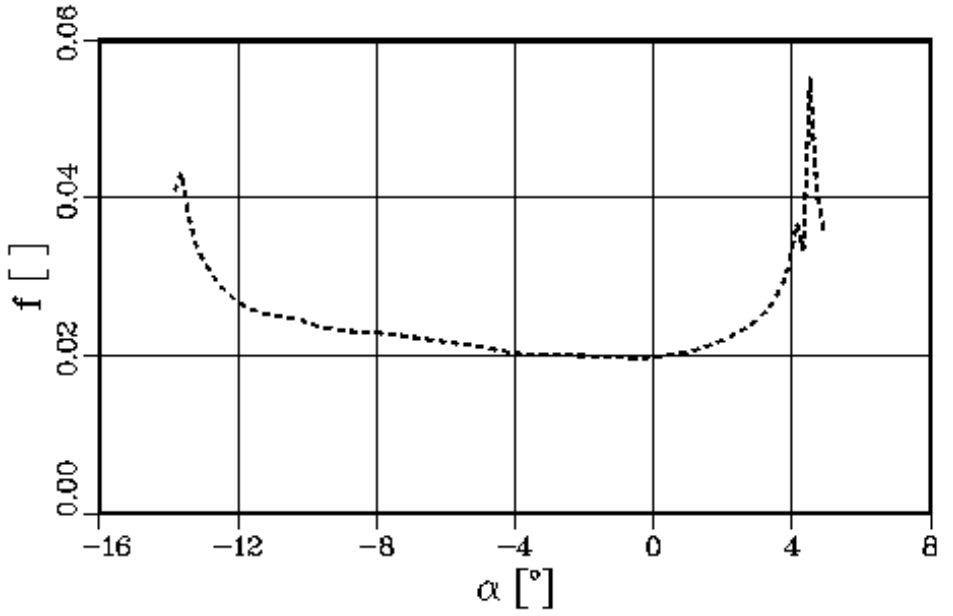

Figure 43. Darcy-Weisbach friction factor f in the eighth node ($x = 420$ mm) of Pipe l_1 as a function of the crank angle α. The rack setting was 15 mm.

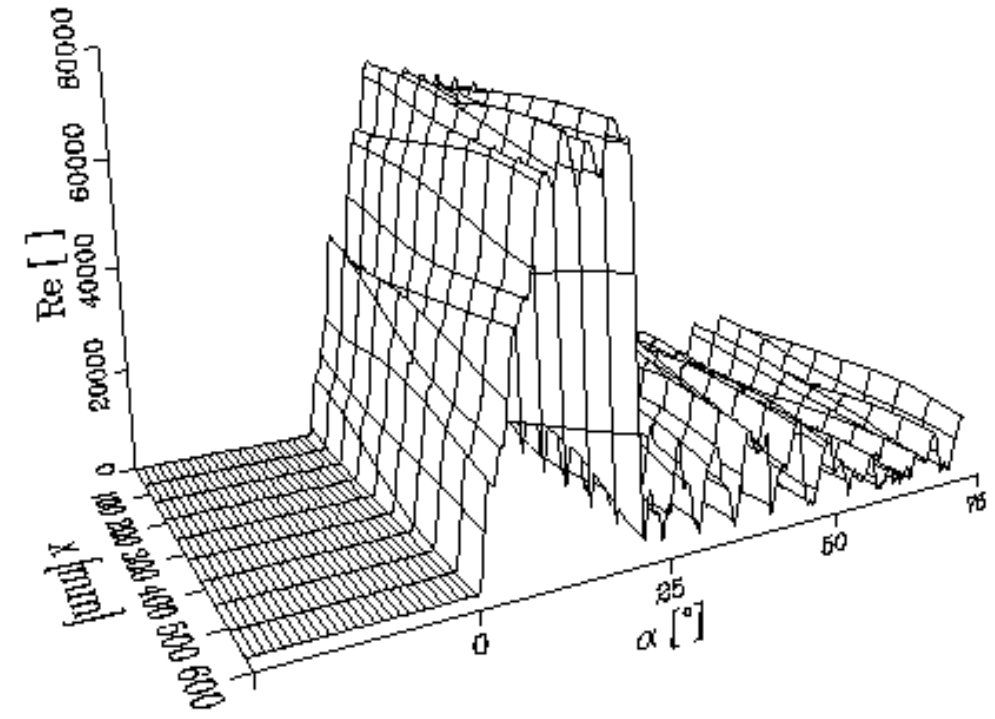

Figure 44. Reynolds number Re in Pipe l_1 as a function of the distance x and crank angle α. The rack setting was 22 mm.

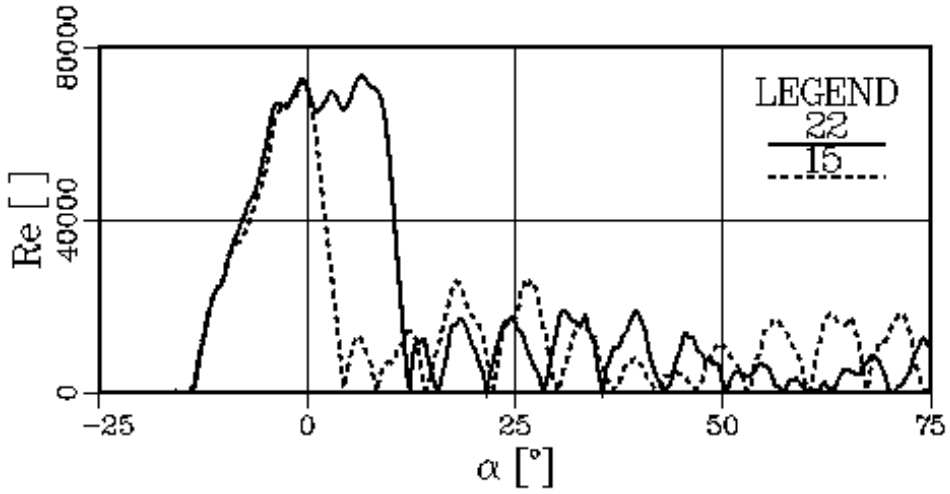

Figure 45. Reynolds number Re in the eighth node of Pipe l_1 ($x = 420$ mm) as a function of the crank angle α. The rack settings were 22 mm and 15 mm.

setting the pressure continues to rise up to a crank angle of 10 °. The cavitation points are clearly visible in the pressure curves.

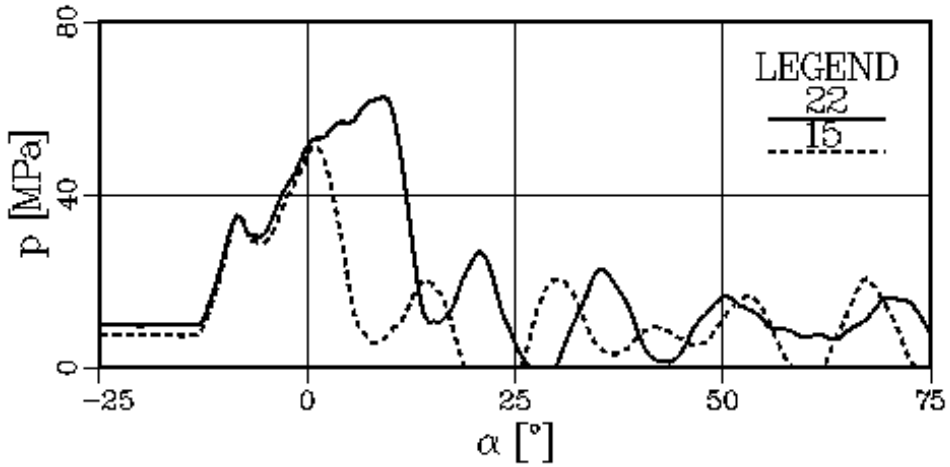

Figure 46. Pressure p in Container bu_1 of unknown pressure as a function of the crank angle α. The rack settings were 22 mm and 15 mm.

The cavitation volume in Container bu_1 is presented in Figures 47 and 48 as a function of the crank angle at two rack settings. At a rack setting of 22 mm, the average cavitation volume during the calculation period is 0.14 mm^3. At a rack setting of 15 mm it is 1.97 mm^3. At the smaller rack setting, three cavitations occur, whereas at the greater rack setting, one cavitation is detected.

9.3 Flow passage cj_1

Figure 49 presents the mass flow rate of the fluids flowing through Flow passage cj_1 as a function of the crank angle at rack settings of 22 mm and 15 mm. At both rack settings, the flow begins almost simultaneously. At the high rack setting, the flow continues for much longer than at the lower rack setting. At a rack setting of 22 mm, when the crank angle exceeds the value 20°, after-injection starts.

The Reynolds number has been calculated on the basis of the geometric cross-section area of Passage cj_1 (Appendix A.5). As a matter of fact, the shape of the curve for the Reynolds number (Figure 50) resembles the shape of the curve for the mass flow rate. At a rack setting of 22 mm, the highest Reynolds number during the main injection is approximately 23500, and,

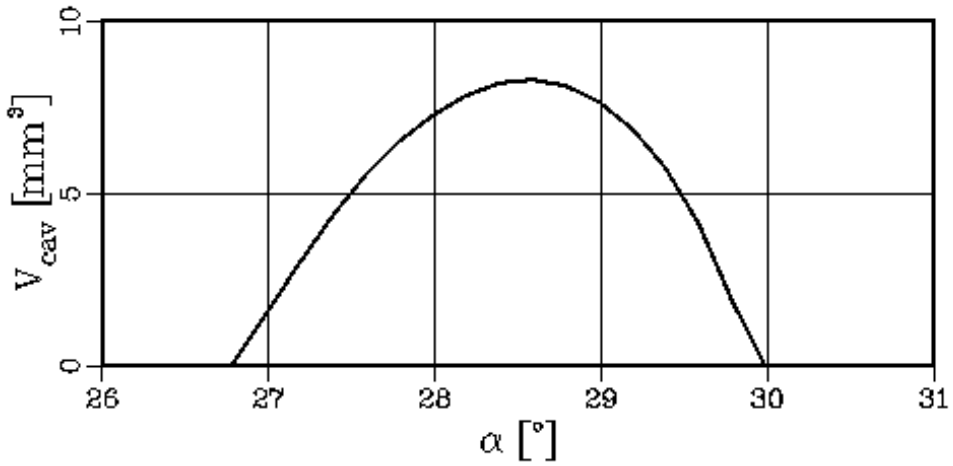

Figure 47. Cavitation volume V_{cav} in Container bu_1 of unknown pressure as a function of the crank angle α. The rack setting was 22 mm.

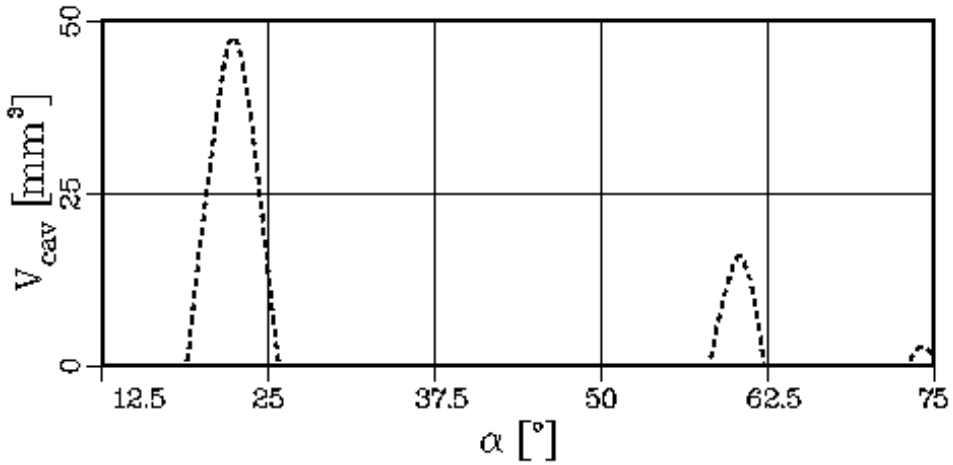

Figure 48. Cavitation volume V_{cav} in Container bu_1 of unknown pressure as a function of the crank angle α. The rack setting was 15 mm.

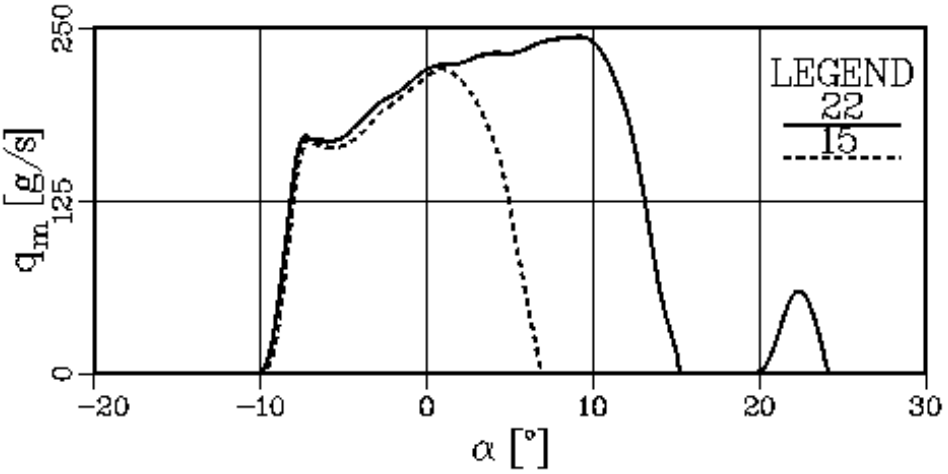

Figure 49. Mass flow rate q_m through Flow passage cj_1 as a function of the crank angle α. The rack settings were 22 mm and 15 mm.

during the after-injection, approximately 4700. At a rack setting of 15 mm, the Reynolds number reaches its highest value of 21200.

9.4 Container bubk$_1$ of unknown pressure

Figure 51 presents the pressure in Container $bubk_1$ of unknown pressure as a function of the crank angle. The parameter is the rack setting. When Flow passage cj_1 is closed, the pressure in this container is assumed to equal the pressure in Known pressure container bk_2. At a rack setting of 22 mm, the after-injection is detected as a pressure rise in the proximity of the crank angle 22°.

9.5 Flow passage cg$_1$

9.5.1 Rack setting of 22 mm

Figure 52 shows the fictive flow coefficient, dimensionless pressure drop, and Reynolds number in Flow passage cg_1 as a function of the crank angle.

The main injection begins at a crank angle of −10.4°. Since the Reynolds number is small at the beginning of the main injection, the fluid flows in laminar fashion in Flow passage cg_1.

The Reynolds number exceeds the turbulent flow limit at a crank angle of −9.5°, as a result of which the flow becomes turbulent. The fictive flow

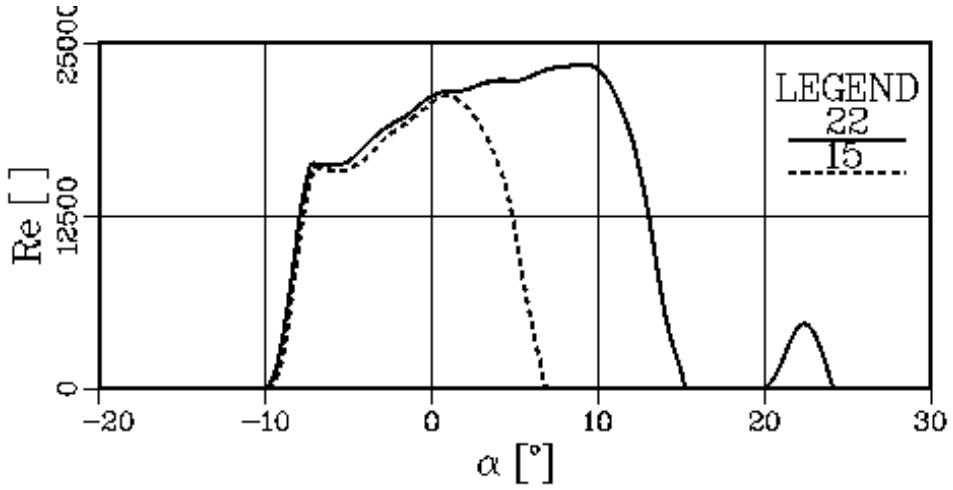

Figure 50. Reynolds number Re in Flow Passage cj_1 as a function of the crank angle α. The rack settings were 22 mm and 15 mm.

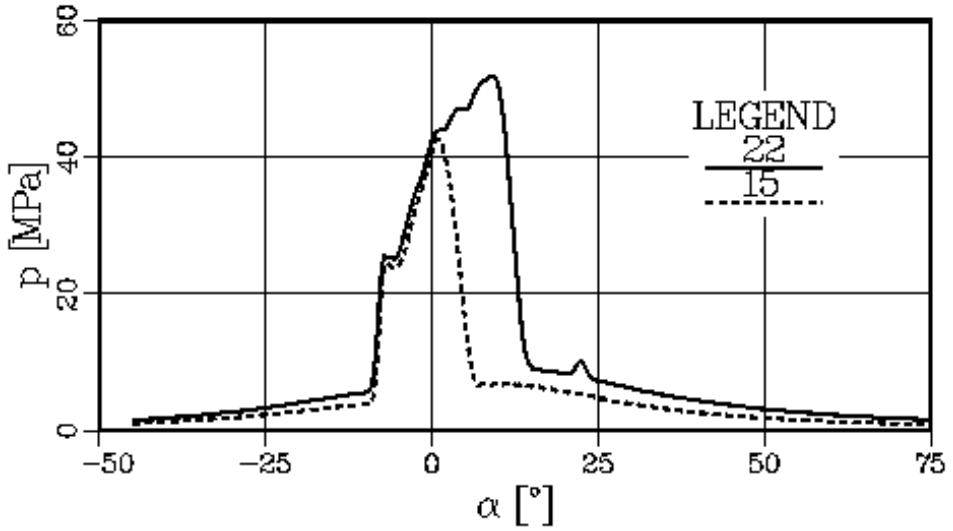

Figure 51. Pressure p in Container $bubk_1$ of unknown pressure as a function of the crank angle α. The rack settings were 22 mm and 15 mm.

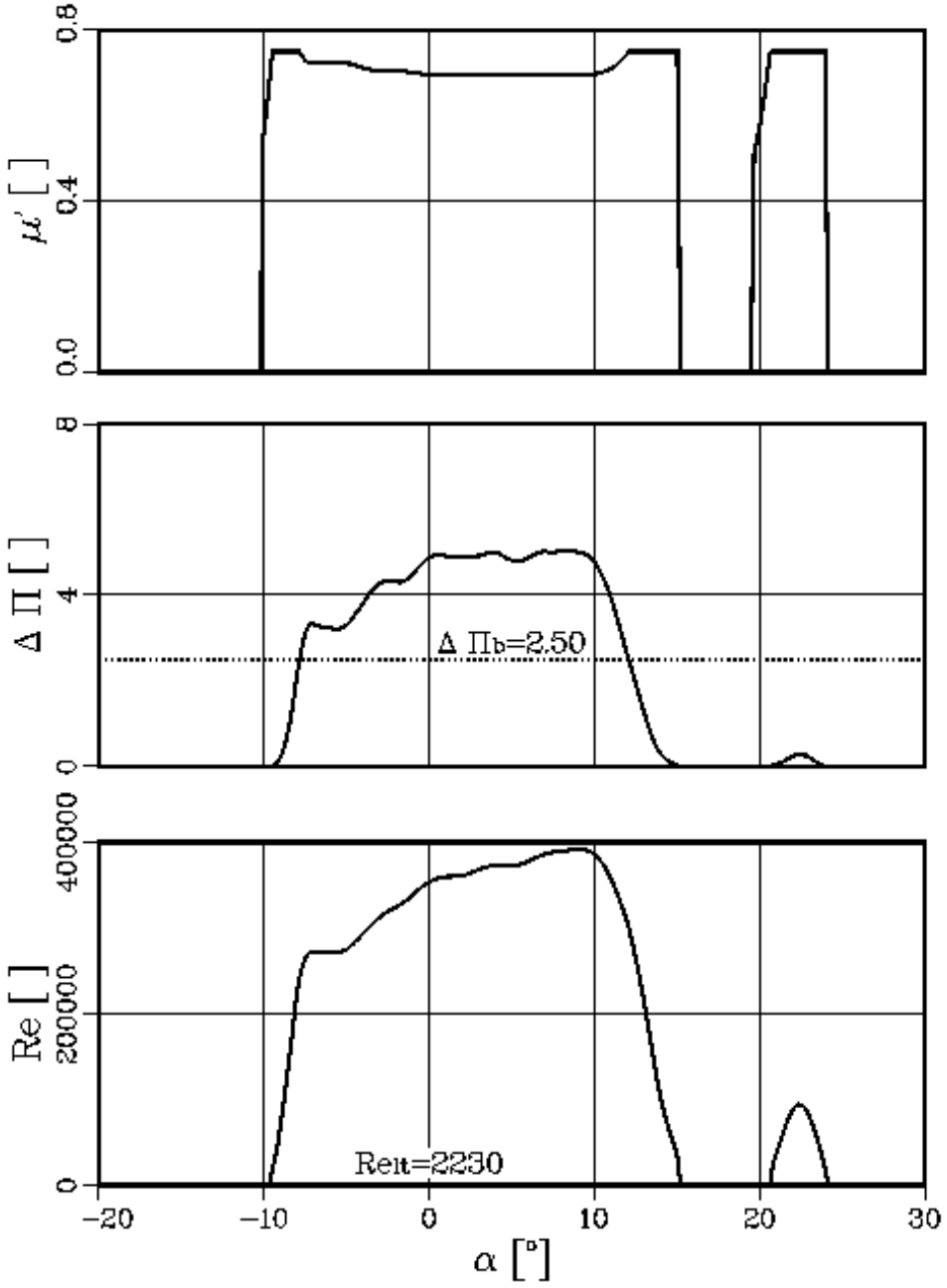

Figure 52. Fictive flow coefficient μ', dimensionless pressure drop $\Delta\Pi$, and Reynolds number Re in Flow passage cg_1 as a function of the crank angle α. The rack setting is 22 mm, $\Delta\Pi_b$ is the critical dimensionless pressure drop, and Re_{lt} is the Reynolds number on which the flow turns from a laminar into a turbulent one.

coefficient is constant in the turbulent flow.

When the critical dimensionless pressure drop is exceeded at a crank angle of -7.9 °, cavitation begins in the flow passage. The lowest fictive flow coefficient of the cavitating flow is by 7.5% lower than the fictive flow coefficient of the turbulent flow. Cavitation continues up to a crank angle of 12.1°, until the critical dimensionless pressure drop is reached. From this crank angle onwards, the flow continues to be turbulent up to a crank angle of 15.2°. Thereafter, the main injection ends abruptly.

The after-injection begins at a crank angle of 19.4°. The flow remains laminar through the subsequent 1.4°. The turbulent flow continues through 3.1°. The after-injection ends very rapidly. During the after-injection, the flow is not cavitating in Passage cg_1.

Table 4 presents the share of the mass flowing during each flow type in comparison with the overall mass of either the main injection or the after-injection. In the main injection, the mass injected during the laminar flow is practically negligible compared with the masses that flowed during the turbulent and the cavitating flows. The bulk of the fuel is injected while the flow is cavitating.

Table 4. Share of the fuel mass flowing through Flow passage cg_1 during the laminar, turbulent, and cavitating flow of the overall mass flowing during the main or after-injection. The rack setting was 22 mm.

Flow	Main injection [%]	After-injection [%]
Laminar	0.1	4.9
Turbulent	8.7	95.1
Cavitaing	91.2	

During the after-injection, the majority of the fuel is injected from the turbulent flow of Passage cg_1.

Figure 53 presents the mass flow rate through Flow passage cg_1 as a function of the crank angle.

Figure 54 shows the flow velocity in a hole of the injection valve calculated according to the geometric flow area. During the main injection, the highest flow velocity is 222 m/s and during the after-injection, 55 m/s.

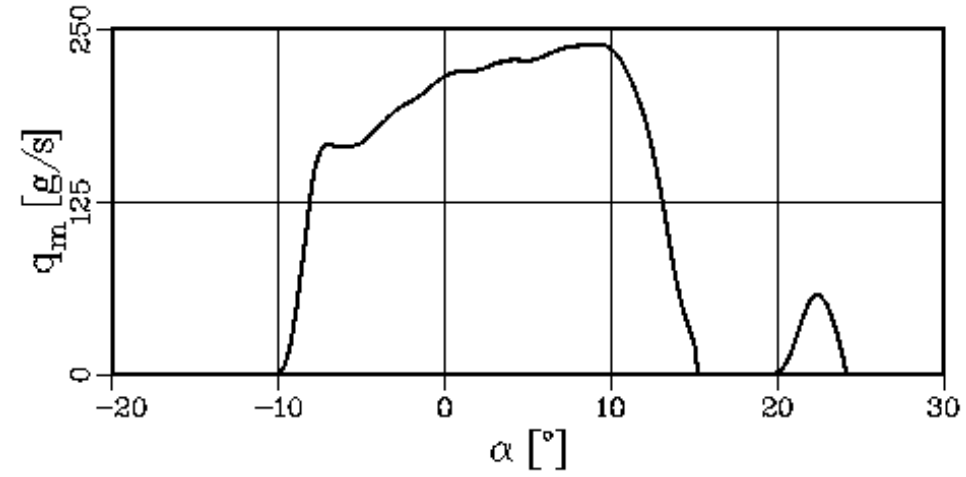

Figure 53. Mass flow rate q_m through Flow passage cg_1 as a function of the crank angle α. The rack setting was 22 mm.

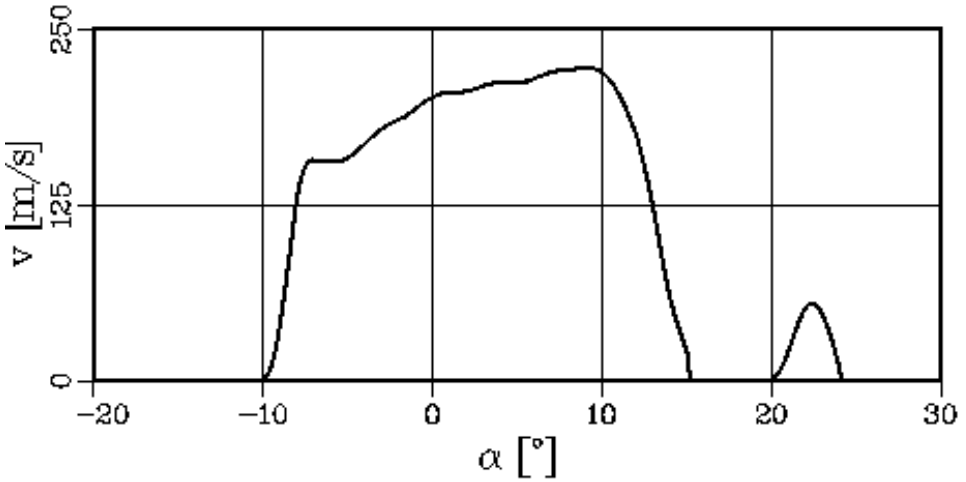

Figure 54. Flow velocity v calculated according to the geometric cross-section area in Flow passage cg_1 as a function of the crank angle α. The rack setting was 22 mm.

9.5.2 Rack setting of 15 mm

Figure 55 presents the fictive flow coefficient, the dimensionless pressure drop, and the Reynolds number in Flow passage cg_1 as a function of the crank angle. At this rack setting, no after-injection occurs.

The injection begins at a crank angle of $-10.1°$. The flow is initially laminar. The flow becomes turbulent at a crank angle of $-9.2°$. The flow remains turbulent until the dimensionless pressure drop becomes higher than the critical dimensionless pressure drop at a crank angle of -7.8 °. Now, the flow starts to cavitate. The flow cavitates up to a crank angle of 4.5 °. The flow is turbulent at the crank angle range of 4.5 through 6.7°. The laminar flow is over after 0.1° the termination of the turbulent flow.

The lowest fictive flow coefficient of the cavitating flow is lower than 10.8 % than the fictive flow coefficient of the turbulent flow.

Table 5 shows the share of the mass flowing through Passage cg_1 of the injection mass per shot in different types of flow. A very small quantity is injected in laminar flow compared with the overall mass. The highest amount of fuel is injected from the cavitating flow of Passage cg_1.

Table 5. Share of the fuel mass flowing in different types of flow through Flow passage cg_1 to the injection mass per shot. The rack setting was 15 mm.

Flow	Proportion [%]
Laminar	0.1
Turbulent	10.9
Cavitating	89.0

Figure 56 shows the mass flow rate in Flow passage cg_1 as a function of the crank angle.

Figure 57 presents flow velocity at the geometric cross-section area. The highest velocity is 241 m/s. At a rack setting of 15 mm, the pressure in Container bk_1 of known pressure is lower than at a rack setting of 22 mm. Therefore, the maximum velocity is higher at the lower setting than at the higher setting.

9.6 Needle $\mathbf{vn_1}$

The lift curves for Needle vn_1 are presented in Figures 33 and 34. Figure 58 presents the velocity of Needle vn_1 as a function of the crank angle at rack

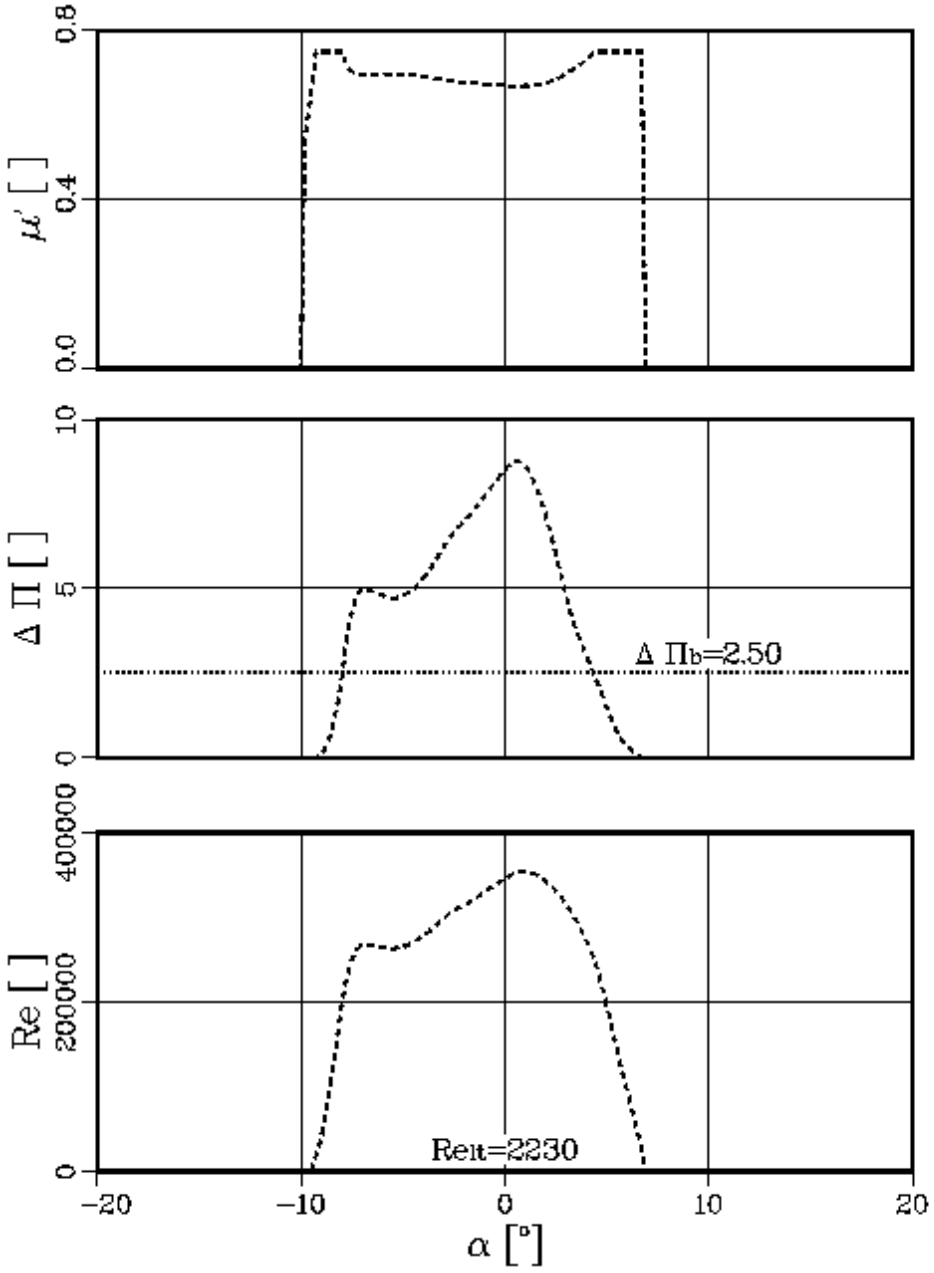

Figure 55. Fictive flow coefficient μ', dimensionless pressure drop $\Delta\Pi$ and Reynolds number Re in Flow passage cg_1 as a function of the crank angle α. $\Delta\Pi_b$ refers to critical dimensionless pressure drop, Re_{lt} to the Reynolds number on which the flow turns from a laminar into a turbulent one. The rack setting was 15 mm.

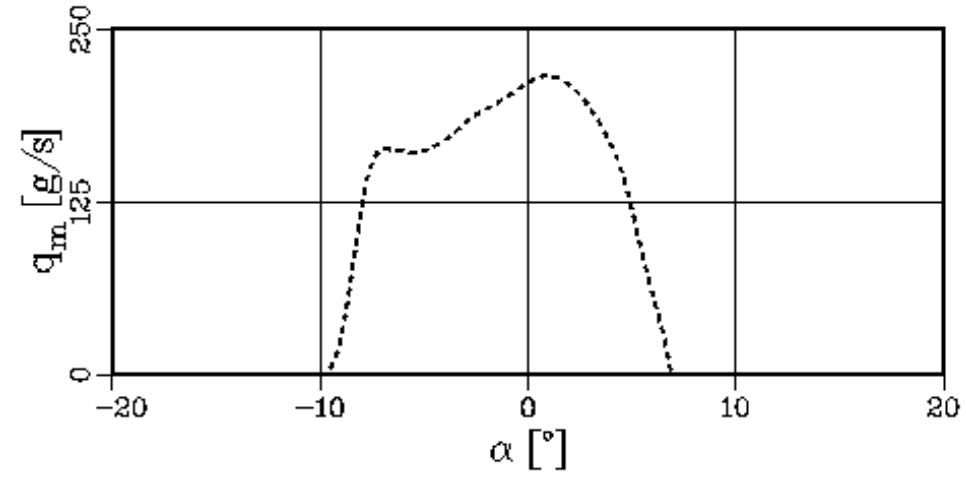

Figure 56. Mass flow rate q_m through Flow passage cg_1 as a function of the crank angle α. The rack setting was 15 mm.

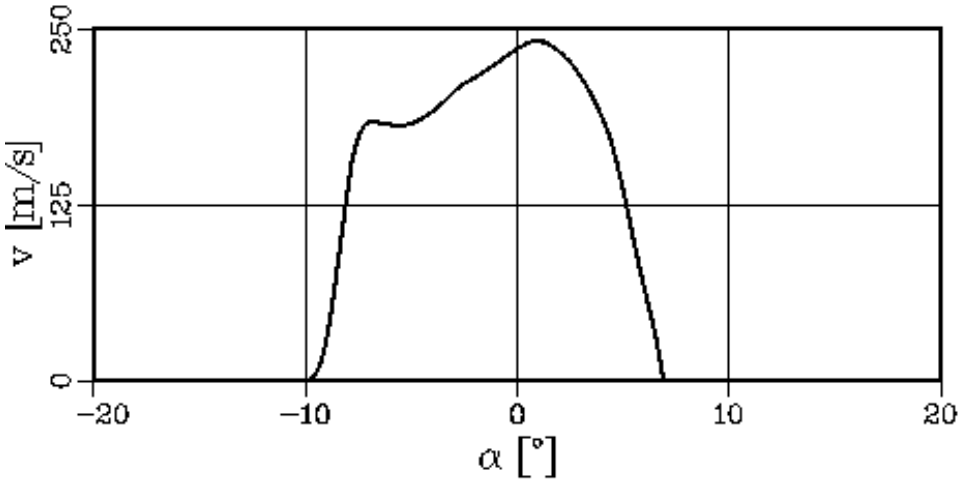

Figure 57. Flow velocity v calculated according to the geometric cross-section area of Flow passage cg_1 as a function of the crank angle α. The rack setting was 15 mm.

settings of 22 mm and 15 mm. When Needle vn_1 rises to its upper limiter for the first time, the velocity curve at both rack settings is almost identical. The needle collides with the upper limiter at a velocity of 1.8 m/s.

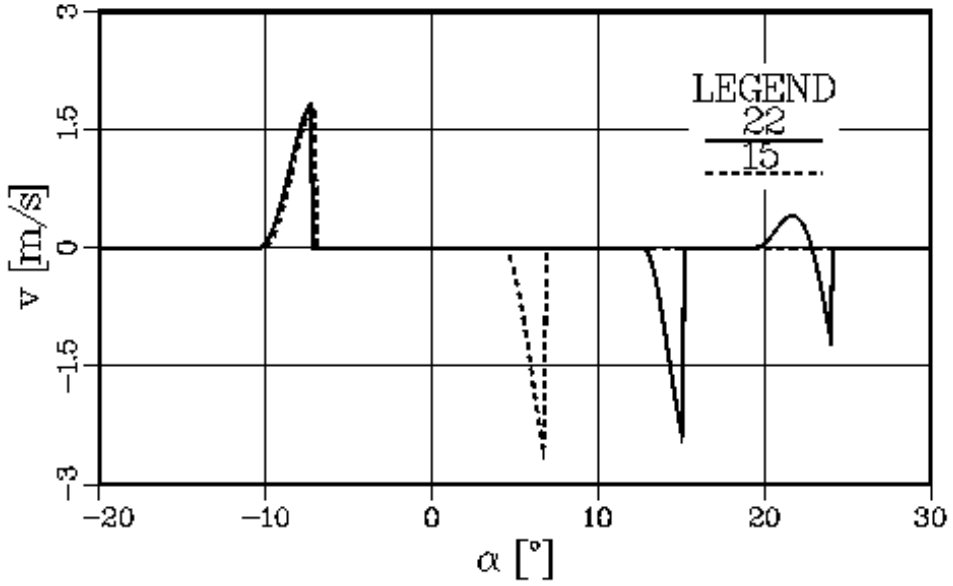

Figure 58. Velocity v of Needle vn_1 as a function of the crank angle α. The rack settings were 22 mm and 15 mm.

At the lower rack setting, the needle initially goes down and collides with the seat at a velocity of -2.5 m/s. At the higher rack setting the needle collides with the seat for the first time at a velocity of -2.3 m/s.

At a rack setting of 22 mm, after-injection occurs. Now, the needle does not rise to the upper limiter. At the end of the after-injection, the needle collides with the seat at -1.1 m/s.

Figure 59 presents the acceleration of Needle vn_1 as a function of the crank angle with the rack setting as a parameter. The highest acceleration of the needle in the opening phase is 4084 m/s^2 and in the closing phase -6356 m/s^2.

9.7 Laminar flow s_1

Figure 60 shows the Reynolds number in Laminar flow s_1 as a function of the crank angle at rack settings of 22 mm and 15 mm. The Reynolds number remains small all through the flow. In such a gap, the flow turns from a

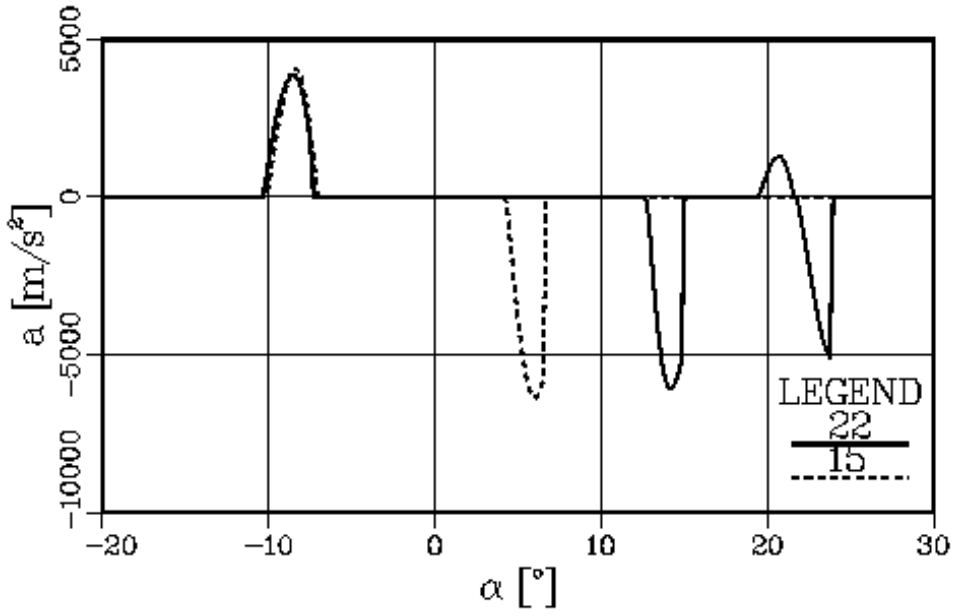

Figure 59. Acceleration a of needle vn_1 as a function of the crank angle α. The rack settings were 22 mm and 15 mm.

laminar into a turbulent one at a Reynolds number of 1400. Thus, the fluid flows well in a laminar fashion in the elementary unit s_1.

The mass flow rate in Laminar flow s_1 is presented in Figure 61 as a function of the crank angle at two rack settings. The pressure in Container bu_1 of unknown pressure was higher before the beginning of the injection than in Container bk_3 of known pressure. For that reason, there is fluid running through Laminar flow s_1 before the injection. The mass flow rate through Laminar flow s_1 is, for the most part, dependent on the pressure of Container bu_1. Therefore, the shape of the curve for the mass flow rate is approximately the same as that of the pressure curve of Container bu_1 (Figure 46).

Table 6. Mass flowing through Laminar flow s_1 during the entire calculation period, the main injection, and the after-injection at rack settings of 22 mm and 15 mm.

Rack setting	[mm]	22	15
Overall injection	[mg]	2.425	1.625
Main Injection	[mg]	1.245	0.662
After-injection	[mg]	0.112	

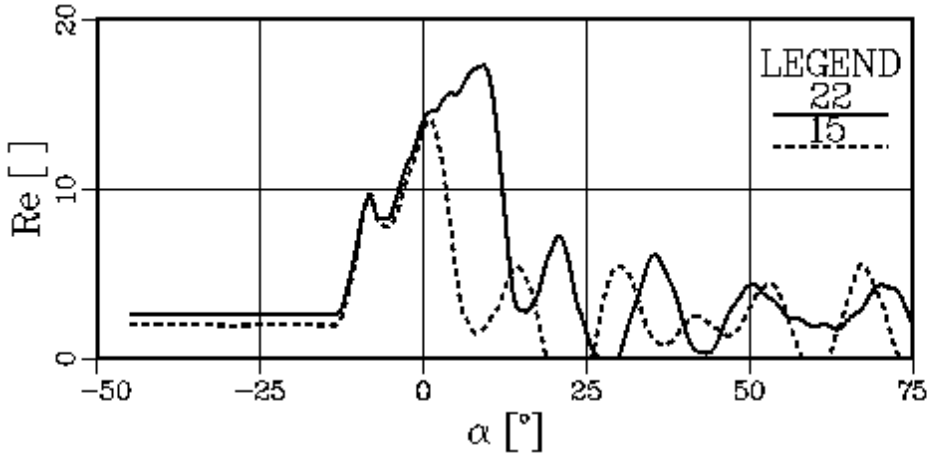

Figure 60. Reynolds number Re in Laminar flow s_1 as a function of the crank angle α. The rack settings were 22 mm and 15 mm.

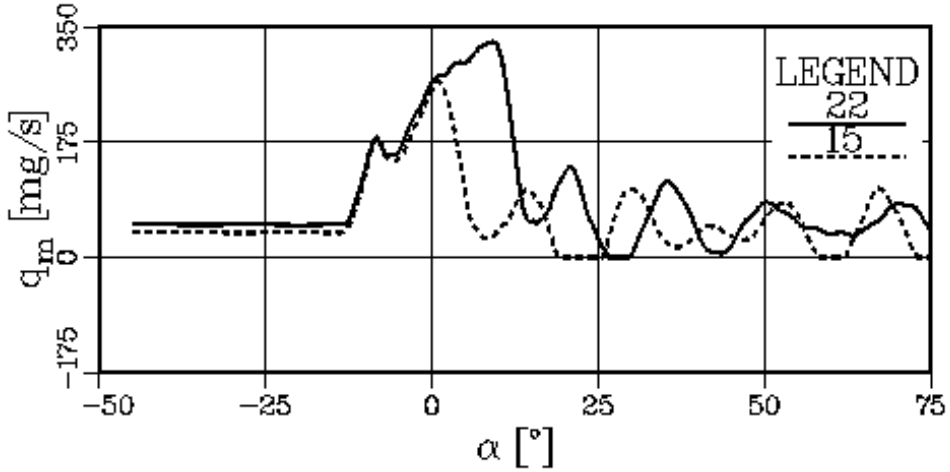

Figure 61. Mass flow rate q_m in Laminar flow s_1 as a function of the crank angle α. The rack settings were 22 mm and 15 mm.

Table 6 shows the mass that has flowed through Laminar flow s_1 during the entire calculation period, the main injection, and the after-injection. When the rack setting is 22 mm, the overall mass, passed through the laminar flow, is 0.23 % of the injection mass per shot. With a 15 mm rack setting, the respective overall mass is 0.29 % of the injection mass per shot.

When the rack setting is 22 mm, 51.3 % of the overall mass passed through the laminar flow flows during the main injection. With this rack setting 4.6 % of the overall mass flows during the after-injection.

At a rack setting of 15 mm, 40.7 % of the entire mass of the calculation period flows during the main injection.

10 Discussion

The results calculated with the program contain a number of error sources, such as:

1. the fictive flow coefficient of the gap between the needle and the seat of the injection valve, and of the injection valve holes, had to be measured using deficient measuring equipment. Since the injection mass per shot was calculated using the measured fictive flow coefficients, the injection mass became too small. For that reason, new fictive flow coefficients were defined for these two flow passages, so that the injection mass calculated with these flow coefficients is approximately equal to the measured injection mass. Since the fictive flow coefficients could be selected from among a wide range, the adoption of new fictive flow coefficients was relatively arbitrary;

2. the injection mass per shot was measured from a running engine with the aid of the fuel mass flow rate. The injection mass was assumed to be equal in each cylinder. Therefore, the precise size of the injection mass of the measured cylinder is not known;

3. the injection mass per shot is an average of at least 325 working cycles. The pressures of the high-pressure pipe and the lift of the injection valve needle were measured as an average of ten working cycles. Hence, the injection mass does not necessarily correspond to the other measured values;

4. the measured pressure curves and the curve for the needle lift are average curves. Not even one individually measured curve needs to be identical with the average curve. On the other hand, the measured pressures and the needle lift varied only to a minor extent during the measuring period;

5. the properties of the fuel were taken from a number of sources. This factor may cause errors in the calculated results;

6. the cavitation model of both the pipe and the container of unknown pressure is simple. With the cavitation models employed, only the sensitivity of the system to cavitation can be detected;

7. the model of the injection valve is rough. The flow of the fuel in the bores of the injection valve body and tip can be calculated separately. In addition, the junctions of the bores should be modeled. This kind

of model of the injection valve, which would be far more detailed than the present one, may reduce the pressure oscillation after the main injection;

8. the needle of the injection valve is assumed to be stiff in a similar fashion to the seat of the needle and the upper limiter. Modeling the elasticity of the needle may enhance the accuracy of calculation. However, the lift curves calculated with a stiff needle do not differ to a great extent from the measured lift curve;

9. the model is one-dimensional. Presumably, the accuracy of the calculation of the pipe would not be improved even if the flow were calculated in two or three dimensions. On the other hand, a multi-dimensional modeling of containers of unknown pressure may increase the calculation accuracy of the entire model.

The program is not solely tied to the injection system of a diesel engine. Since the model was assembled from elementary units, the model is flexible. From elementary units, various general hydraulic models can be assembled by means of which one-dimensional time-dependent fluid flow can be calculated.

The low-pressure side of the injection system, the common-rail injection system, and the flow in the cooling system are appropriate new applications of the software in diesel engines.

With the program, detailed information of the flow in the injection system can be provided. No other publications are known in which the following results have been presented:

1. the amount amount of interpolation, velocity, calculated coefficient for fluid friction, and the Reynolds number in the high-pressure pipe;

2. the Reynolds number and mass flow rate between the needle and the seat of the injection valve;

3. the fictive flow coefficient of injection valve holes, dimensionless pressure drop and Reynolds number as a function of the crank angle, and the fluid mass flowing through the holes in the course of laminar, turbulent, and cavitating flow;

4. the velocity and acceleration of the injection valve needle;

5. the Reynolds number and mass flow rate of the leakage of the injection valve.

When this research work was started, no program appropriate for the calculation of the injection process was available. In the course of the latter period of the study, three commercial injection programs were published: HYDSIM by AVL,GT-FUEL by Gamma Technologies, and FINJECT [12] by Ricardo. These programs are primarily intended for designing an injection system, not specifically for analyzing flow. A major weakness in the commercial programs is that the solution methods included therein are accurately known only to the manufacturing companies. The user is not able to change the models of such programs, and neither is he enabled to add novel features thereto. Only values of certain variables can in general be output from the programs.

The code of calculation used in conjunction with this work has been developed, throughout, using homogeneous principles suitable for large programs. The models employed and the solution methods are known. The source code, written in a standardized programming language, is available. The program needs one subroutine library only. This mathematical library is generally available. Desired calculation values can be output from the program without any hindrance. The models and solution routines employed can be developed or changed substantially, and, if necessary, the code itself can be enlarged. Owing to these properties, the present program is highly appropriate for calculating time-dependent fluid flow.

11 Conclusions

1. In calculating high-pressure pipe flow, the amount of interpolation remained in a good range throughout the activity. Hence, the linear model developed for the interpolation of the R and S points of the characteristic grid works, at least in the calculated instances.

2. After the beginning of the main injection, the fluid flows in the high-pressure pipe in an almost constantly turbulent fashion.

3. The Reynolds number achieves such high values in the high-pressure pipe that the Darcy-Weisbach friction factor for turbulent flow cannot be calculated using Blasius' equation. In contrast, Colebrook's equation is valid in all instances.

4. During part of the main injection, the Darcy-Weisbach friction factor of the high-pressure pipe is approximately constant. The Darcy-Weisbach friction factor of the high-pressure pipe cannot, however, be assumed to be constant during the whole injection period.

5. The Reynolds number between the needle and the seat of the injection valve is relatively large. The flow in this flow passage cannot be controlled. Therefore, it is not known at which Reynolds number the flow of the fluid in this passage turns from a laminar into a turbulent one.

6. In the course of the main injection, most of the fuel is injected from the cavitating flow of the holes of the injection valve into the cylinder. The mass to be injected from the turbulent flow of the holes cannot, however, be omitted. During the laminar flow of the holes, relatively little fuel is injected into the cylinder.

7. During the after-injection, the flow does not cavitate in the injection valve holes. Now, most of the injection takes place from the turbulent flow of the injection valve holes, and the fuel mass injected during the laminar flow also affects the mass of the after-injection.

8. When the engine runs at full load, the needle of the injection valve collides with its upper limiter at a velocity of approximately 1.8 m/s. At slightly above the half load, the collision speed of the needle with the upper limiter is of the same order of magnitude. At the end of the main injection, the needle collides with the seat at a higher speed than in a collision with the upper limiter. The acceleration of the needle of the injection valve reaches high values.

9. The leakage of the injection valve needle can be modeled as a laminar flow. The fuel mass that flows through the leakage is insignificant compared with the injection mass per shot.

10. Targets for further research related to the present model are as follows:

    (a) the fictive flow coefficient of the gap between the needle and the seat of the injection valve and of the injection valve holes needs further research. These fictive flow coefficients should be measured in time-dependent flow using either a Bosch pipe [3] or Zeuch's method [40];

    (b) engine tests are less appropriate for testing a model of an injection system. A model for an injection system should be tested with separate test equipment in which a mass for one injection, the lift of the needle, and the pressures needed can be measured simultaneously. In the test equipment, the pressure can be measured at more locations than in the injection system of the engine. In addition, the volume flow rate of the fluid flowing through the holes of the injection valve can be measured as a function of time with this type of equipment;

    (c) it would be desirable to use the injection system of a modern diesel engine for testing the model, and

    (d) the effect of the changes of different parameters of the injection system on the injection process is calculated with the program. The properties of the fuel, the fictive flow coefficient of the gap between the needle and the seat and the holes of the injection valve can be listed as such variables.

11. Reference [25, pp. 34–35] deals with the possibilities of how to develop the model, and presents rough estimates of the time needed for enhancing the model. The following properties could be added to the model:

    (a) the calculated pressure of the high-pressure pipe oscillates after the main injection more powerfully than the measured pressure. Therefore, an air-relief model is needed to calculate the flow in the high-pressure pipe. References [46, pp. 136–155] and [24, pp. 53–57] deal with one air-relief model. The programming of the air-relief model is estimated to take 720 working hours;

    (b) the model is supplemented with an injection pump. Programming the model for the injection pump is predicted to take 1100 working

hours. The measurement of the fictive flow coefficients of the flow passages of the injection pump may take about 480 working hours;

(c) the low-pressure side is modeled, which will take 350 working hours;

(d) the injection valve is modeled in greater detail than in the present model;

(e) when the fluid flows from the pipe to the container or in the reverse direction, losses are entailed;

(f) if a high-pressure injection system is modeled, the effect of elasticity of the high-pressure pipe on the injection process has to be defined.

12 Summary

The injection of fuel controls the combustion in the cylinder of a diesel engine, because of which the progress of the injection has to be well controlled. The objective of this research work was to study the injection process in the injection system of a medium-speed diesel engine with the aid of a computer program.

The program was written in the Fortran language. The program was assembled from objects representing the parts of the injection system. The injection system of the program consists of a high-pressure pipe and an injection valve. The injection pump was replaced by pressure measured at the junction of the injection pump and the high-pressure pipe.

The fuel was modeled as a fluid object. The properties of the fluid are dependent on pressure and temperature. The properties of the fluid need not be the same in different parts of the injection system.

The injection pump, the cylinder, and the leakage container of the injection valve are containers of known pressure. The pressure in the container of known pressure is known as a function of time.

The flow of the high-pressure pipe was calculated in a pipe object in which the one-dimensional fluid flow is solved using a method of specified time intervals. This method is an application of the method of characteristics. The segregation of vapor is modeled in the form of concentrated vapor cavitation. In the calculation method, the points of the characteristic grid of the preceding point of time had to be interpolated. For this interpolation, a method was developed in which the speed of the pressure pulse between two consecutive pipe nodes is assumed to be linearly proportional to the pressure.

The pressure and sac containers of the injection valve are described as containers of unknown pressure. At any point in time, the pressure at each point of the container of unknown pressure is assumed to be equal. The pressure in the container is solved by means of an equation derived from the definition of the coefficient of bulk modulus of elasticity. When the pressure in the container is lower than the vapor pressure of the fluid, the volume of the segregated vapor is calculated using an equation derived from the continuity equation.

The gap between the needle and the seat of the injection valve is modeled as a flow passage controlled by the valve. The volume flow rate through such a passage is dependent on the fictive flow coefficient, the geometric cross-section area of the passage, the density of the fluid, and the pressure drop across the passage. The fictive flow coefficient is assumed to be a function of the valve lift.

The holes of the injection valve are described as a constant-aperture flow

passage. The volume flow rate through the passage is solved using the same equation as in the flow passage controlled by the valve. The fictive flow coefficient of the flow passage with constant holes is modeled by a combination of the Giffen-Muraszew and Schmitt models. The fictive flow coefficient is calculated in different ways in the laminar, the cavitationless turbulent, and the cavitating flows.

The needle of the injection valve is classified as valve. The motion of the valve is solved by means of equations of motion.

The leakage of the needle is processed as laminar flow. In this kind of object, the Reynolds number is small.

The measuring equipment of the fictive flow coefficients of the flow passages proved less appropriate. The pressure after the passage could not be adjusted, and neither was it possible to reach a high enough pressure.

The model was applied to the injection system of a medium-speed Wärtsilä 324 TS engine. In the running test engine, the pressure was measured at three points of the injection system and in the cylinder. In addition, the motion of the needle and the injection mass per shot were determined.

The calculated and the measured results were compared using two rack settings, the one corresponding to full load and the other to about half load. The calculated and the measured results corresponded moderately well to each other, except that the calculated injection mass at both positions was clearly smaller than the measured mass. As the values for the fictive flow coefficients of the flow passages could not be measured reliably, new fictive flow coefficients were sought by means of calculation. The calculated and the measured injection masses with these corrected fictive flow coefficients were of approximately equal magnitude at both rack settings. The ultimate results were calculated with the new fictive flow coefficients.

In the calculation, the interpolation of the points of the characteristic grid of the high-pressure pipe was successful. After the beginning of the injection, the fluid flows turbulently in the high-pressure pipe throughout the injection period. At approximately half load, the flow cavitated in a few nodes of the high-pressure pipe.

In the pressure container of the injection valve, the flow cavitated at both loads.

In the gap between the needle and the seat of the injection valve, the Reynolds number reached relatively high values. In the course of the main injection, most of the fuel entered the cylinder from the cavitating flow of the injection valve holes. Part of the fuel was injected from the turbulent non-cavitating flow of the holes. The share of the fuel injected from the laminar flow of the holes was insignificant.

At full load, after-injection occurred. In the course of the after-injection,

the flow did not cavitate in the holes of the injection valve.

At approximately half load, the highest flow velocity in the injection valve holes was approximately 240 m/s. At full load the highest flow velocity was about 220 m/s.

The acceleration of the injection valve needle reached high values. At the beginning of the main injection, the needle collided with the upper limiter at a velocity of 1.8 m/s at both rack settings.

In the leakage of the needle, the Reynolds number remained small at both loads. The mass of the leakage flow was negligible compared with the injection mass per shot.

With the aid of the program developed, the flow in the injection system of a diesel engine can be examined in detail. The program is flexible and it is written in a standardized programming language.

References

1. Alliévi, L., Allgemeine Theorie über die veränderliche Bewegung des Wassers in Leitungen. Berlin, Julius Springer, 1909.

2. Becchi, G., Analytical Simulation of Fuel Injection in Diesel Engines. SAE Paper 710568, 1971, 30 pp.

3. Bosch, W., Der Einspritz-Indikator, ein neues Meßgerät zur direkten Bestimmung des Einspritzgesetzes von Einzeleinspritzungen. MTZ 25(1965)7, pp. 268–282.

4. Chaudhry, M., Applied Hydraulics Transients. 2nd Edition, New York, Van Norstrand Reinhold Company, 1987, 521 pp.

5. De Juhasz, K., Graphical Analysis of Transient Phenomena in Linear Flow. Journal of the Franklin Institute, April-June 1937, pp.463, 643, 655.

6. Dow, R., Fink, C., Computation of some Physical Properties of Lubricating Oils at High Pressures, Part I. Journal of Applied Physics, Vol. II, May 1940, pp. 353–357.

7. El-Erian, M., Simulation and Control of Transient Flow in the Diesel Injection System. Dissertation, the University of Michigan (Mechanical Engineering), 1972, 151 pp.

8. El-Erian, M., Wylie, E., Bolt, J., Analysis and Control of Transient flow in the Diesel Injection System. Part 1 – the Analytical Control Method. SAE Paper 730661, 1973, 17 pp.

9. El-Erian, M., Wylie, E., Bolt, J., Analysis and Control of Transient flow in the Diesel Injection System. Part 2 – Design Results of Controlled After-Injection. SAE Paper 730662, 1973, 17 pp.

10. Erdmann, H.-D., Untersuchungen zum Einfluss von Toleranzen bei Dieseleinspritzeinlagen auf den Einspritzverlauf und den auf den Motorbetrieb. Dissertation, Die Fakultät für Maschinenbau und Elektrotechnik der Universität Carola-Wilhelmina zu Braunschweig, 1983, 171 pp.

11. Fairbrother, R., J., Computer Simulation of Fuel Injection for Direct-Injection Diesel Engines. Thesis, Thermofluids Section, Department of Mechanical Engineering, Imperial College of Science, Technology and Medicine, University of London, 1994, 188 pp.

12. Fairbrother, R., Simulation of Pump-Line-Nozzle Diesel Fuel Injection System with the FINJECT code. Detroit, Proceedings of the Second Ricardo Software International User Conference, February 28, 1997, 14 pp.

13. Ficarella, A., Laforgia, D., Contribution to The Simulation of Injection System for Reciprocating Internal Combustion Engines. SAE Paper 885016, 1988, 10 pp.

14. Ficarella, A., Laforgia, D., Fluiddynamische Erscheinungen in Einspritzanlagen. MTZ 52(1990)1, pp. 28–34.

15. Fomin, Hydrodynamische Berechnung des Einspritzsystems von Schiffsdieselmotoren. Moskau, Meertransport, 1959.

16. Fox, R., McDonald, A., Introduction to Fluid Mechanics. Singapore, John Wiley & Sons, 1985, 741 pp..

17. Giffen, E., Muraszew, A., The Atomization of Liquid Fuels. London, Chapman & Hall ltd, 1953, 246 pp.

18. Goyal, M., Modular Approach to Fuel Injection System Simulation. SAE Paper 780162, 1978, 8 pp.

19. Guide to the Expression of Uncertainty in Measurement. BIBM, IEC, IFCC, ISO, IUPAC, IUPAP, OIML. International Organization for Standardization, 1993, 101 pp.

20. Hardenberg, H., Die Geometrischen Strömungsquerschnitte von Lochdüsen für Direkteinspritzdieselmotoren. MTZ 45(1984)10, pp. 427–429.

21. Huber, E., Scaffitz, W., Experimentelle und theoretische Arbeiten zur Berechnung von Einspritzanlagen von Dieselmotoren (Teil 1). MTZ 27(1966)2, pp. 35–42.

22. Juva, A., Diesel Fuel Oil and Automotive Transportation. Seminar on Contemporary Development in Automotive Transportation, Espoo, Helsinki University of Technology, Department of Mechanical Engineering, 1988, 31 pp. (in Finnish)

23. Kaario, O., Pokela, H., Kjäldman, L., Tiainen, J., Larmi, M., LES and RNG Turbulence Modeling in DI Diesel Engines. SAE Paper 2003-01-1069, 2003.

24. Kiijärvi, J., The Principles of Diesel Fuel Injection System Modeling and Defining Flow Parameters. Licenciate's Thesis, Helsinki University of Technology, Department of Mechanical Engineering, 1993, 133 pp. (in Finnish)

25. Kiijärvi, J., A Model of the Transient Flow in the Diesel Fuel Injection System, the final report of the MOBILE 101T research project. Espoo 1996, Helsinki University of Technology, Internal Combustion Engine Laboratory, Report 68, 38 pp. (in Finnish)

26. Klüsener, O., Druckstösse in Kraftstoffleitungen und Characteristiken-Verfahren. MTZ 23(1962)1, pp. 5–9.

27. Kortelainen, J., Development of a Measurement Equipment for the Fuel Injection System of the Medium Speed Diesel Engine and Evaluation of Simplified Fuel Injection System Models. Master's Thesis, Helsinki University of Technology, Department of Mechanical Engineering, 1995, 102 pp.(in Finnish)

28. Kumar, K., Gaur, R. R., Gaur, R. D., Babu, M., A Finite Difference Scheme for the simulation of a Fuel Injection System. SAE Paper 831337, 1983, 24 pp.

29. Köhler, W., Untersuchungen an gleichdruckentlasteten Einspritzsystemen von Dieselmotoren. Dissertation, Die Fakultät für Maschinenwesen der Technischen Universität Hannover, 1972, 116 pp.

30. Liljenfeldt, G., On the Construction and Use of Fuel Systems for Heavy Fuel Oil. Seminar on Contemporary Development in Automotive Transportation, Espoo, Helsinki University of Technology, Department of Mechanical Engineering. 1988, 38 pp. (in Swedish)

31. Meyer, B., Object-oriented Software Construction. USA, Prentice Hall, 1988, 534 pp.

32. Notz, H., Beitrag zur experimentellen Ermittlung des Einspritzverlaufs am schnellaufenden Dieselmotor. Dissertation, Technische Universität München, Lehrstuhl für Verbrennungskraftmaschinen und Kraftfahrzeuge, 1986, 153 pp.

33. Parsons, J., Harkins, R., Investigation of Fuel Injection System Cavitation Problems on the MV James R. Baker, MV Mesami Miner, and William J. De Lancey. Marine Technology 22(1985)3, pp. 219–237.

34. Pischinger, A., Pischinger, F., Gemischbildung und Verbrennung im Dieselmotor. 2. Auflage, Wien, Springer Verlag, 1957, 206 pp.

35. Ralston, A. Numerical integration methods for the solution of ordinary differential equations. In: Ralston, A., Wilf, H., Mathematical Methods for Digital Computers. New-York, John Wiley & Sons, 1960, pp. 95–109.

36. Schmitt, T., Untersuchungen zur stationären und instationären Strömung durch Drosselquerschnitte in Kraftstoffeinspritzsystemen von Dieselmotoren. Dissertation, Fakultät für Mashinenwesen und Elektrotechnik der Technischen Hochschule München, 1966, 124 pp.

37. Sitkei, G., Kraftstoffbereitung und Verbrennung bei Dieselmotoren. Berlin/Göttingen/Heidelberg, Springer Verlag, 1964, 224 pp.

38. Sobel, D., Lehrach, R., A Hydro-Mechanical Simulation of Diesel Fuel Injection Systems. SAE Paper 870432, 13 pp.

39. Swamee, P., Jain, A., Explicit Equations for Pipeflow Problems. Proceedings of ASCE, Journal of Hydraulic Division, 102, HY5, May, 1976, pp. 656–664.

40. Takamura, A., Ohta, T., Fukushima, S., Kamimoto, T., A Study on Precise Measurement of Diesel Fuel Injection Rate. SAE Paper 920360, 9 pp.

41. Thiemann, W., Zur Bestimmung des Einspritzverlaufs bei Dieseleinspritzanlagen bei Gleichraumentlastung. MTZ 49(1988)5, pp. 207–217.

42. Vogel, W., Simulation von Einspritzvorgängen auf einen digitalen Kleinrechner. MTZ 35(1974)9, pp. 282–287.

43. Wannenwetsch, P., Egler, P., A User-Friendly Program System for Digital Simulation of Hydraulic Equipment. SAE Paper 850532, 1985, 7 pp.

44. Wuori, P., Introduction to Fluid Mechanics. Espoo, Otatieto Oy, 1990, 161 pp.(in Finnish)

45. Wylie, E., Bolt, J., El-Erian, M., Diesel Fuel Injection System Simulation and Experimental Correlation. SAE Paper 710569, 1971, 14 p.

46. Wylie, E., Streeter, V., Fluid Transients. Third Printing, Ann Arbor, FEB Press, 1985, 384 pp.

47. Young, F., Cavitation. Great Britain, McGraw-Hill Book Company (UK) Limited, 1989, 418 pp.

A Initial values of the program

A.1 Fluid

For the fluid of the model, light diesel oil was used. Since there were no chances to measure the properties of diesel oil in the study, they were taken from two different sources. A number of the values of diesel oil had to be estimated.

The properties of light-weight diesel oil are stored in a data base. In the data base, the speed of the pressure pulse in the diesel oil [21] is presented as a function of pressure and temperature . The density in the initial pressure [21] is dependent on temperature. The initial pressure is 100 kPa. The dynamic viscosity [22] and the estimated vapor pressure are functions of temperature. In addition, the data base includes the molar mass of vapor.

The input file defining the properties of the fluid object was created with the preprocessing program `DlObj`. The preprocessing program reads the data base containing the temperature of the fluid and the properties of diesel oil as inputs. In the calculation, 40 °C was assumed as the temperature of each liquid object. The initial values of the liquid object are presented below at this constant temperature.

The speed c of the pressure pulse in diesel oil is calculated with the equation

$$c[\mathrm{m/s}] = 1551.48[\mathrm{m/s}] + 5.0045 \cdot 10^{-6} p[\mathrm{Pa}] - 6.9163 \cdot 10^{-15} (p[\mathrm{Pa}])^2, \quad (65)$$

where p denotes pressure. The highest speed of the pressure pulse is 2457 m/s. At this moment, the pressure is 362 MPa. If the pressure exceeds the above value in the calculation, the speed of the pressure pulse is assumed to be the maximum magnitude.

The density of diesel oil is calculated using the polynomial

$$\rho[\mathrm{kg/m^3}] = 818.67[\mathrm{kg/m^3}] + 5.8738 \cdot 10^{-7} p[\mathrm{Pa}] - 1.3846 \cdot 10^{-15} (p[\mathrm{Pa}])^2. \quad (66)$$

When the pressure is 212 MPa, the density of diesel oil reaches its highest value of 881 kg/m^3. If the pressure exceeds the value 212 MPa, the density will be given its maximum value.

At 40 °C the dynamic viscosity of diesel oil is $1.723 \cdot 10^{-3}$ Ns/m^2. At the selected temperature, the pressure of diesel oil vapor is assumed to be 50 kPa.

The molar mass of diesel oil vapor is assumed to be equal to the molar mass of air, this being 28.9644 kg/kmol. When the gas constant is $8.31433 \cdot 10^3$ J/(kmol K), temperature 40 °C and vapor pressure 50 kPa, 0.5562 kg/m^3 is obtained as the vapor density of diesel oil by Equation 5.

A.2 Containers of known pressure bk_1, bk_2 and bk_3

In Figures 62 and 63, the pressure is shown in Containers of known pressure bk_1 and bk_2 as a function of time at tested loads. Time is the variable of the calculation code. A post-processing program can convert the results into functions of crank angle. The pressure in Container bk_3 of known pressure was assumed to be 100 kPa at both rack settings.

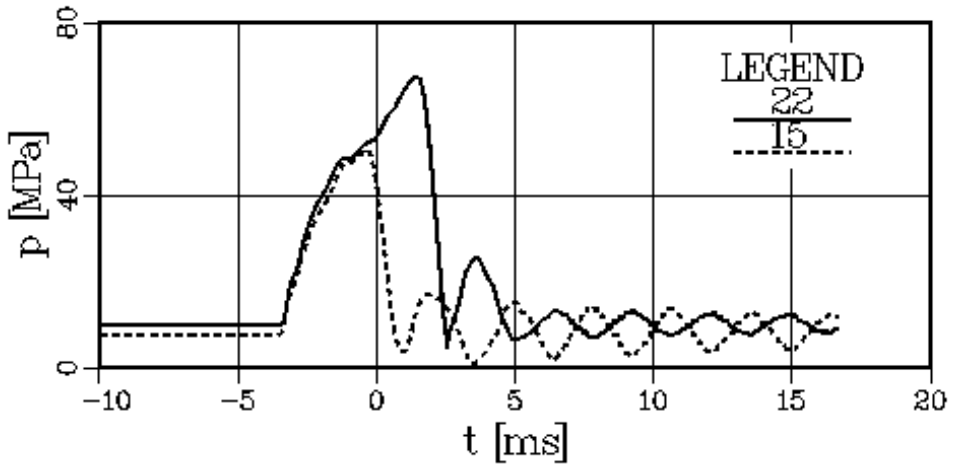

Figure 62. Pressure p in Container bk_1 of known pressure as a function of time t. The rack settings were 22 and 15 mm.

A.3 Pipe l_1

The length of Pipe l_1 is 600 mm and the inner diameter 2.6 mm. The relative roughness of the inner surface was assumed to be 0.0001.

A.4 Container of unknown pressure bu_1

When Needle vn_1 is closed, the volume of Container of unknown pressure bu_1 is 4308.9 mm^3. The controlling area of Needle vn_1 in Container bu_1 is 25.918 mm^2.

A.5 Flow passage cj_1 controlled by valve

Table 7 shows the initial values of Flow passage cj_1 controlled by the valve as a function of valve lift. The difference between the calculated and the

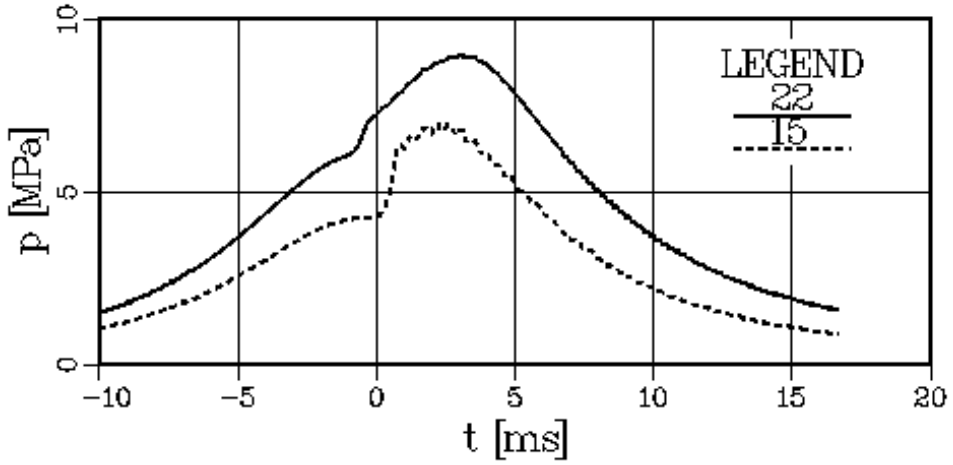

Figure 63. Pressure p in Container bk_2 of known pressure as a function of time t. The rack settings were 22 and 15 mm.

measured injection masses per shot with measured fictive flow coefficients is too great. Therefore, new fictive flow coefficients were determined by calculation. The new fictive flow coefficients were used in calculating the ultimate results.

When Needle vn_1 is closed, the original value of the fictive flow coefficient is 0.7. This value was not, however, measured. The value has been defined to be such that when the needle opens, a sufficient quantity of the fluid flowed between the two containers of unknown pressure connected by a passage. When the needle is closed, no fluid flows through the passage.

The natural length of the passage is needed in order to calculate the Reynolds number. The natural length and the geometric cross-sectional area of the passage were calculated with equations derived by Hardenberg [20] using the NeedleSeat program [24, pp. 124–127].

A.6 Container of unknown pressure $\mathbf{bubk_1}$

The volume of Container of unknown pressure $bubk_1$ is 17.370 mm^3 and the cross-sectional area of the part controlling the needle vn_1 is 3.1416 mm^2.

A.7 Constant-aperture flow passage $\mathbf{cg_1}$

The constant-aperture Flow passage cg_1 includes eight holes, the diameter of which was 0.45 mm. New values had to be calculated for the quantities

Table 7. The initial values of Flow passage cj_1 controlled by the valve. Valve lift x, the measured fictive flow coefficient μ'_{ori}, new fictive flow coefficient μ'_{opt}, natural length l, and geometric cross-section area A_g.

x [mm]	μ'_{ori} [ ]	μ'_{opt} [ ]	l [mm]	A_g [mm^2]
0.0	0.700	0.910	0.0000	0.0000
0.1	0.654	0.850	0.0707	0.3664
0.2	0.605	0.786	0.1442	0.7217
0.3	0.643	0.836	0.2169	1.0456
0.4	0.666	0.866	0.2907	1.3428
0.5	0.711	0.924	0.3662	1.6114
0.6	0.750	0.975	0.4448	1.8485

illustrating the fictive flow coefficient.

On measured values, the fictive flow coefficient μ' of laminar flow is calculated with the equation

$$\mu' = 0.422 + 4.652 \cdot 10^{-3}\sqrt{Re}, \tag{67}$$

where Re denotes the Reynolds number. On the new values, the value of the fictive coefficient of the laminar flow is obtained with the equation

$$\mu' = 0.493 + 5.442 \cdot 10^{-3}\sqrt{Re}. \tag{68}$$

When the Reynolds number exceeds a value of 2230, the flow in Passage cg_1 turns from a laminar into a turbulent one. The measured fictive flow coefficient of the turbulent non-cavitating flow is 0.642 and the flow coefficient determined by calculation is 0.750.

The turbulent flow in Passage cg_1 starts to cavitate when the dimensionless pressure drop exceeds 2.50. The measured fictive flow coefficient of the cavitating flow is calculated using the equation

$$\mu' = 0.543\sqrt{1 + 1/\Delta\Pi}, \tag{69}$$

where $\Delta\Pi$ denotes the dimensionless pressure drop. The fictive flow coefficient of the cavitating flow determined by calculation, is

$$\mu' = 0.634\sqrt{1 + 1/\Delta\Pi}. \tag{70}$$

A.8 Needle vn_1

The controlling area of Needle vn_1 in Container $bubk_1$ is 3.1416 mm^2 and in Container bu_1 25.918 mm^2. The pressure affecting these areas struggles to open the valve. The pressure in Container bk_3 presses to have the valve closed. The controlling area of the needle in this container is 38.485 mm^2.

The moving mass of Needle vn_1 is 61.69 g and the greatest lift 0.6 mm. The spring rate closing the needle is 0.27841 MN/m and spring initial force 622.04 N. For the damping coefficient, 26.211 kg/s was calculated by Vogel's Equation 40.

A.9 Laminar flow s_1

In Laminar flow s_1, the diameter of the piston is 7.0 mm, the length of the gap 28.7 mm, and the clearance 5.5 μm.